2015

Shock Interaction with Substrate in a Shock Induced Spray Process

Kevin Mrozinski
University of Windsor

Shock Interaction with Substrate in a Shock Induced Spray Process

By

Kevin Mrozinski

A Thesis
Submitted to the Faculty of Graduate Studies
through the Department of
Mechanical, Automotive and Materials Engineering
in Partial Fulfillment of the Requirements for
the Degree of Master of Applied Science
at the University of Windsor

Windsor, Ontario, Canada

2015

SHOCK INTERACTIONS WITH SUBSTRATE IN A SHOCK INDUCED SPRAY PROCESS

By:
Kevin Mrozinski

APPROVED BY:

_____

Dr. R. Carriveau
Department of Civil and Environmental Engineering
University of Windsor

_____

Dr. D. Ting
Department of Mechanical, Automotive and Materials Engineering
University of Windsor

_____

Dr. J. Villafuerte
Industrial Advisor
CenterLine (Windsor) Limited

_____

Dr. G. Rankin, Co-Advisor
Department of Mechanical, Automotive and Materials Engineering
University of Windsor

_____

Dr. B. Jodoin, Co-Advisor
Department of Mechanical Engineering
University of Ottawa

February 17th, 2015

Declaration of Co-Authorship / Previous Publication

I. Co-Authorship Declaration

I hereby declare that this thesis incorporates material that is the result of joint research through the University of Windsor under the co-supervision of Dr. Gary Rankin, the University of Ottawa under the co-supervision of Dr. Bertrand Jodoin, and Windsor Centerline Limited with Dr. Julio Villafuerte acting as an Industry Advisor. Darryl Beneteau also aided the initial stages of this research, primarily in design of the apparatus and acquisition of equipment through Centerline Limited. In all cases, the key ideas, primary contributions, data analysis and interpretation, were performed by the author.

I am aware of the University of Windsor Senate Policy on Authorship and I certify that I have properly acknowledged the contribution of other researchers to my thesis, and have obtained written permission from each of the co-author(s) to include the above material(s) in my thesis. A copy of these letters/emails are provided in Appendix F.

I certify that, with the above qualification, this thesis, and the research to which it refers, is the product of my own work.

II. Declaration of Previous Publication

This thesis includes one original paper that has been previously published/submitted for publication in peer reviewed conference proceedings, as follows:

Thesis Chapter	Publication title/full citation	Publication status*
Chapter 2,3,4	D. Beneteau, K. Mrozinski, G.W. Rankin and B. Jodoin, *Shock Induced Spray Process: Flow Visualization of The Substrate Impact Region*, Proceedings of The Canadian Society for Mechanical Engineering International Congress 2014. Toronto, ON, June 1 – 4, 2014.	Published.

I certify that I have obtained a written permission from the copyright owner(s) to include the above published material(s) in my thesis. I certify that the above material describes work completed during my registration as graduate student at the University of Windsor.

I declare that, to the best of my knowledge, my thesis does not infringe upon anyone's copyright nor violate any proprietary rights and that any ideas, techniques, quotations, or any other material from the work of other people included in my thesis, published or otherwise, are fully acknowledged in accordance with the standard referencing practices. Furthermore, to the extent that I have included copyrighted material that surpasses the bounds of fair dealing within the meaning of the Canada Copyright Act, I certify that I have obtained a written permission from the copyright owner(s) to include such material(s) in my thesis.

I declare that this is a true copy of my thesis, including any final revisions, as approved by my thesis committee and the Graduate Studies office, and that this thesis has not been submitted for a higher degree to any other University or Institution.

ABSTRACT

To further the knowledge of the Shock Induced Spray Process (SISP), an experimental apparatus which simulates Centerline's Waverider thermal spray gun was created which uses an unsteady flow to propel solid particles onto a substrate by the use of a shock wave to produce a coating. Experiments were conducted at a variety of operating supply pressures, firing frequencies, and stand off distances. A qualitative analysis was done using a custom Schlieren system along with a high speed camera. Insight into the flow behaviour in the SISP was established with the definition of six distinct phases. The formation of a bow shock, which is known to be detrimental to the SISP operation, is shown to be more prominent in the cases with higher supply pressure and close proximity of the apparatus exit to the substrate than with changes in firing frequency.

DEDICATION

If I Have Seen Further It Is By Standing On The Shoulder Of Giants.

– Sir Isaac Newton

Discoveries are not always instant or planned.

This is for anyone furthering any area of research

for unknowingly they may be building the foundation to a great discovery.

ACKNOWLEDGEMENTS

I would like to fully thank both of my thesis supervisors, Dr. Gary Rankin and Dr. Bertrand Jodoin, for their continued guidance and encouragement during my time as a graduate student. Their knowledge and patience was key to allow me to fully enjoy my time at the University of Windsor.

I would also like to thank Darryl Beneteau who first began work on this project and accepted me to come aboard to aid in the research of this thermal spray technology. I would further like to thank Dr. Julio Villafuerte for his direction and Centerline (Windsor) Limited for their industrial contributions to the project. They, along with NSERC and the Ontario Centres of Excellence, provided the funding and in kind contributions, without which this work would have been impossible.

Of course I would like to thank my parents, Margaret and Marek Mrozinski for their continued support and encouragement to pursue a post graduate education which I now know will pay off in the long run. Finally I would like to heart fully thank my long-time girlfriend Caitlin Towsley for all her support, patience, encouragement, love and resilience through these years.

Thank you all so much!

TABLE OF CONTENTS

List of Tables

List of Figures

Nomenclature

Symbols

a	Area
c	Speed of Sound
B_{PP}	Uncertainty in Instrument
D	Diameter
Fps	Frames per Second
M	Mach Number
P_{Peaki}	Peak Pressure Value
$\emptyset$	Phase Duration
p	Pressure
SOD	Stand off Distance
T	Temperature
V	Velocity
x	Axial Position
γ	Gas Constant
F_R	Frame Rate
S	Sensitivity
R	Resolution
C_D	Cycle Duration
WC_D	Uncertainty in Cycle Duration
P_{MR}	Pressure Transducer Maximum Range Value
$WP\emptyset$	Uncertainty in Percentage Phase Duration

W_{CW}	Uncertainty in Width of Channel
W_{CH}	Uncertainty in Height of Channel
W_{AC}	Uncertainty in Area of Channel
W_{PP}	Uncertainty in Peak Pressure
$W\emptyset$	Uncertainty in Phase Duration
W_{TP}	Uncertainty in Image Capture
W_{SP}	Uncertainty in Supply Pressure
$P_{Peakavg}$	Average Peak Pressure Value
$t_{v,95}$	Student t Distribution Value
T_{CS}	Temperature Coefficient of Sensitivity
E_{min}	Pressure Transducer Minimum Voltage
P_{PP}	Uncertainty in Average Peak Pressure
t_{LF}	Time of Last Frame in Phase
t_{FF}	Time of First Frame in Phase
I	Interval of Pressure Gauge
W_f	Uncertainty in Frequency
B_f	Uncertainty in Oscilloscope
P_f	Uncertainty in Cycle Duration
f_i	Inverse of Cycle Duration Value
f_{avg}	Average Frequency Value

Subscripts

1	Relating to Zone 1	2	Relating to Zone 2
3	Relating to Zone 3	4	Relating to Zone 4
a	Atmospheric		

Chapter 1 Introduction

In this chapter, a background of thermal spray processes is given focusing on certain types; Flame, Detonation Gun, High Velocity Oxy Fuel (HVOF) and Cold Gas Dynamic Spraying (CGDS), to show the variations of techniques available. This will also include a description of a newer variation of CGDS called the Shock Induced Spray Process (SISP) which is the main object of this thesis.

1.1 Thermal Spray Process

Thermal spray processes are an effective way to increase both the performance and longevity of a material by improving its surface properties. Though there are many different thermal spray processes, the common feature for most of them is that molten or semi-molten particles are deposited onto the desired substrate to be coated. Depending on the specific spray process, the particles use either more thermal energy or more kinetic energy to cause them to adhere to the substrate upon impact. These particles deform plastically due to shear straining forces and embed themselves onto the substrate. How these particles increase performance of the base layer relies on the type of particles in the feedstock and their density. Current technologies allow spray of a wide range of materials such as metals, ceramics and cermets, however continued research is being conducted to maximize deposition efficiency and coating properties. Depending on the material used, thermal spray processes are able to increase the corrosion, wear and oxidation resistance, electrical insulation and many other important qualities [1].

The first thermal spray device was Schoop’s flame spray gun, patented in the 1900's, which was a hand held unit [2]. The technique has evolved primarily in its

automation as it was realized that application of many thin layers of coating provided a higher quality, typically spraying at 2-4 ft/s (0.6-1.2 m/s) [3]. There are two types of flame sprayers, powder fed or wire fed. In a powder fed flame gun, Figure 1, an oxygen fuel flame is produced near the end of the nozzle and the particles are accelerated through this area and heated through contact with the exiting combustion gases. The thermal energy of the flame melts, or partially melts, these particles prior to their impact and adherence to the substrate. The wire fed flame gun works in a similar fashion however, instead of particles being injected into the flow, a wire is melted at the exit and the resulting droplets propelled by a dispersing gas such as compressed air. The flame fuel temperature will vary from 2700 K to 3170 K, the lower value obtained with methane and the higher value with acetylene [2,4]. Particle velocities are in the range of 80-100 m/s at a stand off distance of 120-250 mm [3]. Though flame spraying is the oldest method it is still used today, mostly for wear protection coating production in a variety of industries such as steel, chemical, glass producing and mining.

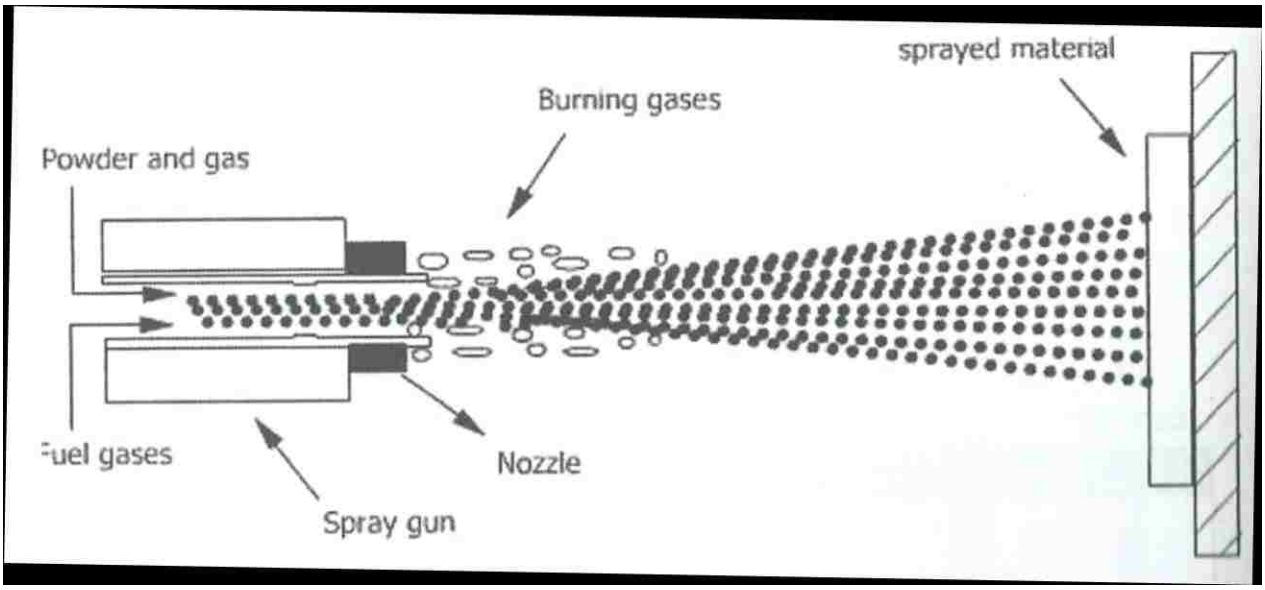

Figure 1 Schematic of the Flame Spray Process
Reproduced with Permission [4]

The detonation gun, or D-gun, spray process was developed more than 50 years after the flame spray process by Union Carbide Industrial Gases (now Praxair, Inc.) [2]. As one can deduce from the name, the detonation gun uses a combustion method to accelerate particles onto a substrate. As seen in Figure 2, the apparatus resembles an engine block with a combustion chamber, three valves, a spark plug and a powder inlet. The process begins with acetylene and oxygen being released through their respective valves while the spray powder is fed from the back of the gun. The chamber is ignited by the spark plug resulting in a detonation wave that travels down the barrel taking the powder particles with it. The particles use the kinetic and thermal energy from the explosion to obtain a speed upwards of 1000 m/s and a temperature of 4500 K with a typical stand off distance of 100 mm. Since the detonation gun is capable of operating at a repetition rate of anywhere between 1 to 15 Hz the chamber must be clear of all remnants of the previous cycle so after the gas is ignited the third valve opens to purge the chamber with an inert gas such as nitrogen. Referring back to the engine analogy, the chamber experiences high temperatures and must be cooled which is typically done with liquid water [2,5]. It is important to note that, unlike the flame spray technology, this is an interrupted flow process.

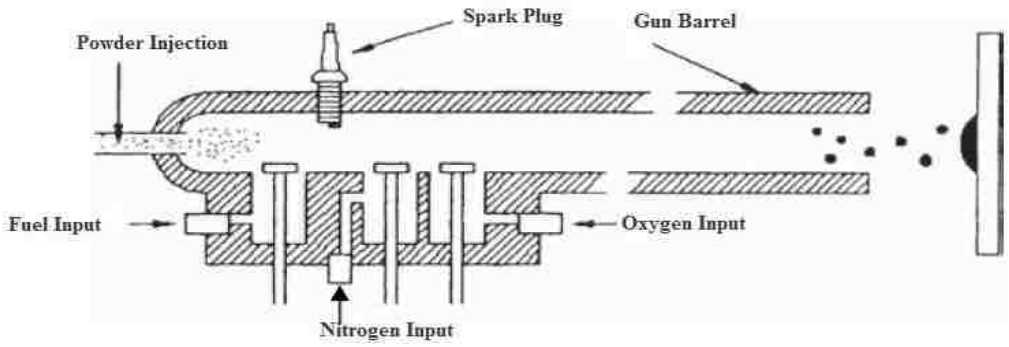

Figure 2 Schematic of a Detonation Gun Spray Process
Reproduced with Permission [4]

Similar to the detonation gun spray technology, High Velocity Oxy Fuel spraying also uses a combustion chamber within its gun. The main difference is that the burning is constant due to continually fed paths of the oxygen and fuel into the combustion chamber. This is similar to the flame spraying technique except that the gases are pressurized up to 1 MPa. The flame reaches a temperature of around 3000 K but the particles have a higher kinetic energy than thermal energy in this process with the flow reaching speeds up to 2000 m/s due to the use of a de Laval nozzle [6]. The result, due to the high velocity, is a coating of high density, bond strength and toughness [7]. The stand off distance is typically in the 150 mm to 300 mm range. There is also research being conducted on a method called suspension spraying that feeds the particles with a carrier liquid instead of gas. Although nano-structured coatings can be sprayed the method is not yet well developed [8].

One of the newest spray methods is the Cold Gas Spray coating process which was invented by accident [9]. In the 1980's a Russian research team was designing atmospheric re-entry vehicles and used a supersonic wind tunnel with metallic particles as a tracer for flow visualization. Beyond certain flow speeds, however, the particles

formed a coating similar to a thermal spray process. This technique was soon patented and is being investigated by researchers all over the world and some manufacturers now offer commercial cold spray systems. Figure 3 shows a diagram of the basic configuration of this process. The gas enters the apparatus under high pressure, up to 5 MPa, where some of the gas travels directly to the powder feeder and the rest runs through a heating coil that warms the gas up to 1100˚C. The two gases then meet within the barrel of the gun where they travel through a converging diverging de Laval nozzle that forms a supersonic jet. The particles enter this jet and are ejected from the barrel at a speed between 600 to 1000 m/s. As the name would suggest, the temperature of most of the impacting particles is only in the range of 400 K to 500 K, below the melting temperature of most sprayed metals and ceramics however, some particles experience a molten impact [9,10]. This is a steady flow process with a nozzle area that is 10 to 15 mm^2 and a stand off distance of 5 to 25 mm. The important advantage of this technique is that since the majority of particles are not molten during their flight they experience less oxidation than in other spray processes which creates a higher quality coating for technical applications [10].

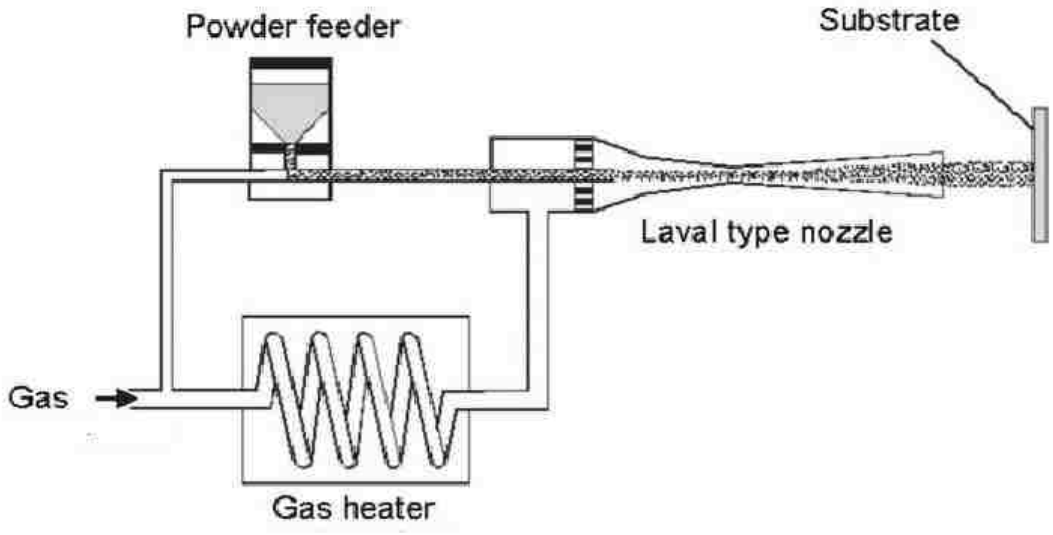

Figure 3 Schematic of a Cold Gas Dynamic Spray
Reproduced with Permission [5]

1.2 Shock Induced Spray Process

The Shock Induced Spray Process (SISP), Figure 4, was invented by Dr. Bertrand Jodoin from the University of Ottawa and co-advisor to this project. Similar to CGDS, the SISP propels particles well below their melting temperatures onto a substrate, however in a periodic rather than continuous manner. Unlike the CGDS case in which the particles experience a large cooling rate as they travel through the nozzle, they maintain most of their thermal energy as they leave the SISP nozzle. This is achieved through the use of compression waves, generated by the opening of a valve which coalesce to form a shockwave that travels down the barrel and out the exit of the nozzle. The strength of the shockwave depends on the pressure difference on the two sides of the valve; typically the barrel section will be at atmospheric conditions as it is open to atmosphere at the exit. The particles are dispensed into the barrel through a powder feeder but are first preheated to reduce the amount of heat transfer from the propellant

gas to the particles. Since the flow is pulsed, the gas volume is limited therefore the gas can potentially lose too much thermal energy to the particles which would decrease the effectiveness of the coating obtained with this technique. This implies there is a maximum number of particles that each flow can effectively spray. After the shockwave passes the powder in the barrel it creates a high speed intermediate temperature flow of gas that heats and accelerates the particles. Traveling within this zone the particles are heated thus lowering the required critical velocity, which is the required velocity that the particle must reach in order to adhere to the substrate. This is an advantage compared to the CGDS process in which passage through the diverging portion of the nozzle cools the particles [11,12].

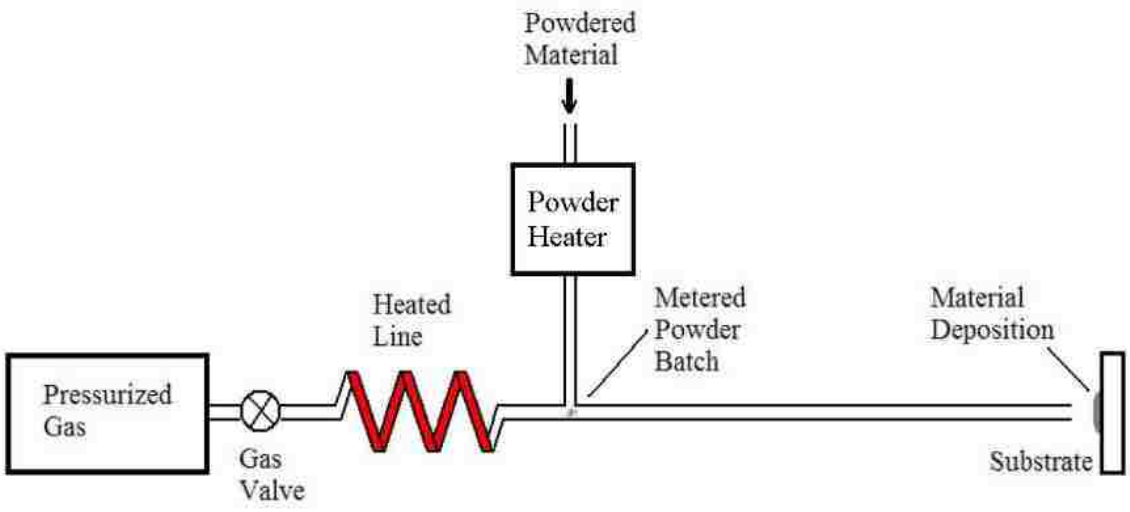

Figure 4 Schematic of a Shock Induced Spray Process
Reproduced with Permission [13]

Since the flow fluctuation occurs at a certain frequency controlled by the valve, it exits the nozzle as pulses that contain clusters or lumps of the feedstock material as shown in Figure 5. This has been shown to be capable of depositing very hard particle materials such as silicon carbide. In the CGDS process only 22% of these particles were

found on the substrate when injected in a 60% feedstock powder where the SISP saw a 42% deposition percentage [14]. It is thought that the cluster of particles do not bounce off the substrate as much as in the CGDS case due to the fact that the initial impact creates a softer area on which the rest of the cloud of particles can adhere [14].

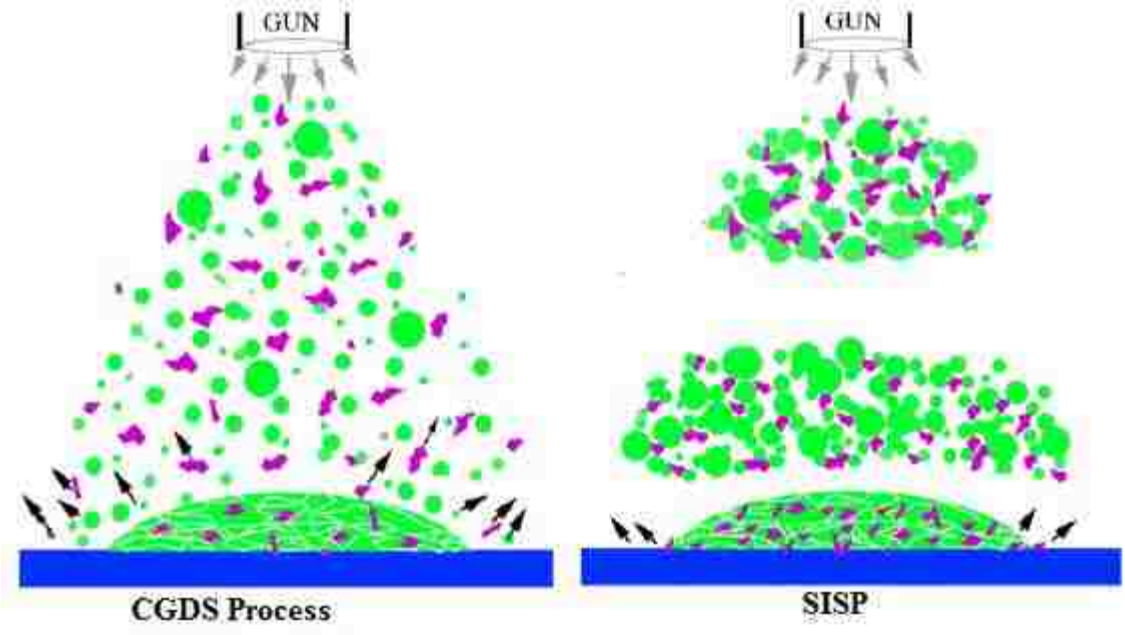

Figure 5 Comparison of Exit Flows from CGDS and SISP
Reproduced with Permission [14]

Chapter 2 Literature Review

This chapter will first take a look at the Schlieren technique and then the fundamentals behind normal shock waves and their formation in compressible flows. Next, the three conditions for supersonic flow exiting a nozzle are explained with a more detailed analysis on shock diamonds and their variation with exit Mach Number. This will lead to a discussion of the interaction of the flow and the substrate, more specifically the formation of the Bow shockwave and its influence on the flow. The shock tube and this experiment's SISP are then described with references to previous research conducted in this field. Finally, the objectives of this project are presented.

2.1 Schlieren Method

Schlieren photography has been in existence for over a century and is closely related to a simpler technique called the shadowgraph [15]. Whenever there is an in-homogeneity of density within the medium being observed, the density variations deflect the light in such a way that some regions become brighter and some darker (shadows) which can be captured on an image called a shadowgraph. The shadowgraph produces images in which darkness or greyscale level is proportional to the second spatial derivative of the density variation within the field of view [15]. To provide a higher quality image the Schlieren technique incorporates a series of lenses to capture even the slightest deflection of light through the variable density body. The result is the ability to capture very small changes in density due to pressure and temperature allowing the visual capture of interactions of gas and particles on a macroscopic level [16]. This can be seen in Figure 6 which is a typical lens based Schlieren system. Light originates from a source

(A) then is concentrated by a converging lens (B) onto a spatial filter (C) results in light beams of uniform intensity which travel through a collimating lens (D) through the area of interest then into a de-collimating lens (F) where they are directed onto a filter or in most cases a razor blade edge (G) and finally into a viewing plane or camera (H). If there is no density change present in the area of interest the light travels path 1 and displays a simple uniform light image in the viewing plane. When a different density field exists within the area of interest (D) then the light which travels path 2 when no density field exists will travel path 3. The light in path 3 is slightly deflected due to the different refractive index which can be due to a local change in temperature, pressure. Since it is deflected when it passes the second lens it is not focused onto the knife's edge as path 2 is but is blocked by the knife and therefore it appears as a dark section on the viewing plane. The knife edge is the key component of the Schlieren system and must be correctly adjusted in order to obtain an image with a greyscale level proportional to the first spatial derivative of the density variation in the area of interest [16]. The ideal position for the knife edge is on the optical axis at a location where the diameter of the beam leaving the de-collimating lens matches that of the spatial filter applied to the initial light source. This will create an equal distribution of light intensity on the viewing plane allowing for a crisp contrast to capture regions with low density gradients [15,17,18]. The result is an image far superior to the shadowgraph as shown in Figure 7 where the plumes of a candle can be clearly seen. Though visually appealing, the Schlieren photography method is only a qualitative tool and must be used in conjunction with other methods to obtain quantitative measurements.

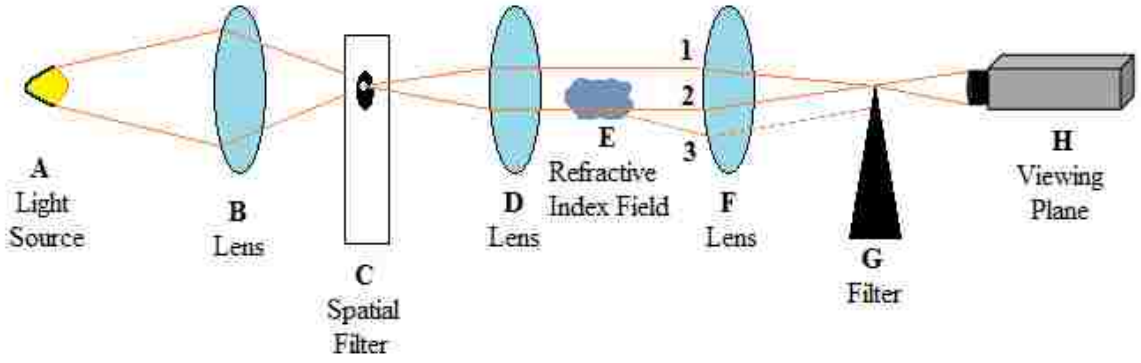

Figure 6 The Schlieren Method

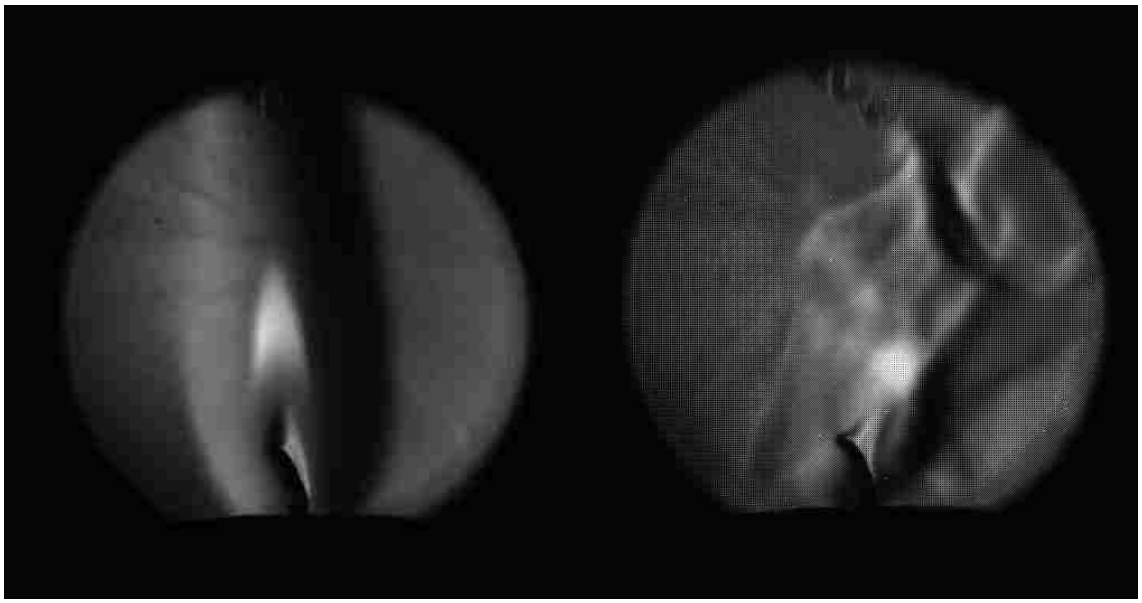

Figure 7 Schlieren Images of the Plume of a Candle

2.2 Fundamental Steady Compressible Flow Concepts

When a supersonic flow encounters a certain condition of high downstream pressure the pressure increase can occur through an abrupt change in the fluid properties such as static temperature, pressure, density and velocity [18]. This condition is referred

as a normal shock wave which is a wave form acting normal to the flow direction. Standing or stationary shocks usually occur in one plane and can be found in nozzles and ducts. These can be formed when a series of weak compression waves coalesce to form a finite compression shockwave [18]. In addition to stationary shockwaves, shockwaves can also be travelling or moving normal shocks, which can occur whenever there is a rapid change in pressure of a certain magnitude due to an explosion, when an object re-enters the Earth's atmosphere or downstream of a rapidly opened high pressure gas valve. A more detailed explanation of moving shocks is presented later in the shock tube section. When a shockwave is inclined to the flow at an angle it is called an oblique shockwave. A typical example is supersonic flow over a jet aircraft's airfoil.

2.2.1 Steady Supersonic Jets

In a typical cold spray process flow travels through a de Laval nozzle which accelerates the particles to high speeds. Before they impact the substrate, however, they lose a portion of their thermal and kinetic energy [12]. Under certain conditions a normal shock wave will occur in the diverging portion. The position of the standing shockwave is determined by the back pressure, which is the pressure downstream of the nozzle exit. As the back pressure is reduced below the upstream total pressure a point is reached where the nozzle throat becomes choked and the mass flow rate remains constant. Continuing to drop the back pressure leads to the flow becoming supersonic after the throat and decelerated through a normal shock wave to subsonic. If the back pressure is further reduced, this shockwave will be at a position further downstream of the nozzle where it will eventually be positioned just upstream of the exit plane. If the back pressure

is low enough the shock wave will actually bend out of the exit nozzle causing supersonic flow to leave the nozzle. Supersonic flow exiting a nozzle can either be underexpanded, overexpanded or perfectly expanded depending on the relationship between exit pressure and the outside back pressure [19].

When the back pressure is less than the exit pressure then an underexpanded jet forms as shown in Figure 8. First the flow leaves the nozzle in Section 1 at a higher pressure than the back pressure, resulting in the need for an expansion process to occur with the flow directed away from the jet axis in Section 2 and the expansion fan extending towards the centerline. Since the flow must be parallel to the jet axis at the centerline a second, reflected, expansion process must occur to turn the flow back inward so that it is parallel to the axis in Section 3. However the second expansion results in a pressure in this section which is below the back pressure and therefore, the flow must be compressed again to get back to the back pressure. These compression waves combine at the jet axis to form oblique shocks just before Section 4 in which the flow is inward toward the centerline. The oblique shock wave reflects from the jet axis and redirects the flow along the jet centerline in Section 5. The flow in Section 5 is at a higher pressure than the back pressure as was the case in Section 1 so the process restarts itself. This process would continue to repeat forever if not for viscous and turbulent mixing loses which eventually decay the flow [19]. Steady flow in a converging nozzle will result in a decrease of pressure but if the back pressure is low enough the exit flow will be choked and the back pressure could be less than the nozzle exit pressure thus requiring an expansion process. Therefore it is only possible to produce an underexpanded jet with a converging nozzle.

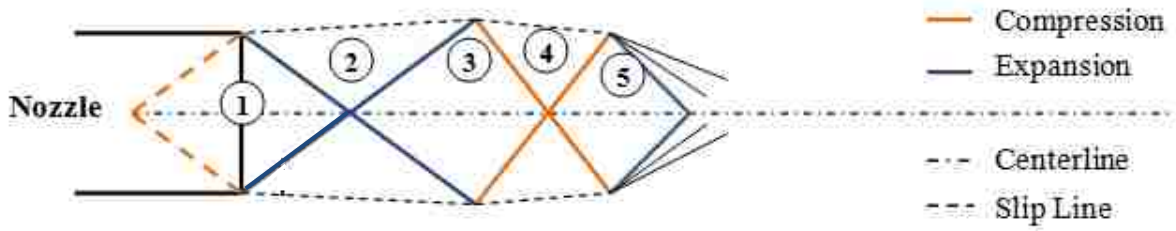

Figure 8 Underexpanded Supersonic Flow Exiting a Nozzle

A perfectly expanded jet can occur when the exit pressure actually matches the outside back pressure which is why it is also called a matched jet flow. In this case no compression or expansion processes occur as shown in Figure 9.

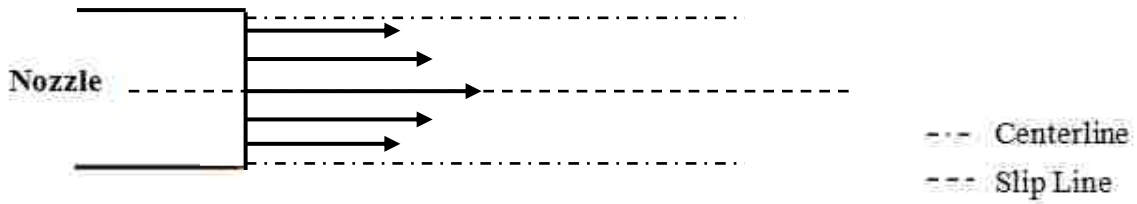

Figure 9 Perfectly Expanded Jet Exiting a Nozzle

For an overexpanded jet to form the back pressure must be greater than the exit pressure of the nozzle. As one would expect the overexpanded process acts as the reverse of the underexpanded process. In Figure 10 the flow leaves the nozzle in Section 1 at a lower pressure than the outside pressure, therefore compression must take place to raise the exiting pressure to the back pressure in Section 2 through the formation of oblique shock waves which direct the flow towards the jet axis. Flow cannot cross the jet axis and

hence a reflected oblique shock wave redirects the flow so that it is parallel to the jet axis in Section 3. The pressure in this section is larger than the back pressure and must expand to drop the pressure back down to the back pressure in Section 4. The reflection of the expansion wave from the jet centerline causes the flow to again be lower than the back pressure in Section 5 and the process repeats once again [19].

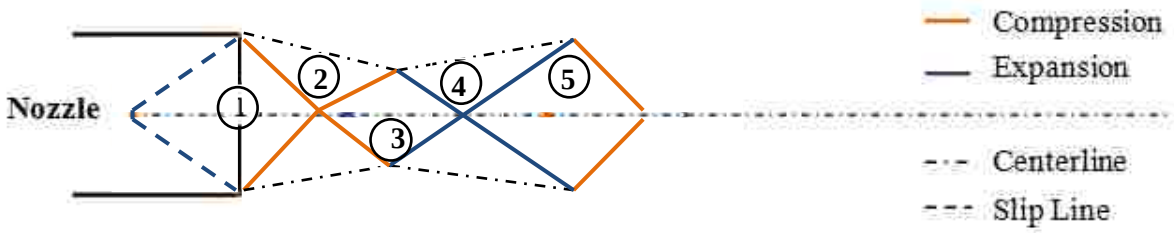

Figure 10 Overexpanded Supersonic Flow Exiting a Nozzle

Shock diamonds are a result of a series of compression waves that create regions of high density and pressure [19]. They are seen in both underexpanded and overexpanded supersonic flows and are evident in the flow exiting a rocket engine. A Schlieren image of the shock diamonds can also be seen in more basic flows, such as high pressure air leaving a straight nozzle shown in Figure 11.

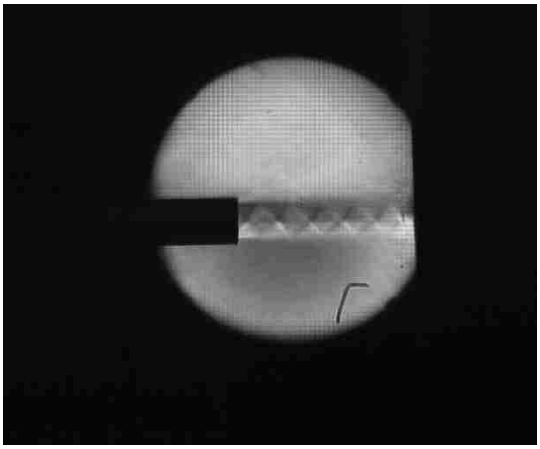

Figure 11 Shock Diamonds in Supersonic Flow Exiting a Straight Nozzle

The easily discernible diamonds also have a unique pressure characteristic. At the midpoint of a diamond where there is a top and bottom vertex, the pressure along the centerline is lower than at the end of a diamond where those vertices come together into one. Figures 12 and 13 show a shock diamond structure`s wavelength along its centerline and the axial pressure ratio for a Mach Number of 1.166 and 2.24 respectively [20]. Clearly a higher Mach Number leads to a longer structure wavelength but also a greater static pressure amplitude along the centerline. Therefore if the jet structure is continually shifting Mach numbers as in an unsteady jet process, a point located on the jet centerline would experience a high pressure region at one time but then a low pressure at another time.

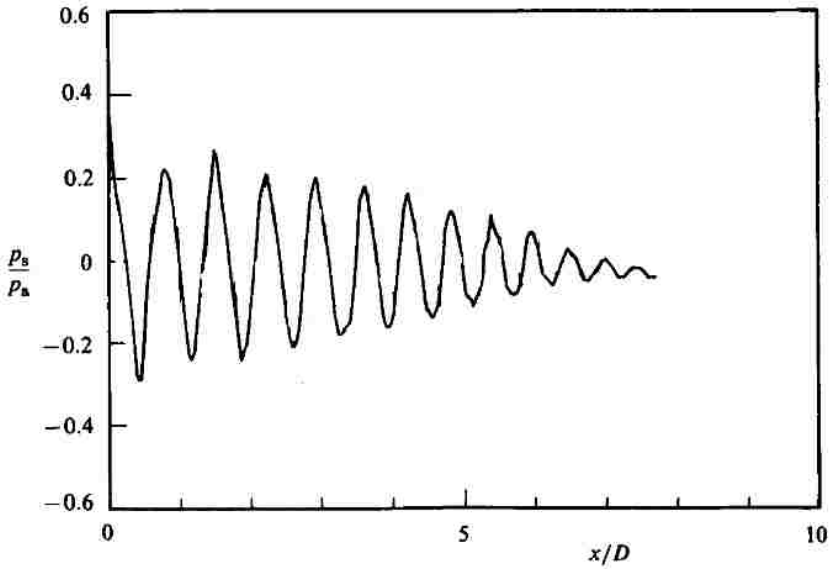

Figure 12 Shock Diamond Structure`s Wavelength at M=1.166 Reproduced with Permission [20]

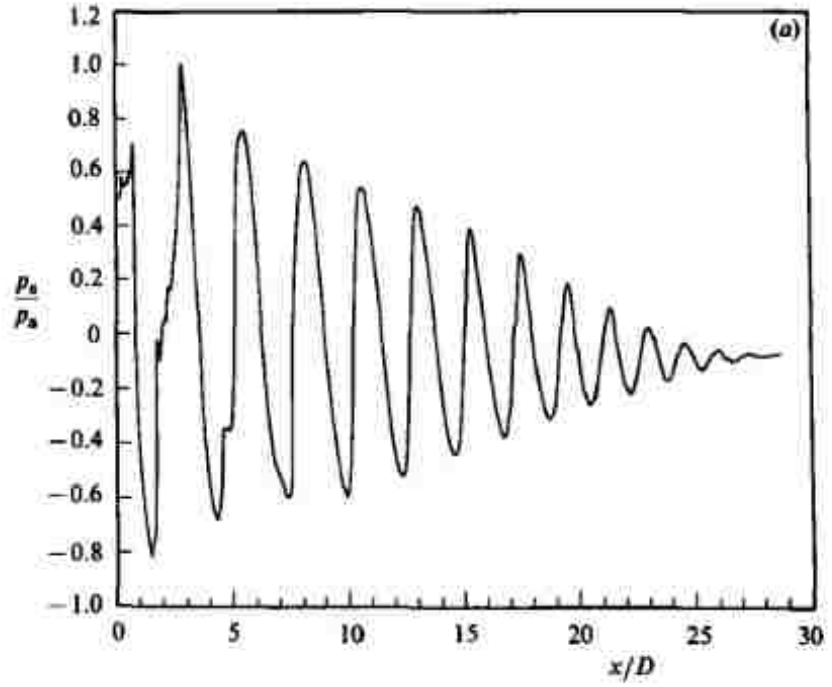

Figure 13 Shock Diamond Structure`s Wavelength at M=2.24 Reproduced with Permission [20]

2.2.2 Steady Supersonic Jet Impacting Substrate (The Bow Shock Wave)

When a supersonic flow in a process such as the CGDS exits a nozzle and impacts the substrate a stagnation zone or bubble forms. This is responsible for the formation of a bow shock as seen in Figure 14. A bow shock forms when the gas particles impact the surface of the substrate which creates a change in both momentum and energy. Newton theorized that when a particle hits a surface it will lose all its momentum normal to the surface but maintain its momentum parallel to the surface [5]. This rapid shift in energy creates microscopic pressure waves which coalesce to form a normal shock near the surface. The oncoming flow intercepts this shock and a radial deflection occurs. If the substrate is positioned normal to the exit nozzle the deflection that occurs is above the maximum deflection angle allowed by oblique shock waves. This creates a curved and detached shockwave also known as a bow shock. This shock has a significant impact on the oncoming flow as it is an unwanted barrier to the substrate that both slows and deflects the particles creating lower deposition efficiency. In one experiment some particle streams with lower velocity could not even penetrate the shock zone and were deflected enough to not impact the surface. The main factor that determines the creation of this type of shockwave is the stand off distance of a thermal spray process [18,21,22].

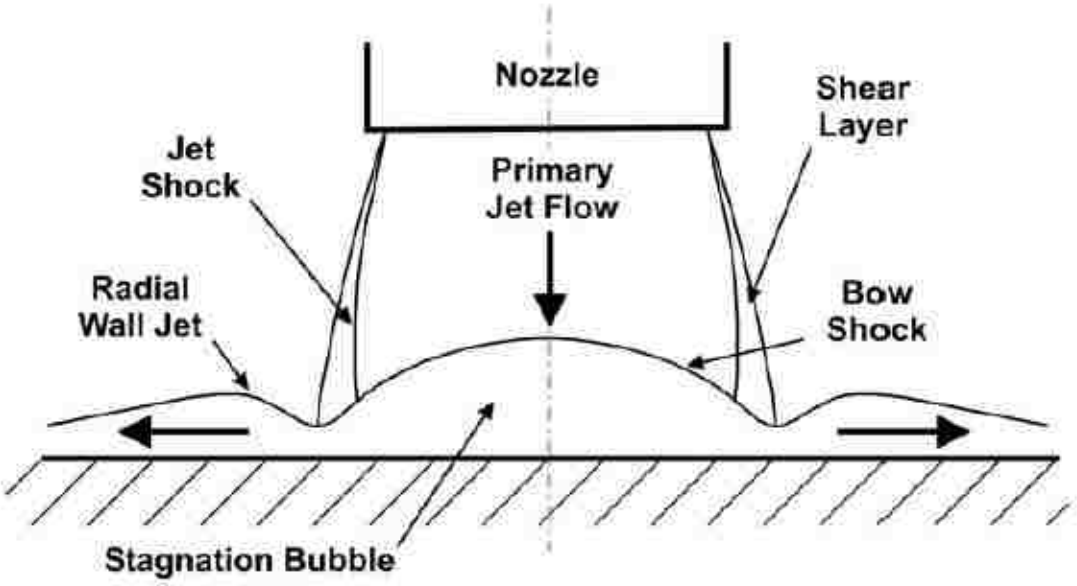

Figure 14 Schematic of a Bow Shock Created by a Supersonic Flow Reproduced with Permission [21]

It is a fact that the bow shock is detrimental to the thermal spray process and specifically the cold spray process where there is constant flow and particle injection [23,24]. Researchers from the University of Cambridge experimented with Helium at 2 MPa and Nitrogen at 3 MPa to investigate the effects of stand off distance on particle velocity, the formation of a bow shock and deposition efficiency [21]. They mapped out three distinct regions and described their effects. First, at a small stand off distance the impact velocity of the particles was decreased by the presence of a bow shock which in turn decreased the deposition rate. The second region at around 60 mm was found to be optimal due to the fact that no discernible bow shock formed and also that the distance to the substrate allowed the particles to stay above the critical velocity threshold. Finally, in region three, the stand off distance is very large resulting in drag forces to develop on the

particles decreasing their velocities before reaching the substrate. They concluded that staying in region two increased deposition efficiency by up to 40 percent for that particular nozzle regardless of what type of gas was used [21].

2.3 Traveling Shock Waves and the SISP

This section deals with the concept of the shock tube and how this relates to the physics behind the SISP. It also includes a review of experimental studies of shock induced flows.

2.3.1 The Shock Tube and Physics Behind the SISP

A shock tube, Figure 15, is a device that contains a high pressure gas at one end called the driver section and a low pressure gas at the other end called the driven, section which are separated by a diaphragm. When the diaphragm bursts this instantaneous change in pressure creates a shockwave that travels downstream and coinciding expansion fan that flows upstream. A contact surface can also be defined which is the physical location or delimitation of the fluid that was on the high side and the fluid that was in the low pressure side prior to diaphragm being burst.

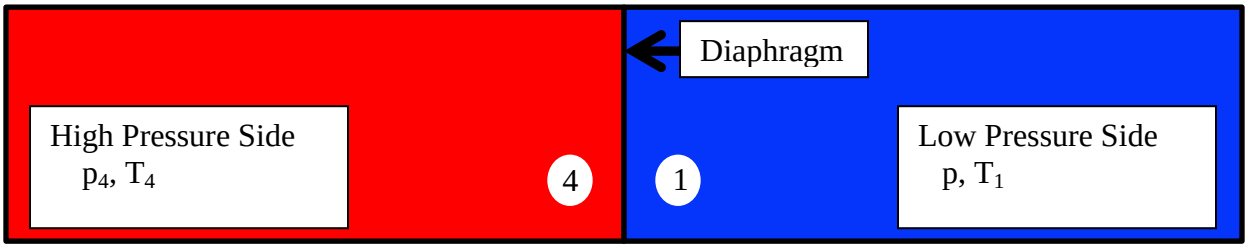

Figure 15 A Diagram of a Shock Tube

The SISP begins much like the shock tube in Figure 15 with Zone 4 being the driver region and Zone 1 the driven region which is being separated by a valve which acts like the diaphragm discussed above, Figure 16a [11]. Once the valve is opened, a series of compression waves is generated, with subsequent waves having a higher pressure, temperature and velocity than the previous, coalescing together as they propagate down the barrel to form a shock wave, Figure 16b. At the same time, a series of expansion or rarefaction waves move backwards into Zone 4 reducing the driver section's pressure until it would reach equilibrium with Zone 1 if the valve is not closed [25]. In Figure 16b, the incident front of the shock wave passes the particles and creates an increase in the pressure and temperature in its wake, Zone 2, which propels the particles toward the exit of the gun exit. [11]. A contact surface, Zone 3, would also exist when Zone 1 and 2 meet, and follow the higher pressure region created by the shockwave but at a slower velocity [25]. This zone is what separated the accelerated gas from the now expanding gas in the driver section. If this was a shock tube the shock wave would reflect off the end boundary and intercept first the contact surface and then the reflected expansion fan from the other boundary end.

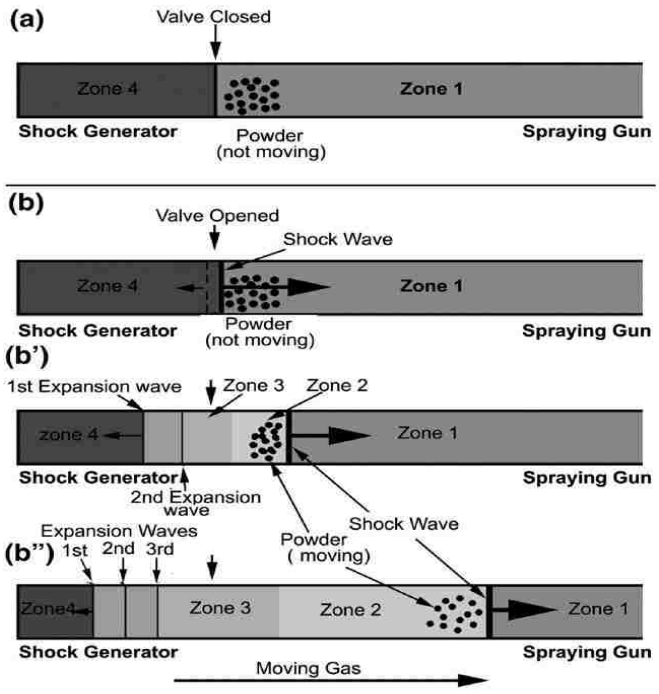

Figure 16 Diagram of the Physics of the SISP
Reproduced with Permission [11]

A one-dimensional model of the process, based on shock wave analysis is presented by Jodoin et al [11]. Given the initial pressures and temperatures before and after the closed valve, the pressure in Zone 2 can be found by solving Equation 1 iteratively. The mass density ratio can then be found from Equation 2; the temperature ratio from Equation 3 and the speed of the shock wave from Equation 4. This shows that the temperature in Zone 2 will have a higher value as seen in Figure 17 [11]. This is the region that propels the particles. The theory assumes that there will be little to no loss of thermal or kinetic energy as in an expanding portion of a typical cold spray gun [26].

$$\frac{p_4}{p_1} = \frac{p_2}{p_1}\left[1 - \frac{(\gamma_4 - 1)\left(\frac{a_1}{a_4}\right)\left(\frac{p_2}{p_1} - 1\right)}{\sqrt{(2\gamma_1)\sqrt{\left(2\gamma_1 + (\gamma_1 + 1)\left(\frac{p_2}{p_1} - 1\right)\right)}}}\right]^{-\left[\frac{2\gamma_4}{(\gamma_4 - 1)}\right]} \quad (1)$$

$$\frac{\rho_2}{\rho_1} = \frac{1 + \frac{\gamma + 1}{\gamma - 1}\left(\frac{p_2}{p_1}\right)}{\frac{\gamma + 1}{\gamma - 1} + \frac{p_2}{p_1}} \quad (2)$$

$$\frac{T_2}{T_1} = \frac{p_2}{p_1}\left(\frac{\frac{\gamma + 1}{\gamma - 1} + \frac{p_2}{p_1}}{1 + \frac{\gamma + 1}{\gamma - 1}\left(\frac{p_2}{p_1}\right)}\right) \quad (3)$$

$$V_s = c_1\sqrt{\frac{\gamma + 1}{2\gamma}\left(\frac{p_2}{p_1} - 1\right) + 1} \quad (4)$$

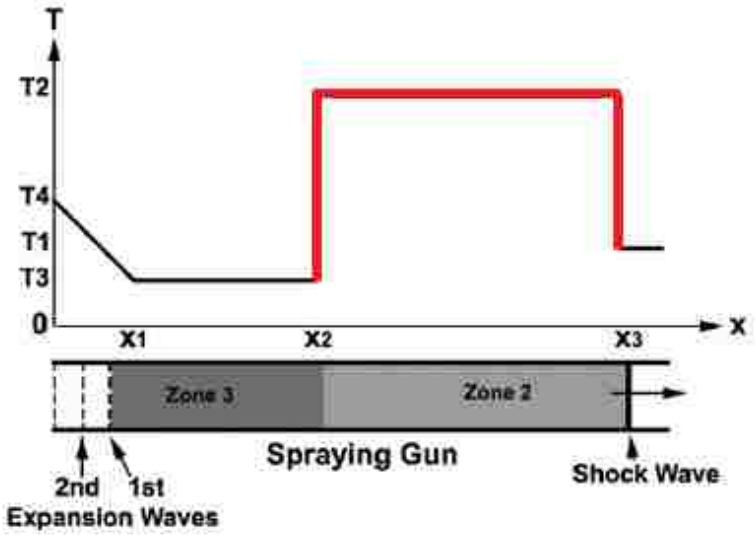

Figure 17 Temperature Graph of SISP Zones
Reproduced with permission [11]

An initial numerical study of the SISP was completed by Karimi et al., [28], using the two dimensional computational fluid dynamic model of an actual geometrical representation of the Waverider thermal spray gun. The results showed that an increase in supply pressure and thus the pressure ratio across the diaphragm, would increase the shock speed as well as the duration of the supersonic flow. Another important element of information discovered was that varying the time in the cycle when particles are injected into the flow has a significant impact on the overall deposition rate onto the substrate based on the particle critical velocity ratio. Other factors that affected the deposition rate are the firing frequency of the valve and the formation of a bow shock. Little information regarding the formation of a bow shock wave in a periodic flow field led to the present experimental study [28].

2.3.2 Experimental Research Involving Shock Induced Flow

There has been minimal research done in the area of pulsating supersonic flow visualization however there is significant research available regarding shock tubes. It is therefore, instructive to make a comparison between one cycle of the pulsating flow with the characteristics seen in a shock tube. Usually these studies are conducted in a circular tube but the flow in this experiment's rectangular cross section is expected to demonstrate many of the same features.

In 1952 Elder and Hass [29] used a Schlieren technique to investigate supersonic flow exiting a nozzle in order to capture the vortex rings created at the shock tube exit as seen in Figure 18. A vortex ring is a direct result of the flow interacting with the wall

boundary layer in the tube which decreases the velocity of the flow [30]. This interaction causes eddies that separate at the nozzle edge to create the vortex rings [31]. Elder and Hass used an electronic delay circuit synchronized with a camera and spark source and were able to capture the initial shock wave leaving the tube as well as the vortex ring that followed but only through repeating the experiment at different time delays to compile a sequence of images.

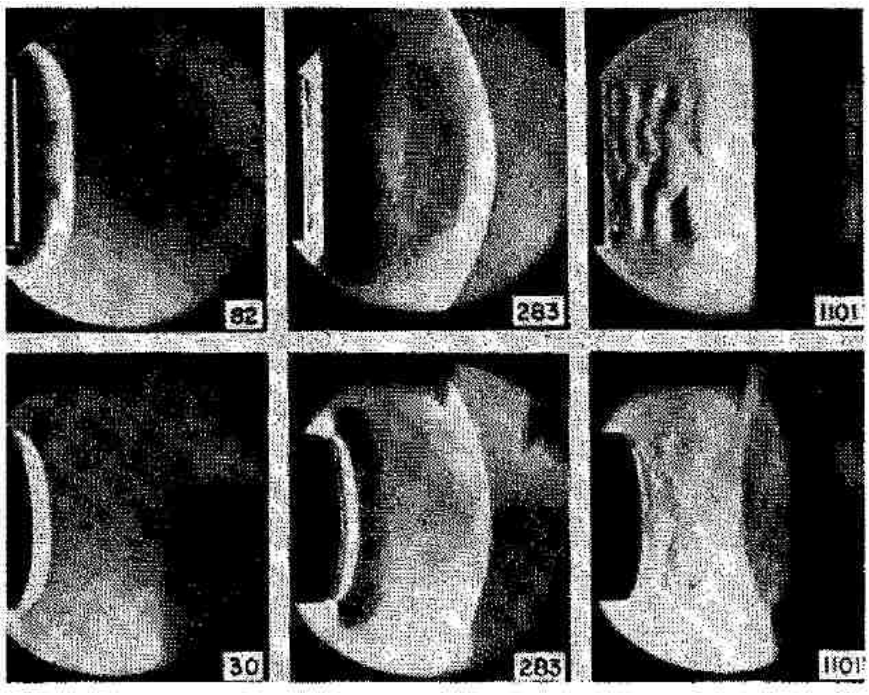

Figure 18 Elder and Hass' Shockwave and Vortex Rings
Reproduced with Permission [29]

As imaging technology has progressed, the ability to capture at extremely high frame rates has enabled us to view and analyze super high speed objects and their interactions with the environment such as a bullet leaving the muzzle of a gun [32]. Similar experimental techniques using a shock tube were conducted by Ishii to explain

the different aspects of a shock wave leaving a nozzle. Ishii described the initial shock wave as the first shock, and then observed a secondary shock and Mach disk that developed into vortices, Figure 19 [33]. This secondary shock was the leading front of the supersonic flow noted by the shock diamonds described earlier. Other researchers also found the flow exiting a nozzle in three distinct stages; initial shock, vortex rings and supersonic flow [34,35,36,37].

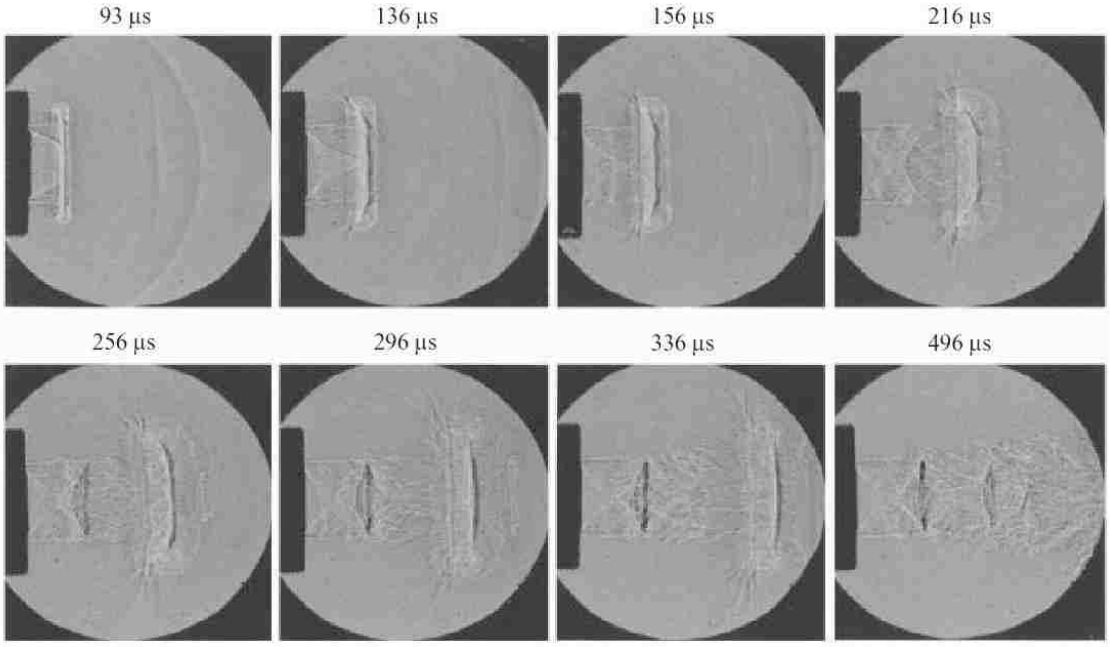

Figure 19 Ishii's Initial Shock, Secondary Shock and Mach Disk Reproduced with Permission [33]

A pulsating flow can also be found in the exhaust pipe of any type of reciprocating engine. As the exhaust valve of the engine opens and closes it acts much like a shock tube diaphragm with the high pressure gases in the cylinder being released into the exhaust pipe. Both Endo [38] and Kimura [39] investigated the flow generated by a pulsating high speed jet exiting a long tube. Though their main goal was to investigate

the noise generated by the shock waves, their experimental set up was similar to the one used in this study. They also found the three main stages of high pressure discharge from a nozzle and noted a shock wave forming in front of the vortex ring much like Ishii's secondary shock, Figure 20. Endo observed that their rotary valve must run around 2000 rpm or 33 Hertz to produce a shock wave.

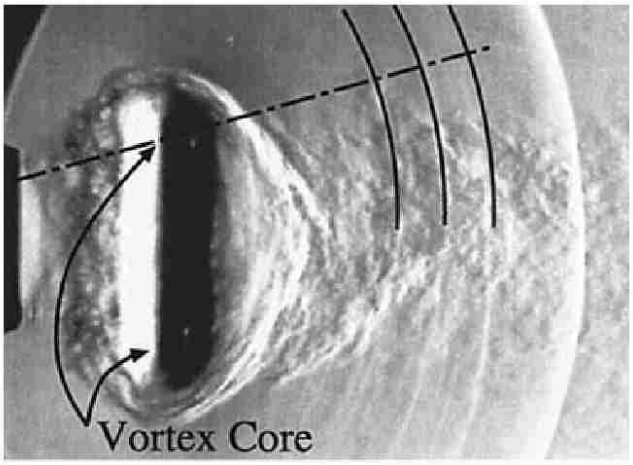

Figure 20 Endo's Schlieren with Initial Shockwave and Vortices Reproduced with Permission [38]

2.4 Objectives

The main objective of this thesis is to experimentally investigate the fluid mechanic flow field at the exit of the nozzle associated with the new Shock Induced Spray Process. The information will be an aid in future designs of Centerline's Waverider SISP Thermal Spray Gun. The work is conducted experimentally within the Jet/Vortex Lab at the University of Windsor's Centre for Engineering Innovation. The specific objectives are listed below:

1. Construct an experimental Waverider apparatus with dimensions similar to those of the actual Waverider manufactured by Centerline Ltd.
2. Construct a working Schlieren apparatus suitable for use with the Waverider facility.
3. Use high-speed photography to capture Schlieren images of the transient compressible flow features produced by this device between the nozzle exit and the substrate and simultaneously collect quantitative data through the use of pressure transducers mounted at strategic locations.
4. Analyze the Schlieren images to draw conclusions regarding the flow as well as map all characteristics for one complete Waverider cycle.
5. Correlate qualitative and quantitative data to discover the effects of initial supply pressure, rotary valve frequency and substrate stand off distance on the substrate central pressure and the flow field in the region between the nozzle exit and the substrate.

Chapter 3 Experimental Facility and Procedure

This chapter begins with an overall description of the experimental flow facility then separately considers the details of each component. The experimental procedure that was followed and the values of the variables considered are then given.

3.1 Experimental Flow Facility

A schematic diagram of the entire experiment facility is presented in Figure 21. Flow initiates from the high pressure (31 MPa), nitrogen tank and passes through a regulator (A) lowering the pressure to the required value. The gas then travels through a hydraulic hose into the Centerline Custom Rotary Motor/Valve assembly (B), the frequency of which is controlled by a proprietary controller box. A PCB Piezotronic 113b24 pressure transducer is located at the exit of the rotary valve to provide a pressure trace from which the frequency can be determined. The gas is then released in pulses creating shock waves that travel into the heater coil which is replaced, in this experiment, by a tube of equal dimensions. After exiting the heater coil, the flow enters the SISP thermal spray apparatus through an inlet section (C) which provides a transition from a circular cross-section which expands into the nozzle. At this point powder would be introduced into the flow however in this experiment it will not be included. The flow then exits the diverging nozzle, (D), passing into the atmosphere, crossing the gap and impacting onto the substrate. The Schileren Apparatus is adjustable to view along the entire SISP Apparatus from inlet to exit. The SISP Apparatus is also able to be positioned at different distances from the substrate to evaluate the affect of the Stand off Distance on the flow.

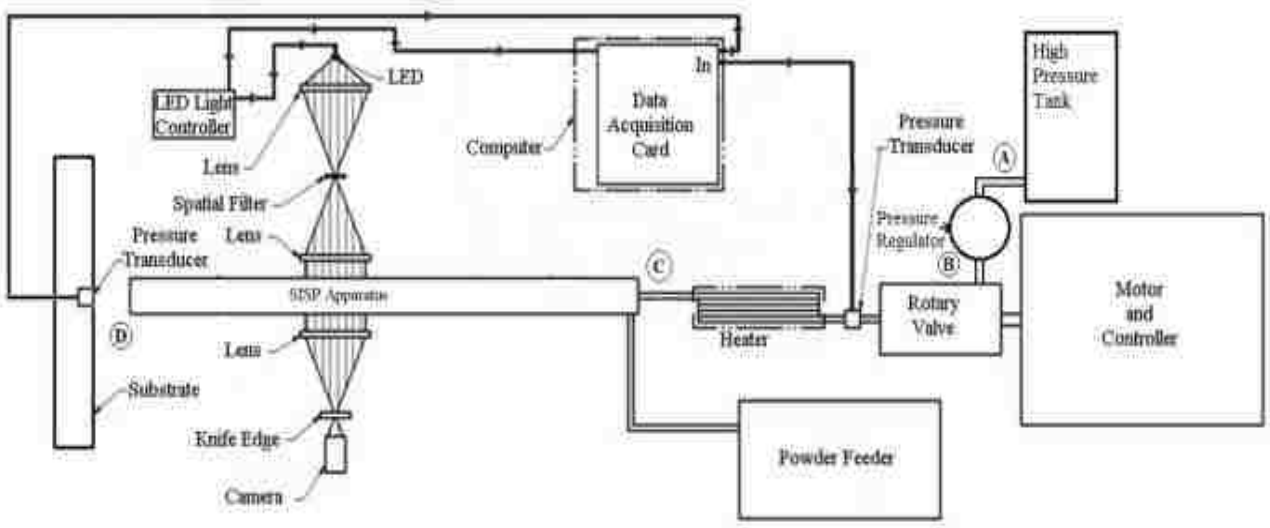

Figure 21 Experimental Set Up

3.2 Centerline Custom Rotary Motor/Valve Assembly

The most important component in the experimental equipment is the custom designed and built rotary valve from Windsor Centerline shown in Figure 22. The three slotted disc as seen in Figure 22b allows the incoming high pressure gas to be systematically blocked and released to the atmospheric pressure within the exit tube which is connected to the thermal spray apparatus. The rotation of the slot disk depends on the frequency dictated by the electric motor controller thus controlling the effective 'pulse firing' of the thermal spray gas.

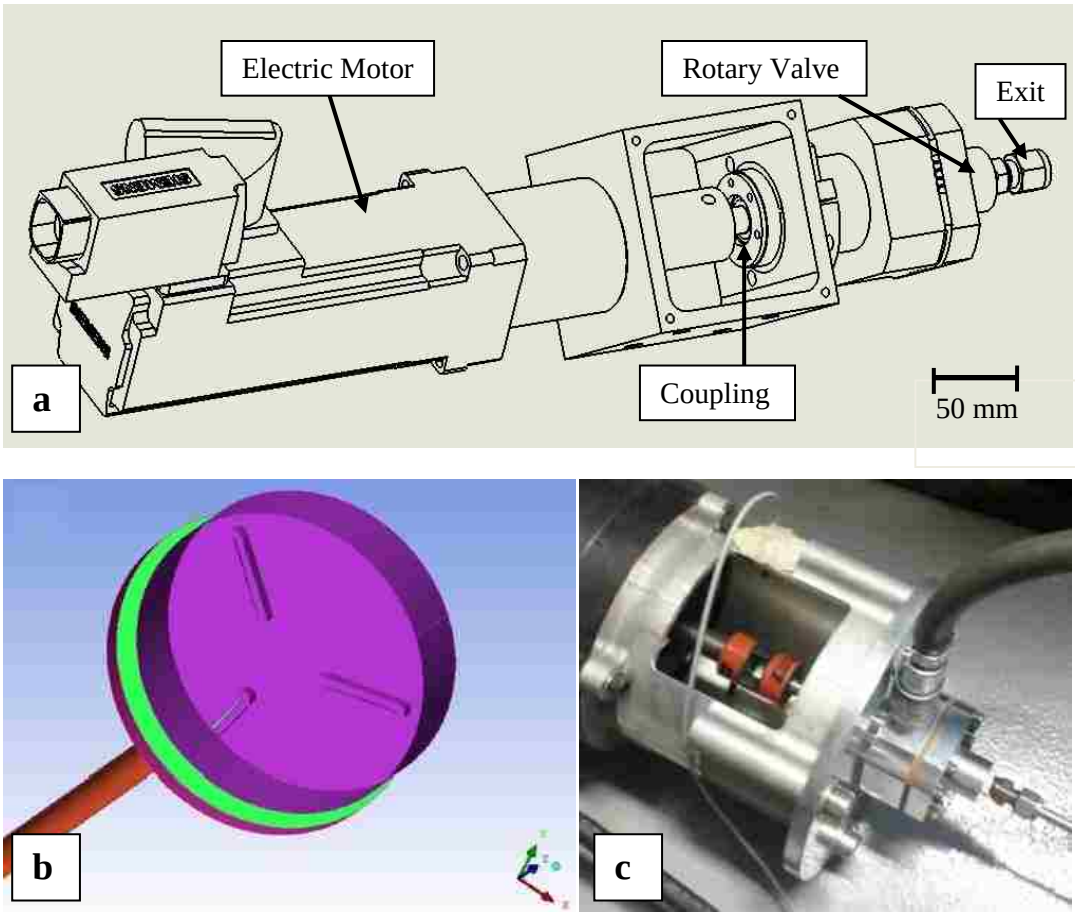

Figure 22 Rotary Motor/Valve Assembly
a) Schematic Drawing
b) Internal Schematic of Rotary Valve Design
c) Photograph of Assembly

3.3 SISP Thermal Spray Apparatus

Once the gas exits the valve apparatus it enters a tube with a length of 1.8 m and internal diameter 4.6 mm which is a dimensionally accurate representation of the heater coil used in the real Waverider device. This lack of heat is acknowledged to alter the density within the flow however it is expected that the main flow characteristic trends will be similar to those at a lower temperature. After exiting the 'heater tube', the flow enters the SISP thermal spray apparatus through an inlet section which provides a

transition from a circular cross-section with a diameter of 3.97 mm to a rectangular area of 6.35 by 4.76 mm as seen in Figure 23 at Point A. This then diverges into a 12.7 x 4.76 mm section within the last 12 cm of the nozzle exit (Point B in Figure 25). To view the flow within the apparatus, a 7 mm glass viewing section was inserted on both sides of the apparatus which expands with the internal divergence into a 14 mm section. In order for the Schlieren to be able to capture images the glass portion was required to be rectangular since a circular glass would deflect the light distorting the Schlieren images. This change should not have a large effect on the flow as the area of the cross section from the Waverider gun is maintained. The glass is also 12.7 mm thick in order to sustain the high pressures used in the experiment. The total length of the apparatus is 0.813 m and also includes a powder feeder inlet for future work involving particle injection. The actual SISP apparatus is shown in Figure 24.

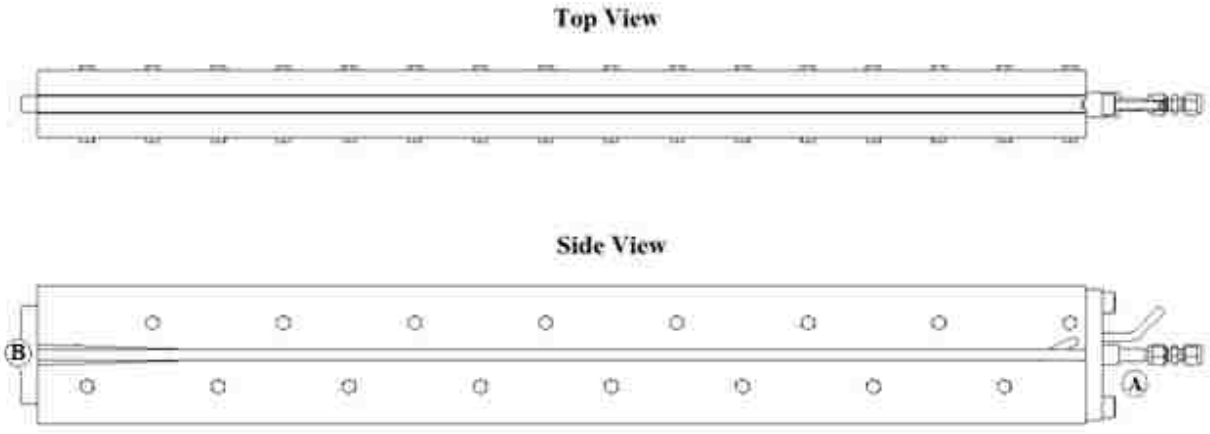

Figure 23 SISP Thermal Spray Apparatus Design

Figure 24 Actual SISP Thermal Spray Apparatus

3.4 Schlieren Apparatus

A schematic diagram of the Schlieren apparatus can be seen in Figure 25 and a photograph of the arrangement is provided in Figure 26. The set-up was built in-house using purchased components. The apparatus includes a Cree Xlamp XM-L LED light source controlled by a Gardasoft RT820F-20 electronic light controller connected to a National Instruments (NI) SCB-68A data acquisition and control card. The light passes through a converging lens with a 460 mm focal length to a spatial filter located at the focal point. The light from the spatial filter falls onto a 175 mm collimating lens which collimates the beam which then passes through the test section (viewing area) of the experiment. Next, the light beam passes through a 200 mm de-collimating lens which focuses it onto a knife edge; the key component of the Schlieren which partially blocks some of the refracted light. Finally, the beam enters the Photron FASTCAM-APX RS

model 250K camera, capable of capturing up to 250,000 frames per second (fps) using a C-mounted Computar M1620-MPV Ultra Low Distortion lens. Adjusting the knife edge of the Schlieren for optimal viewing was a trial and error method however once adjusted it did not need to be changed as the thermal spray apparatus moved perpendicular to the Schlieren rail within the viewing area.

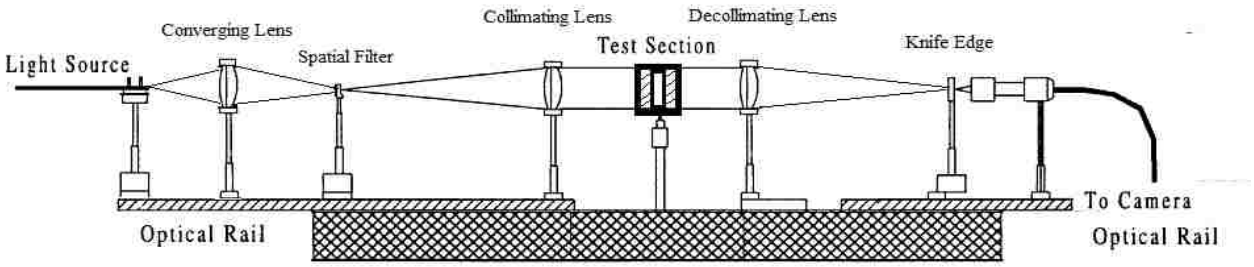

Figure 25 Diagram of Schlieren Apparatus

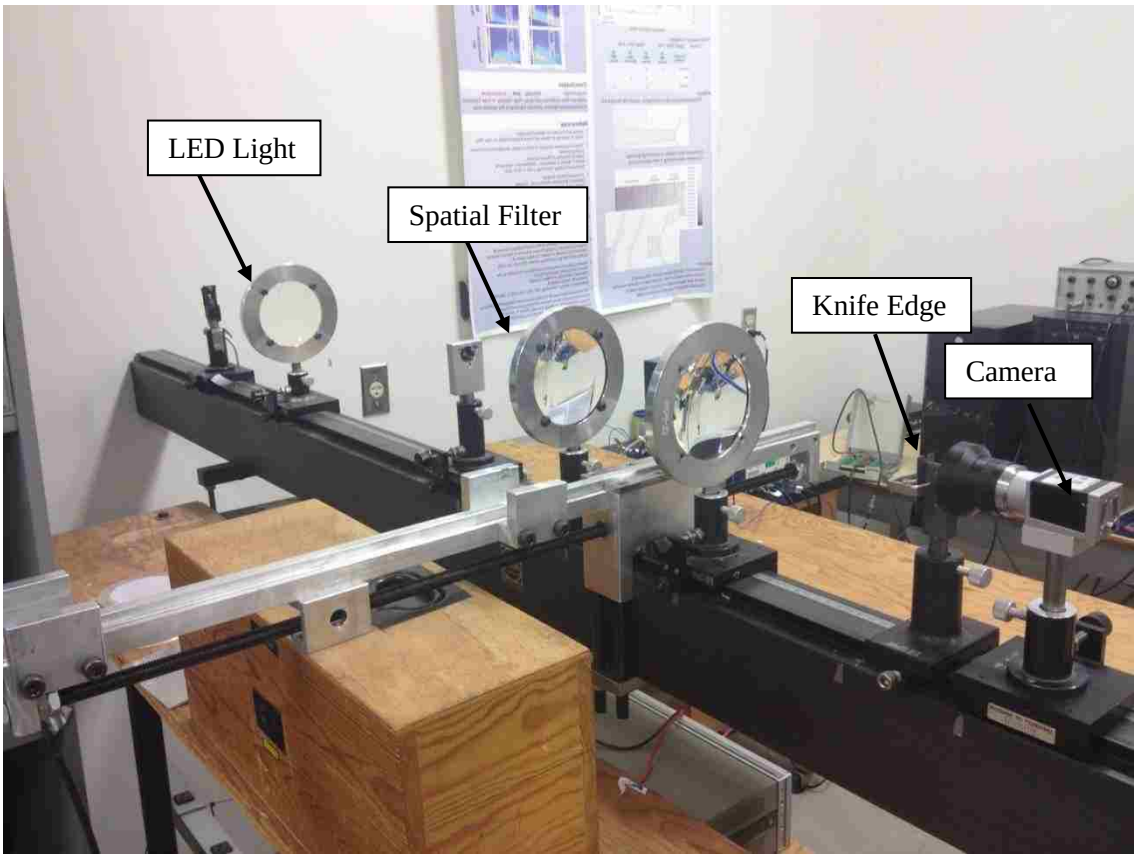

Figure 26 Photo of Actual Schlieren Apparatus

3.5 Substrate, Viewing Area and Camera

A PCB Peizotronics 113B28 pressure transducer mounted flush to the substrate surface is used to measure the substrate impact pressure. The exit portion of the apparatus and substrate are placed in the Schlieren's viewing area, shown in Figure 27, with the substrate at a premeasured stand off distance.

The camera and substrate pressure measurement are triggered using a custom LabVIEW program which is provided in Appendix A. The camera is controlled by the commercially available Photron Viewer software. The frame rate is set at 52500 fps with a shutter speed of 1/246000 seconds. Through preliminary testing this was found to be the optimal frame rate for the required speed while still maintaining a high pixel resolution. The LabVIEW program was also used to capture pressure transducer data at a rate of 52500 samples per second when initiated. Therefore each pressure point coincides with one frame captured by the camera for efficient data analysis.

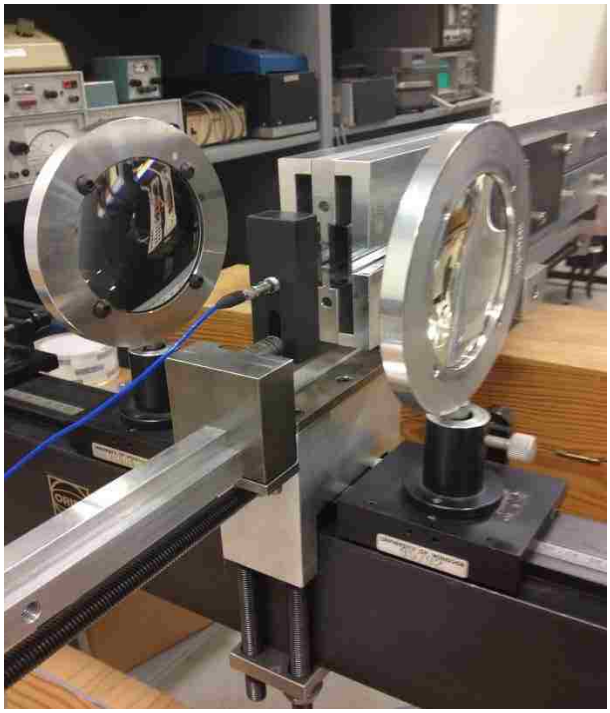

Figure 27 Viewing Area

3.6 Experimental Procedure

Trials were conducted in systematic order starting with the lowest initial pressure, lowest firing frequency and lowest stand off distance. Therefore Trail 1 was a supply pressure of 2 MPa, a valve firing frequency of 5 Hz and a stand off distance of 10 mm.

The first step in the procedure is to position the exit nozzle at the appropriate stand off distance from the fixed substrate for the trial being run, using vernier calipers. The light on the Schlieren apparatus is then initiated and the camera is set in continuous run mode. The position of the nozzle and substrate are verified to be within the viewing area and the exit plane of the nozzle is aligned vertically in the image.

Next the operating supply pressure is set by running the rotary valve at a low angular velocity, releasing the valve on the nitrogen tank and then using the regulator to select the desired supply pressure. Once this is done the rotary valve is set to the desired frequency as measured by the oscilloscope connected to the pressure transducer attached to the rotary valve. A final check of the supply pressure is then made as adjusting the firing frequency could have an effect on the pressure within the line. The nitrogen valve is then turned back off.

The data capture process begins by setting the camera trigger to "standby" mode, initiating the LabVIEW Program and turning on the LED light of the Schlieren Apparatus. The system is now ready to capture pressure data and images once the camera trigger occurs with the opening of the nitrogen valve allowing the gas to be pulsed through the system. The system will now capture each image in accordance to each pressure point captured by the substrate pressure transducer. The resulting data is stored in computer memory using a file naming convention which identifies the supply pressure, pulsation frequency and stand off distance as follows: 2mpa_5hz_10mm_EP1, where EP1 stands for Experiment 1 for Trial 1.

The three independent variables considered in these experiments are; the initial supply pressure, the stand off distance and the rotary valve firing frequency. Table 1 contains all trials that were undertaken in this experiment.

Table 1 Experimental Variables

Initial Pressure (MPa)	2	2	2	2	2	2	2	2	2	2	2	2
Frequency (Hz)	5	5	5	10	10	10	20	20	20	30	30	30
Stand off Distance (mm)	10	20	30	10	20	30	10	20	30	10	20	30

Initial Pressure (MPa)	3.45	3.45	3.45	3.45	3.45	3.45	3.45	3.45	3.45	3.45	3.45	3.45
Frequency (Hz)	5	5	5	10	10	10	20	20	20	30	30	30
Stand off Distance (mm)	10	20	30	10	20	30	10	20	30	10	20	30

Initial Pressure (MPa)	4.8	4.8	4.8	4.8	4.8	4.8	4.8	4.8	4.8	4.8	4.8	4.8
Frequency (Hz)	5	5	5	10	10	10	20	20	20	30	30	30
Stand off Distance (mm)	10	20	30	10	20	30	10	20	30	10	20	30

Chapter 4 Results and Discussion

This chapter presents a detailed analysis of the time dependent flow field between the nozzle exit and the substrate in the shock induced spray process. Consideration of the Schlieren images captured throughout a single cycle reveals some interesting shock phenomena unobservable to the naked eye. Furthermore, these images are correlated with the pressure variation on the substrate to investigate ideal initial conditions for maximum deposition efficiency.

4.1 Cycle Events

Using the commercially available software package (MiDAS), a frame by frame analysis was conducted of each video obtained from the Schlieren system. This process led to the observation of a series of events that occurred within a single flow cycle. Not all of the events that were identified appeared in each and every set of flow and geometrical operating conditions of the SISP.

In order to explain these events in more detail, they are presented in the following sections for the specific case of the SISP operating at a supply pressure of 3.45 MPa with a firing frequency of 10 Hz and a stand off distance of 20 mm.

4.1.1 Appearance of Initial Shock Wave

The start of each cycle could clearly be defined with the appearance of a shock wave front leaving the apparatus as seen in Figure 28 compared to Figure 29 where no shock wave is observed by the Schlieren. Use of this frame in each cycle provided a consistent reference point for analytical purposes. Each image shows the fixed substrate and exit nozzle of the apparatus as highlighted in Figure 28. The shock wave appears as a dark

curve due to the fact that the Schlieren knife edge is oriented in such a way that the image lightness is proportional to the density gradient in the horizontal direction.

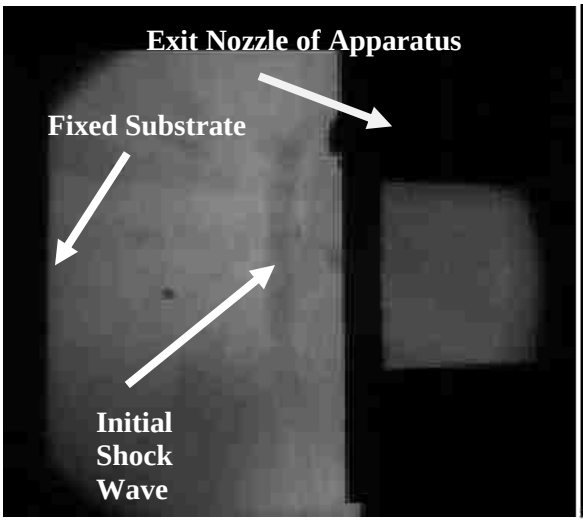

Figure 28
Image with Initial Shock Wave Front

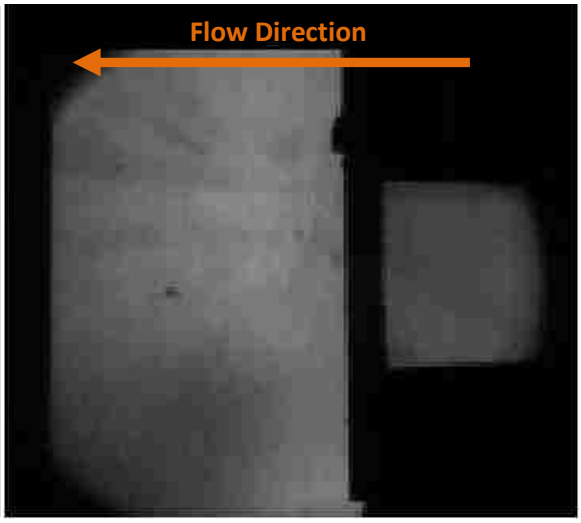

Figure 29
Image with No Shock Wave

4.1.2 Initial Shock Wave Impacts Substrate and Reflects

After crossing the gap between the exit and substrate, the shock wave contacts the substrate carrying enough momentum to be reflected and hence travels back upstream as seen in Figure 30. The reflected shock wave appears light in contrast to the initial shock wave because it is traveling in the opposite direction to the initial wave and therefore the density gradient is of the opposite sign.

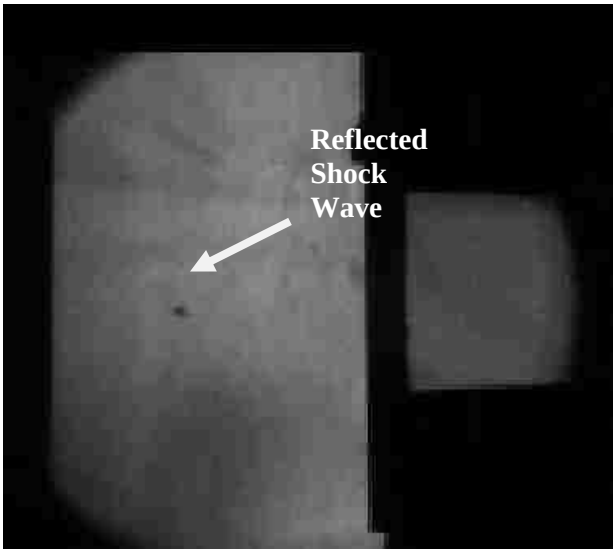

Figure 30 Reflected Shock Wave

4.1.3-4 Reflected Shock Impacts Exit Nozzle and Vortex Ring Formation Leaves Exit Nozzle

For this particular combination of operating conditions events 3 and 4 are observed to happen within the same video frame and hence is considered to occur at the same time. The light coloured reflected shock wave, is seen as it travels away from the substrate and is about to come in contact with the exit nozzle. The shock wave causes a very small change in the substrate pressure reading hence it is unlikely to significantly affect particle motion within the apparatus. The next identifiable feature of the initial flow exiting the nozzle, which is a vortex ring formation, can be seen at the top and bottom portions of the exit nozzle shown in Figure 31.

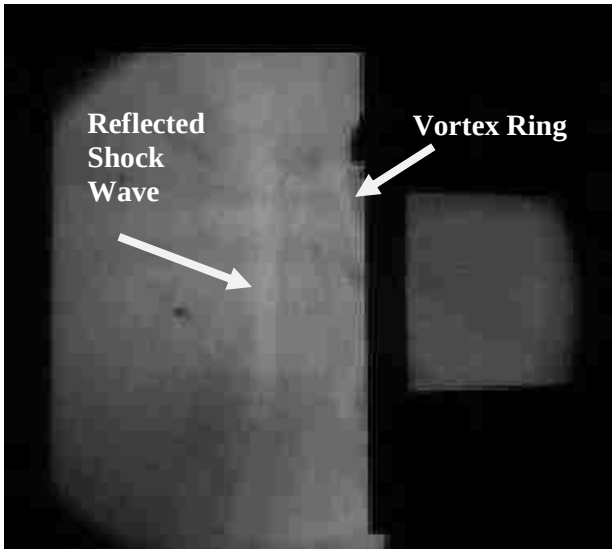

Figure 31 Reflected Shock Wave and Vortex Ring Leaving Exit Nozzle.

4.1.5 Vortex Ring Formation Impacts Substrate

The vortex ring is seen as it crosses the gap close to the nozzle exit in Figure 32 (a). It appears in the form of a reverse 'C' shape that begins to collapse upon itself as it travels across the space toward the substrate in Figure 32 (b). This odd shape is possibly due to the rectangular cross section of the apparatus and the fact that the Schlieren image is formed by integrating the light ray effects along the light ray path. Careful inspection of these images shows a faint secondary shockwave that forms just in front of the vortex as it travels across the open space. Also interesting to note is the initial vortex ring creates weak secondary vortices behind it as seen in Figure 32 (b). As the vortex ring impacts the substrate, as seen in Figure 32 (c), these secondary vortices have all but dissipated. It is important to note that when this vortex ring impacts the substrate there is no pressure rise from the pressure transducer in the substrate meaning the vortex ring does not have the energy required to influence particle motion.

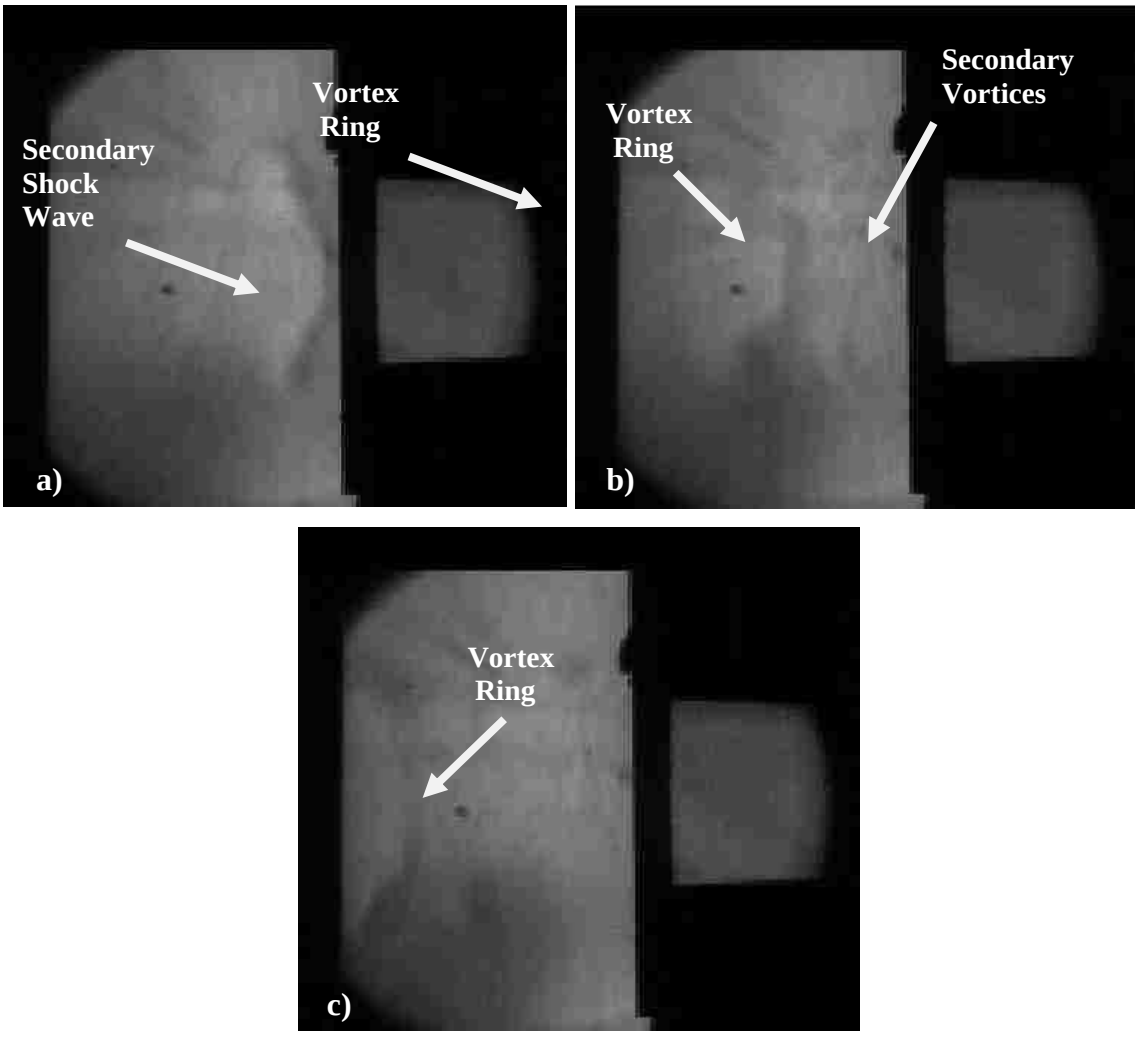

Figure 32 Vortex Ring Travelling Across Gap
a) Near Nozzle Exit
b) Near Middle of Gap
c) As It First Impacts the Substrate

4.1.6 Vortex Ring Formation Dissipates

Upon impact onto the substrate the vortex ring folds outward across the substrate (Figure 33 (a)) and quickly dissipates into the surrounding atmosphere as seen in Figures 33 (b).

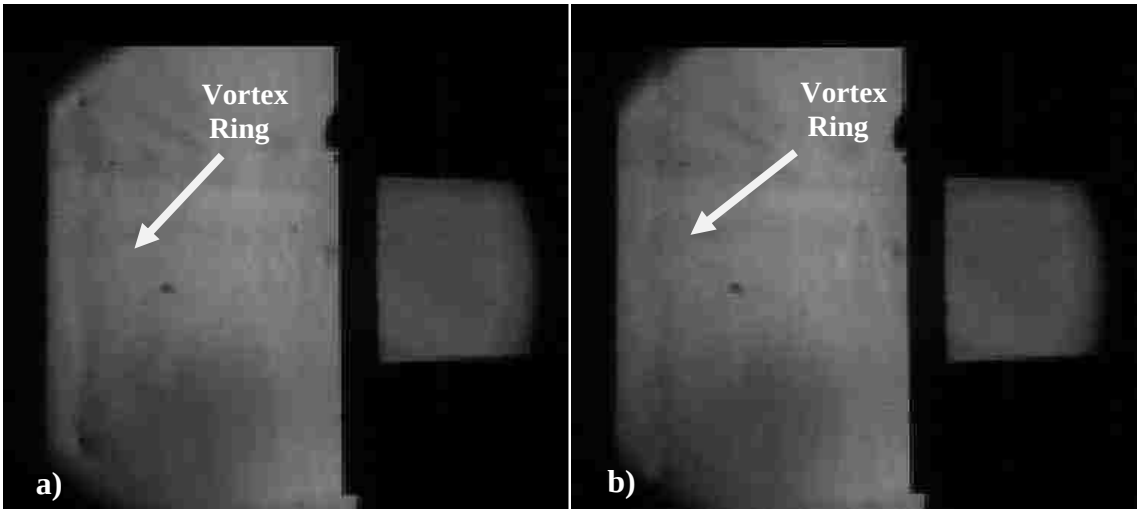

Figure 33 Vortex Impacting and Dissipating on Substrate
a) Impacting
b) Dissipating

4.1.7 Initial Indication of Accelerated Flow

After the vortex ring dissipates, there is a brief period where no significant flow features can be seen near the nozzle exit as shown in Figure 34. There are however, time dependent variations in the shades of grey observed in the video which are not conveyed in the still image. It is speculated that this lack of features in the flow could be caused by subsonic acceleration of the gas in the apparatus. This takes approximately 1.5 ms depending on the SISP operating conditions.

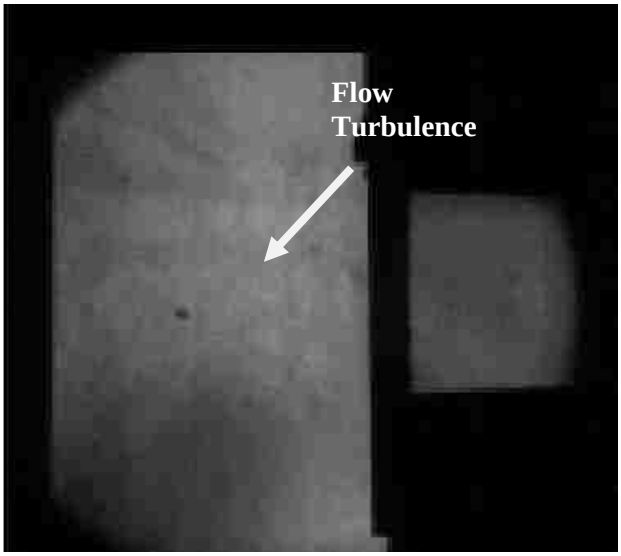

Figure 34 Accelerated Flow Leaving Nozzle

4.1.8 First Appearance of Shock Diamonds in Flow

As mentioned previously, a clear distinction that the flow is indeed supersonic is the formation of shock diamonds within the flow field. In Figure 35 (a) the flow begins to form shock diamonds upon leaving the nozzle. These increase in intensity and hence become more apparent in Figure 35 (b) until they are fully developed as seen in Figure 35 (c).

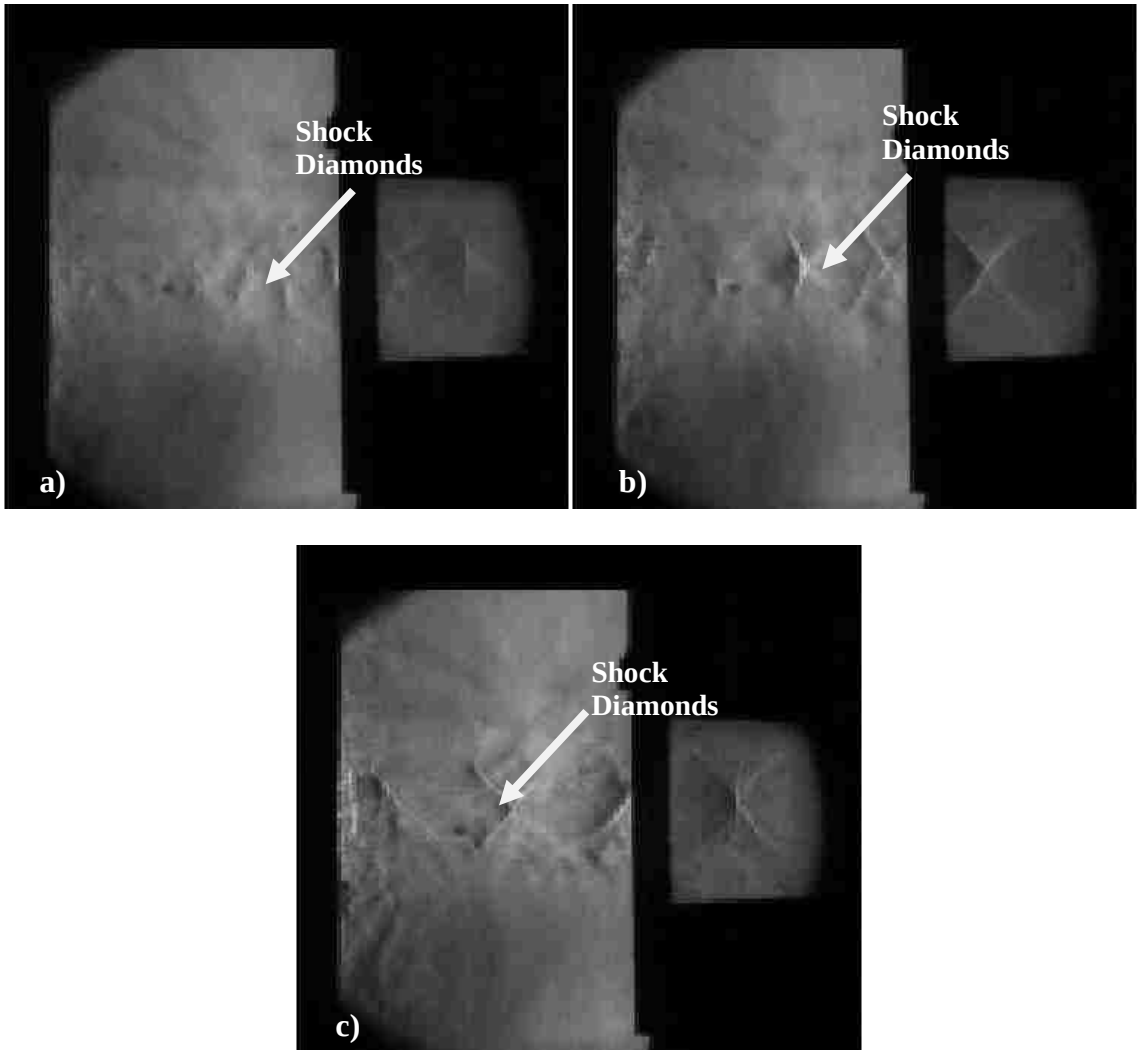

Figure 35 Stages in the Formation of Shock Diamonds
a) Initial Formation
b) Increasing Intensity
c) Fully Developed Diamonds

4.1.9 Formation of Lasting Bow Shock

One of the most interesting phenomena observed in these experiments is the formation of the bow shock on the substrate. As the flow continues to accelerate and impact the substrate a bow shock wave may form depending on the SISP operating conditions. Figure 36 (a) shows the shock diamond pattern for a supply pressure of

3.45 MPa with a frequency of 10 Hz and stand off distance of 20 mm. As supply pressure increased and proximity to the substrate decreased the bow shock becomes more apparent as seen in Figure 36 (b) which corresponds to operating condition of 4.8 MPa supply pressure firing at 10 Hz with a 10 mm stand off distance. The effect of this is further investigated in the next section. Note the term "lasting" bow shock is used because in some cases bow shocks appear but vanish in just a few frames therefore not having a noticeable effect on the substrate pressure.

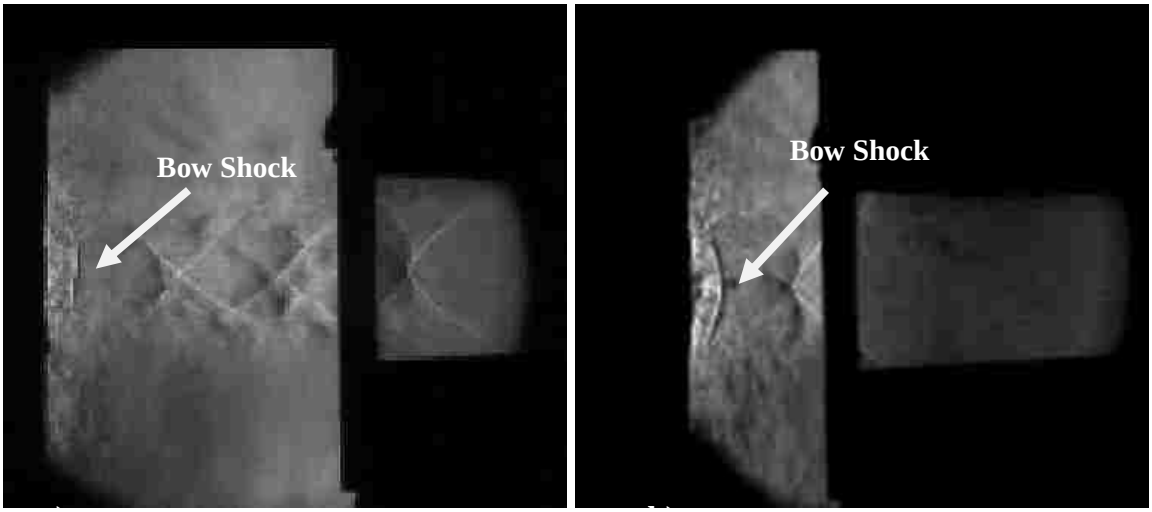

Figure 36 formation of Bow Shock
a) Conditions: 3.45 MPa, 10 Hz, 20mm SOD
b) Conditions: 4.80 MPa, 10 Hz, 10mm SOD

4.1.10 Last Appearance of Bow Shock

The bow shock pattern eventually subsides as evident in Figure 37 and the flow speed begins to decrease due to the valve being closed thus cutting off the driver gas. The last appearance of a bow shock is important as it is needed to calculate the duration of the bow shock which is expected to determine desirable SISP operating conditions.

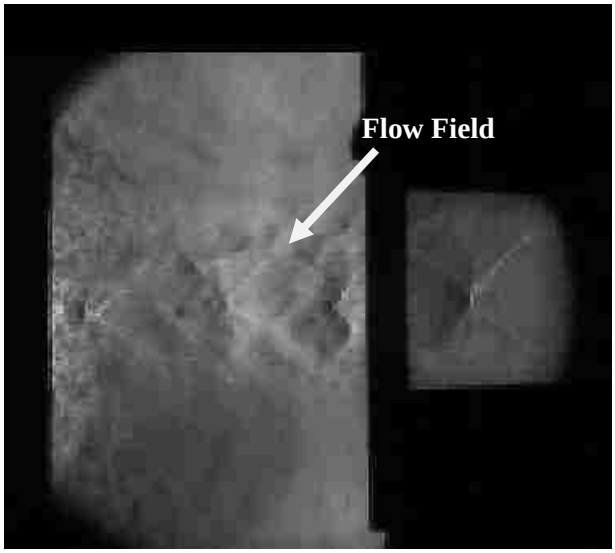

Figure 37 Bow Shock Subsides

4.1.11 Last Appearance of Shock Diamonds

Similar to the last event, it is important to note when the flow decreases its velocity enough to lose the shock diamonds. This would signify the end point where feeding coating particles would be desirable as a decreased flow velocity means lower kinetic energy on impact. The frame indicating the end of the shock diamonds in the flow is seen in Figure 38.

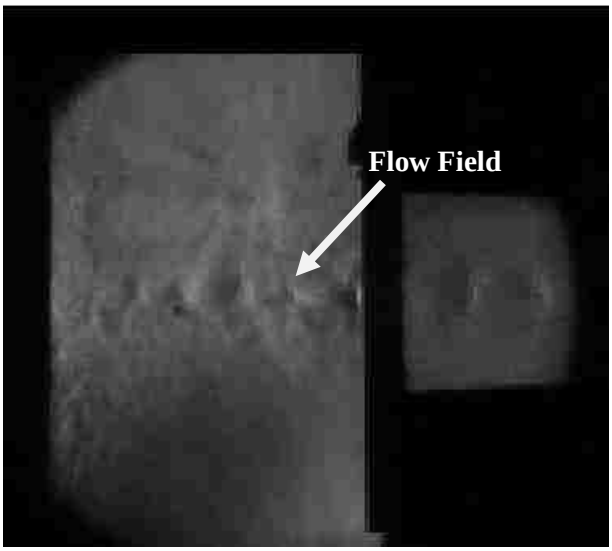

Figure 38 Last Appearance of Shock Diamonds

4.1.12 Completion of the Cycle

The cycles are defined as beginning and ending with the appearance of the initial shock wave. This proved to be a very accurate reference point with a small variation in the cycle time as discussed in the next section. This particular cycle ended with the video frame which includes the next cycle's initial shockwave as shown in Figure 39.

In the preceding sections, a total of twelve events have been identified. In summary they are 1) Appearance of Initial Shock Wave, 2) Initial Shock Wave Impacts Substrate and Reflects, 3) Reflected Shock Impacts Exit Nozzle, 4) Vortex Ring Formation Leaves Exit Nozzle, 5) Vortex Ring Formation Impacts Substrate, 6) Vortex Ring Formation Dissipates, 7) Initial Indication of Accelerated Flow, 8) First Appearance of Shock Diamonds in Flow, 9) Formation of Lasting Bow Shock, 10) Last Appearance of Bow Shock, 11) Last Appearance of Shock Diamonds and 12) Completion of the Cycle. They will be used in a later section to define characteristic phases within the cycle.

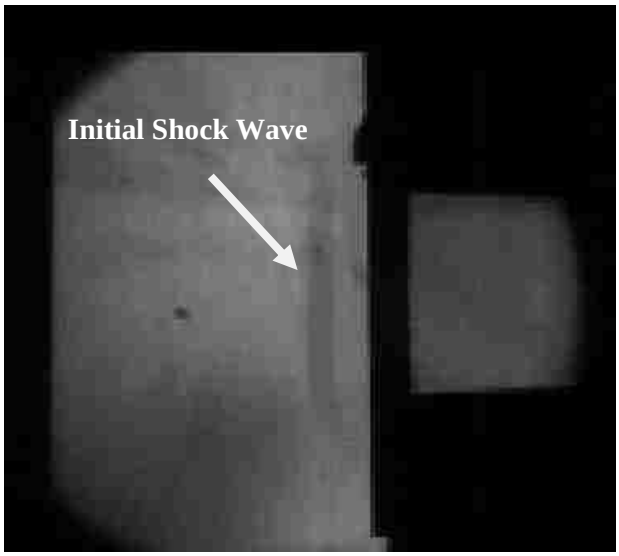

Figure 39 Next Cycle's Initial Shock Wave

4.2 Single Cycle Analysis of Substrate Pressure

Post processing of the data from the pressure transducer mounted into the substrate allowed the Schlieren images of these 12 events to be correlated with the time dependent pressure acting on the center point of the substrate. A total of 585 cycles were investigated and a single cycle was chosen at random from each case to be compared with its Schlieren video to determine the effect that these events have on the pressure traces. Figure 40 is one example of a pressure trace which exhibits all twelve events and it is clear that certain events have a large impact on the substrate pressure, the rest can be found in Appendix B.

The SISP operating conditions which correspond to this graph are a supply pressure of 3.45 MPa, firing frequency of 5 Hz and a stand off distance of 10 mm. The second cycle in the series of cycles captured in each run is selected for analysis in order to eliminate any initial transients.

The flow begins with a slight increase in pressure seen as a bump which coincides with the initial shockwave impacting and reflecting off the substrate. We know, from the video images, a vortex ring exists at this point however, there does not seem to be any significant impact on the substrate pressure caused when it impacts and disperses. The pressure continues to increase slowly and then very rapidly which is the moment that the supersonic flow begins to exit the nozzle. As mentioned before, certain operating conditions produce flows with short lasting bow shocks which can be seen actually decrease the pressure however the flow quickly recovers to increase again. There comes a point in the cycle where the supersonic flow produces a 'lasting' bow shock which drops the pressure about 130 kPa. A possible explanation of this drop is the shape of the Mach diamonds against the substrate immediately before and immediately after the formation of this bow shock. As discussed in the literature review section, the point of high pressure of a shock diamond in a supersonic jet is at a beginning or end of a diamond where only one vertex exists. This high pressure area seems to be acting on the substrate before the bow shock appears and thus the reading of the pressure transducer is high. Once this bow shock forms the Mach number may continue to increase which would cause the pressure peaks to shift and as seen in Figures 12 and 13. This will change the location of the diamonds and their vertices, therefore dropping the pressure as the Mach diamond's center is acting on the substrate. This drop lasts for 0.03 ms of the cycle then the pressure rises once more as the Mach number decreases. After the lasting bow shock ends, the flow begins to gradually decelerate with a few very brief after bow shocks which continue to form until the flow returns to nominal values.

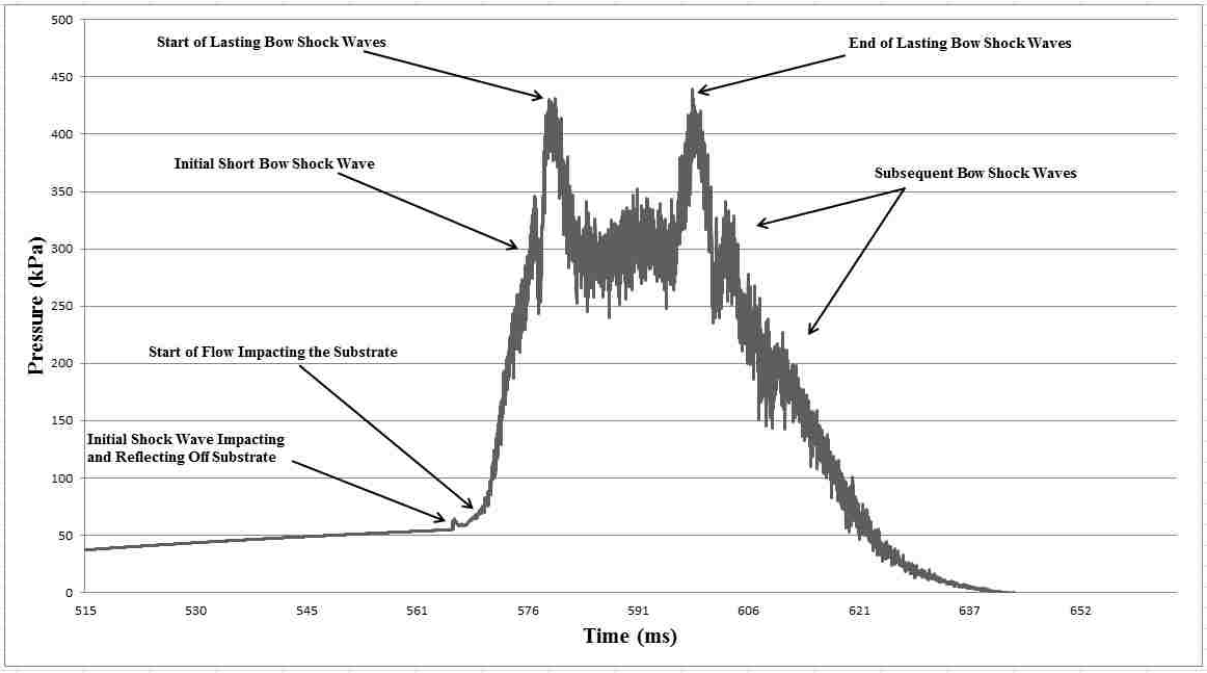

Figure 40 Pressure vs Time of a Single Cycle with Double Peak

This drop in pressure can be seen in the majority of cases however analysis of some of the pressure traces an observable drop cannot be seen. Figure 41 shows the pressure trace from the trial with a supply pressure of 2 MPa with a firing frequency of 10 Hz and a stand off distance of 10 mm. The graph depicts the same initial bump where the shockwave impacts the substrate but then steadily increases into a single peak and then decreases again. For this particular case the bow shock did not form at the substrate which could explain the lack of the double peak shown in Figure 40. However examining the other cases revealed an aspect that was prominent in the majority of the graphs. This was the erratic data points that were first interpreted to be noise in the equipment. Steps were taken to minimize this noise by routing the pressure transducers through a signal conditioner and a low pass filter with a cut off of 63 Hz. The majority of the electromagnetic noise seemed to come from the high powered motor within the rotary

valve which caused the pressure transducer embedded within the substrate to give highly volatile readings. This was greatly reduced but not completely eliminated by replacing the initial metal substrate with a nonmetallic one as seen in Figure 42. There is a minor fluctuation of the pressure of approximately +/- 1.5 kPa, but not to the extent witnessed in the pressure trace graphs; greater than +/- 10 kPa. This lead to the idea that the erratic patterns were possibly the result of instability in the flow stagnation point location and possibly the movement of shock diamond pattern locations in the flow. Since the pressure transducer is embedded into the substrate in a fixed position any fluctuation of the stagnation point at the transducer would have an effect on the reading it acquires. Also when a bow shock forms there is a period of highly volatile flow experienced at the point of contact on the substrate adding to the sporadic data values acquired.

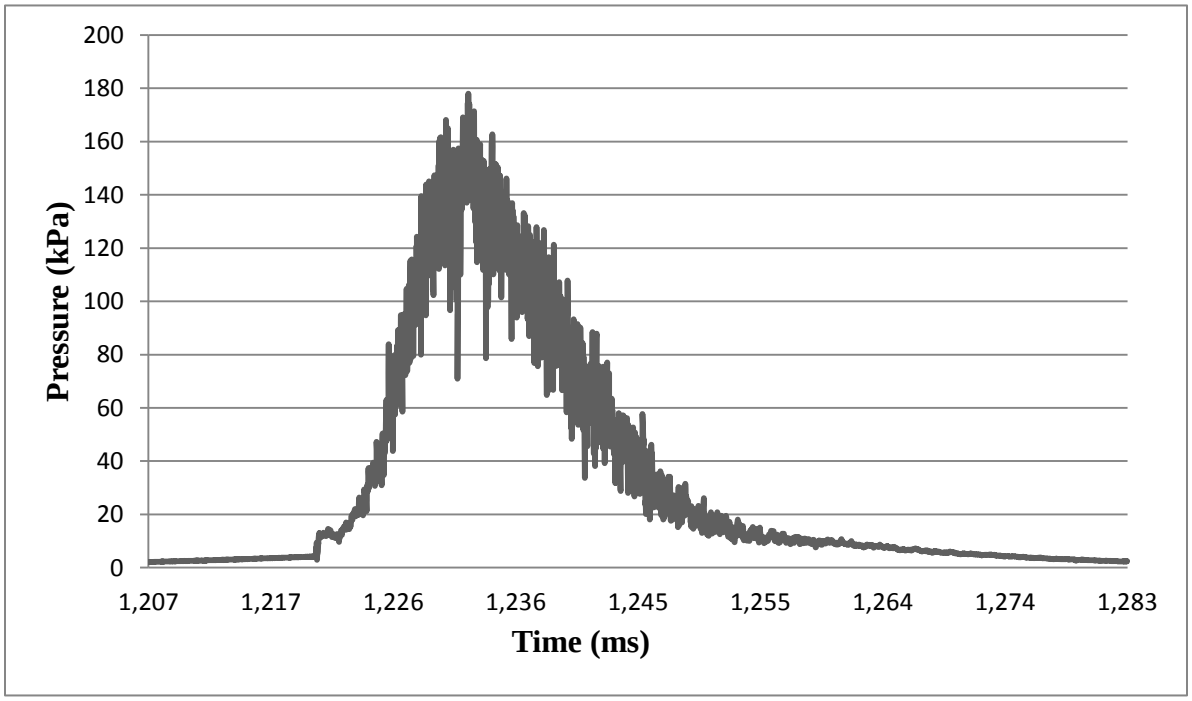

Figure 41 Pressure vs Time of a Single Cycle with Single Peak

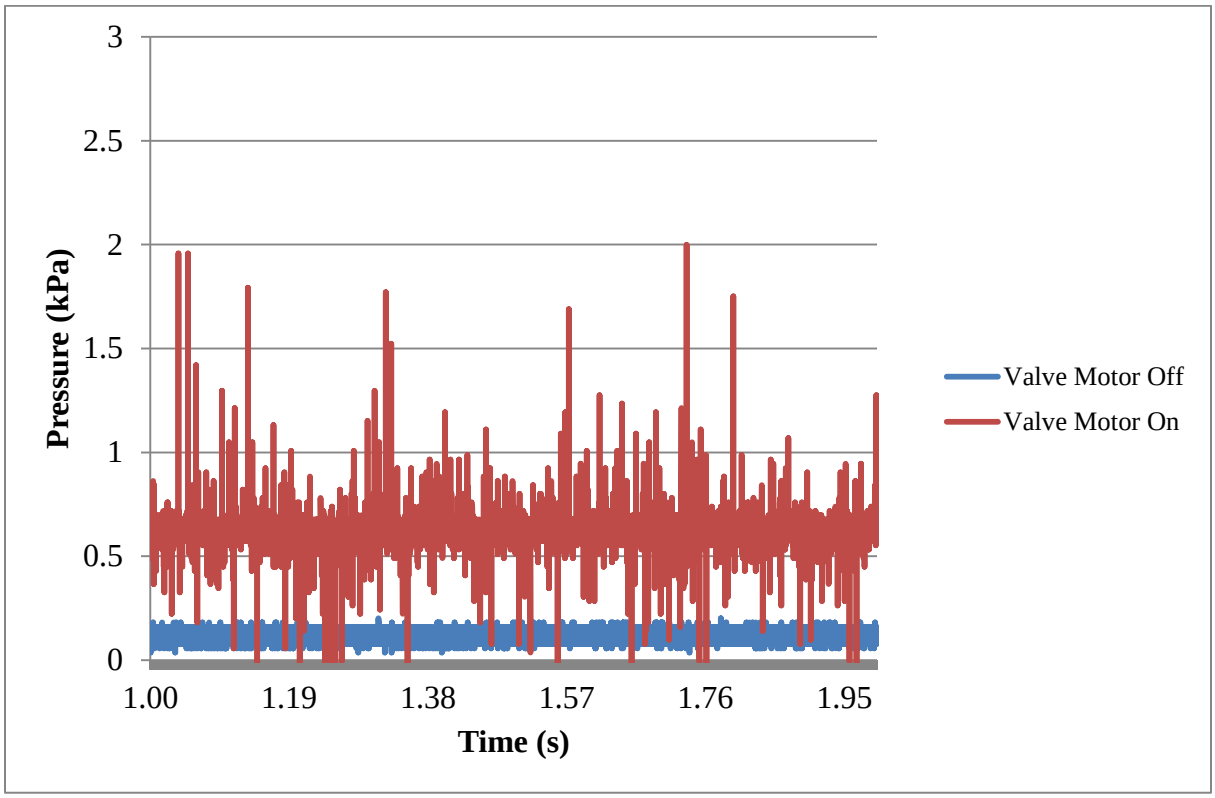

Figure 42 Noise in Pressure Transducer Readings

4.3 Phases of Flow

A video of the Schlieren images of the flow field was made for each of the operating conditions listed in Table 1. A thorough frame by frame examination conducted for five consecutive cycles after continuous operation was established. Each event was marked by the frame number and then converted to time since the frame rate is known. An example of a completed table is shown in Table 2. Note that similar tables for the remaining thirty-five other operating conditions studied are listed in Appendix C. From these tables it is possible to calculate the average duration between events for any given condition. To simplify this process, a single cycle was divided into predefined phases as follows:

Phase 1: The Duration of the Cycle Period - defined as the difference between Event 1 and Event 12 which is the time between the initial shock wave front of the current cycle and that of the next cycle.

Phase 2: The Initial Shock Wave and Its Reflection in the Gap - defined as the difference between Event 1 and Event 3 which is the time between when the initial shock wave is first seen and when the reflected shock impacts the exit nozzle.

Phase 3: The Existence of a Vortex Ring - defined as the difference between Event 4 and Event 6 which is the time required for the vortex ring to leave the nozzle, travel across the gap and dissipate on the substrate.

Phase 4: The Calmness of Flow - defined as the difference between Event 6 and Event 7 which is the time period after the vortex ring dissipates and before the supersonic flow begins to leave the nozzle exit.

Phase 5: The Supersonic Jet - defined as the difference between Event 8 and Event 11 which is the time period between the first shock diamonds formation and when they subside within the flow.

Phase 6: The Presence of a Lasting Bow Shock - defined as the difference between Event 9 and Event 10 which is the time duration of the lasting bow shock wave.

From the data collected from Table 2, a phase table is created and shown in Table 3. The thirty five tables for the other operating conditions considered are located in Appendix D. This will allow for a detailed analysis of how the phases vary at different operating conditions. The standard deviation of each entry was also calculated and included which shows how little variance there exists between repeated cycles. The

portion of the flow from the time when the supersonic flow subsides to the end of the cycle is not considered as it has no important features or functions and makes up the remaining percentage of time duration of Phase 1.

Table 2 Frame Table for a Supply Pressure of 3.45 MPa Firing at 5 Hz at 10mm SOD

Event #	Frame number corresponding to each event				
	Cycle 1	Cycle 2	Cycle 3	Cycle 4	Cycle 5
1	5710	17774	29712	42301	55802
2	5714	17777	29715	42304	55805
3	5715	17778	29716	42305	55806
4	5719	17781	29721	42308	55809
5	5729	17795	29733	42320	55820
6	5740	17802	29741	42338	55834
7	5928	18022	29964	42573	56053
8	6059	18145	30064	42677	56191
9	6247	18335	30223	42863	56392
10	7478	19685	31469	44244	58097
11	8621	20846	32600	45364	59083
12	17774	29712	42301	55802	68402

Table 3 Phase Table for a Supply Pressure of 3.45 MPa Firing at 5 Hz at 10mm SOD

Phase #	Average time duration (ms)	Standard Deviation of time duration (ms)
1	238.83	11.74
2	0.08	0.01
3	0.45	0.08
4	4.13	0.33
5	50.97	2.70
6	26.34	3.65

4.4 Analysis of the Phases

The variation of the average time duration for each of the six phases for all thirty-six operating condition cases is summarized in a single bar graph. Each phase is considered separately in the following paragraphs.

The bar graph corresponding to Phase 1 is shown in Figure 43. In this graph, and all of the remaining graphs, the average time is plotted on the vertical axis against the stand off distance on the axis shown on the left side. The axis on the right side includes sets of operating pressure and frequency. The different frequencies are distinguished by different colors and grouped according to operating pressure which increases along the axis from the origin. As expected, the duration of the cycle is largely dependent on only one factor; the firing frequency of the rotary valve. This follows the logic that if the valve is opened for a significantly large time, the duration of the flow must be longer as well. Note that all the average cycle periods of the 3.45 MPa supply pressure and firing at 5 Hz cases seem to be slightly larger than the rest of the 5 Hz cases. This is due to the actual rotary valve operation at low frequency, being slightly erratic due to the built up of pressure at the inlet which caused a slight variation in the angular velocity throughout the cycle. The fact that both the stand off distance as well as the supply pressure do not have a significant role in changing the duration of the cycle time is an indication that the firing frequency could accurately be controlled.

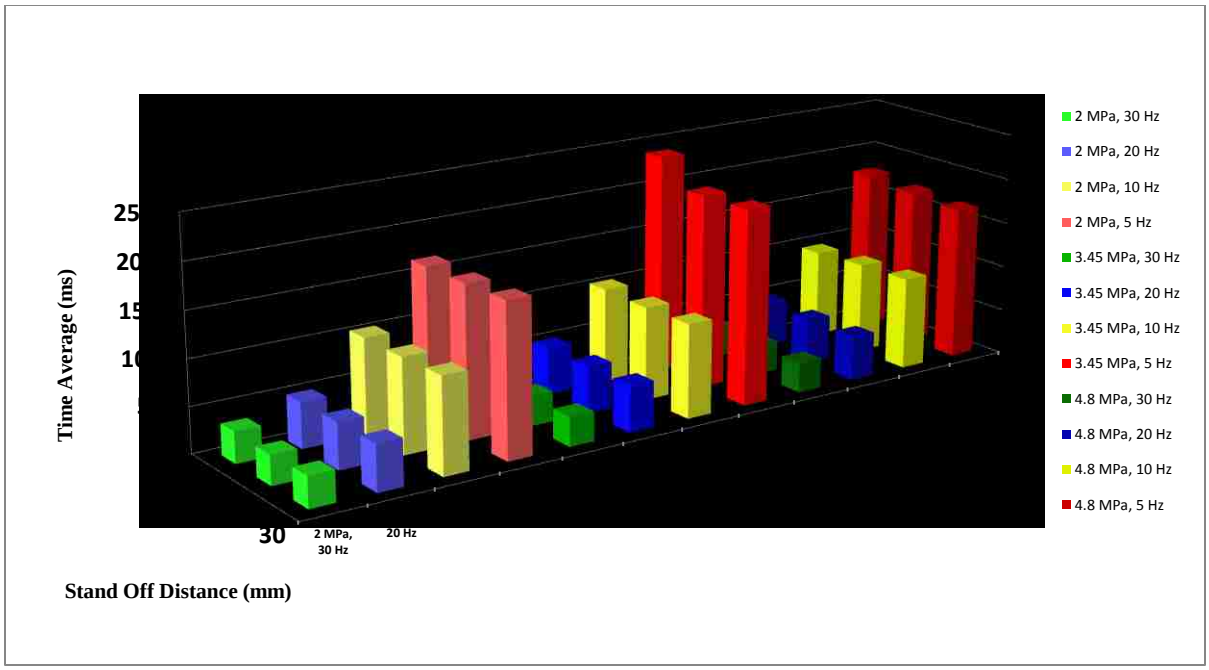

Figure 43 Average Times for Phase 1: Duration of Cycle Period

Figure 44 includes the results for Phase 2 which is the duration of the initial shock wave and its reflection expressed as a percentage of the duration of the total cycle. From this it is clear that the shock wave is only present for a tiny percentage, 0.05-0.25%, of the entire cycle. It also shows that at higher frequencies the time it takes for the shock wave to appear and reflect back is a much larger percentage of the cycle time which is partly due to the lower cycle time at higher frequencies but could also be due to a weaker initial pressure pulse occurring as the firing frequency is raised. This fact will be mentioned later when discussing the results of the pressure experienced on the substrate.

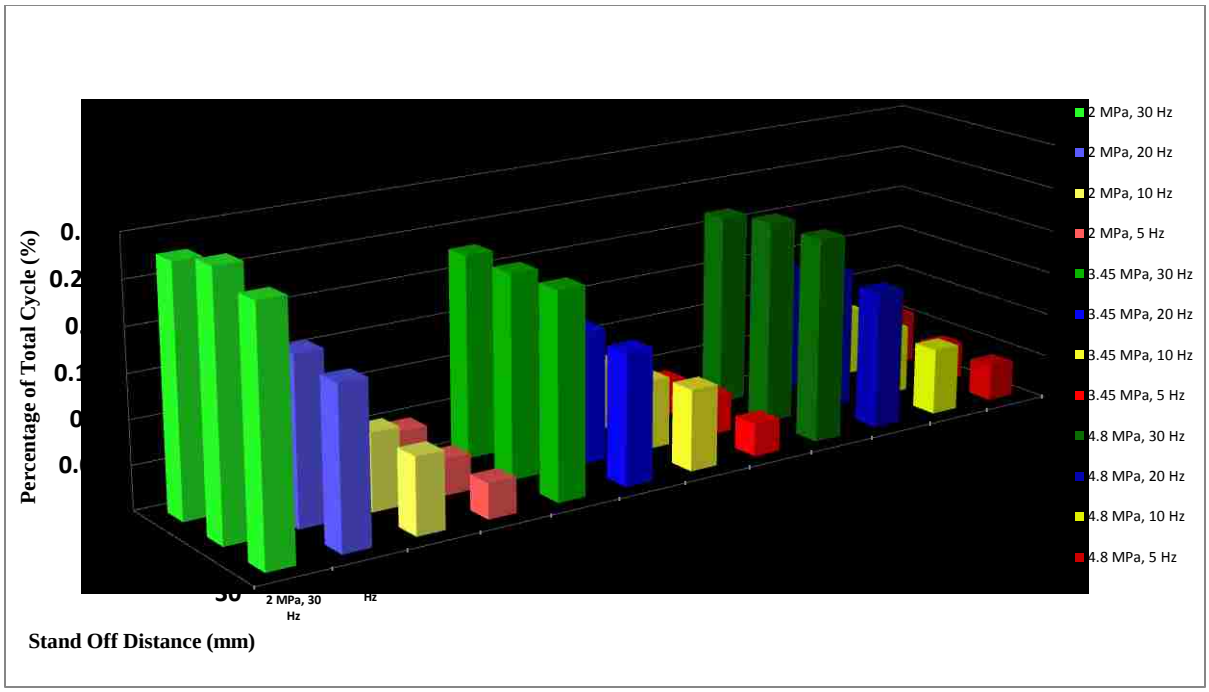

Figure 44 Average Times for Phase 2: The Initial Shock Wave and Its Reflection

The results for the duration of the existence of the vortex ring (Phase 3) are presented in Figure 45. As stated before, the actual vortex ring has no noticeable effect on the substrate pressure, this graph shows how much of an effect the shock wave has on the atmospheric gas already in the apparatus as the bulk flow starts. It would seem that at lower firing frequency the vortex moves faster while at higher frequencies it does not reach the substrate at all. Obviously when the stand off distance is decreased, the vortex impacts and dissipates on the substrate more quickly which coincides with the data.

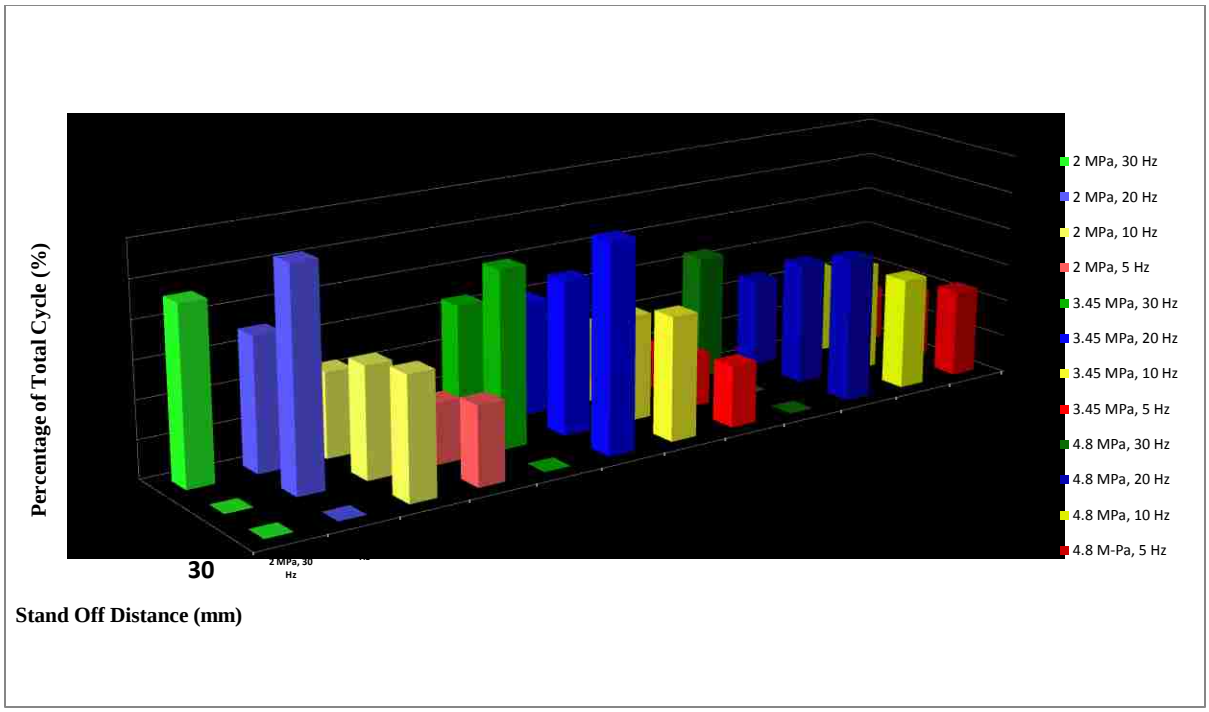

Figure 45 Average Times for Phase 3: Existence of the Vortex Ring

Phase 4 covers the time delay between the dissipation of the vortices and the observable start of the supersonic driven flow leaving the exit nozzle. The average times for this phase are shown in Figure 46. Much like in the case of Phase 1, the delay seems to be highly dependent on the firing frequency of the valve however it would seem that the supply pressure also has an effect. Increasing the supply pressure decreased the time it takes for the driven gas to leave the apparatus and begin to impact the substrate. This means that the flow begins to develop much earlier as well.

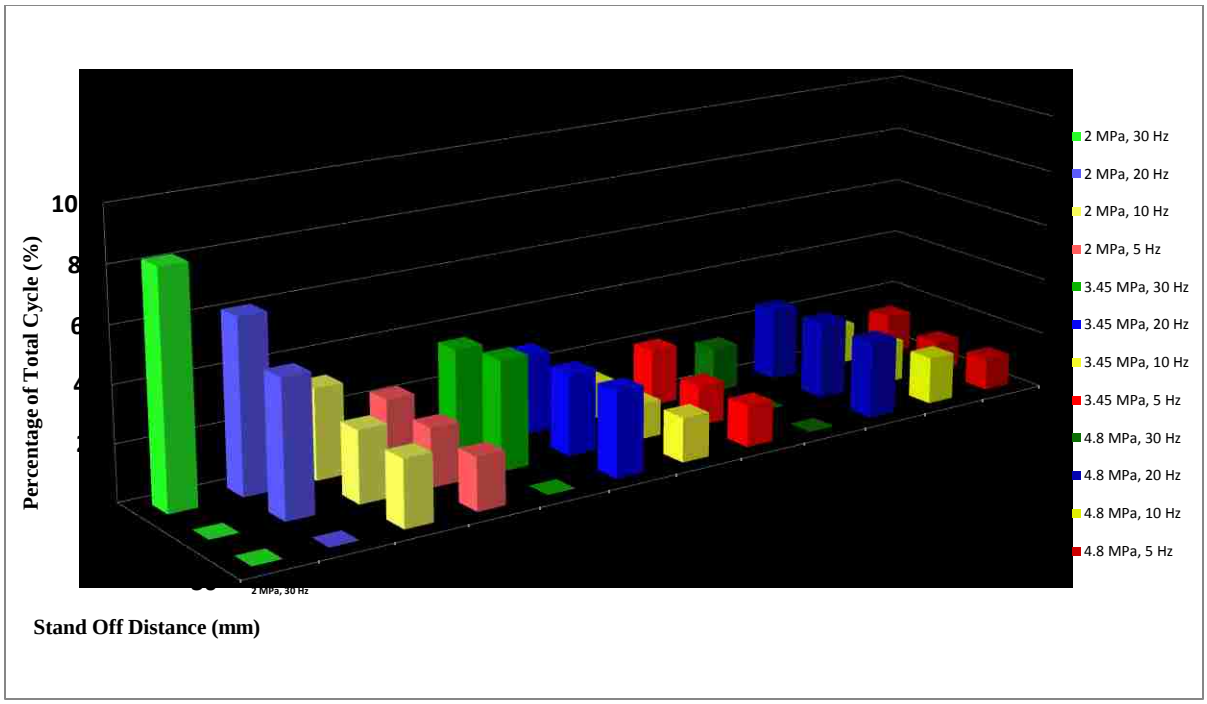

Figure 46 Average Times for Phase 4: The Calmness of the Flow

From Phase 4 one would expect the higher supply pressure regions to have a longer supersonic jet portion of their flow which proves to be the case as seen in the average time duration results for Phase 5 presented in Figure 47. Also noted is the fact that the flow is supersonic for a larger portion of the total cycle in the low frequency cases. The ideal time to inject particles is when the flow is supersonic to maximize the kinetic and thermal energy of the flow. However this flow must reach the substrate to be effective and not be impeded by a bow shock.

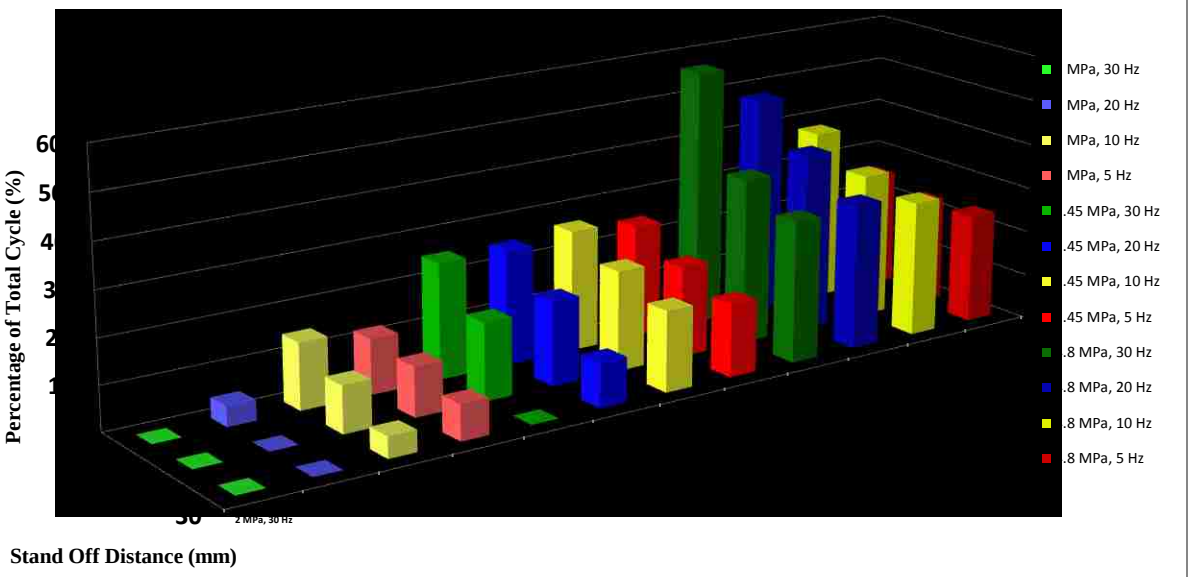

Figure 47 Average Times for Phase 5: The Supersonic Jet

As the particles must reach the substrate at the highest possible velocity for better adhesion, a bow shock at the surface will act to decrease the velocity and thus is not an ideal characteristic. Figure 48 includes the average time duration for existence of a lasting bow shock wave. Though higher initial supply pressures created longer durations of supersonic flow the majority of that flow is impeded by the presence of a bow shock at the substrate. As expected, the case for no bow shock wave at all occurs at the lowest initial supply pressure except for when the frequency is set at 5 Hz with a stand off distance of 10 or 20 mm. For higher initial pressures no bow shock occurs at frequencies of 30 and 20 Hz in all of the 3.45 MPa pressure and all but a stand off distance of 10 mm in the 4.8 MPa case. Finally the other case where no bow shock occurs is at 3.45 MPa firing at 10 Hz at a stand off distance of 30 mm.

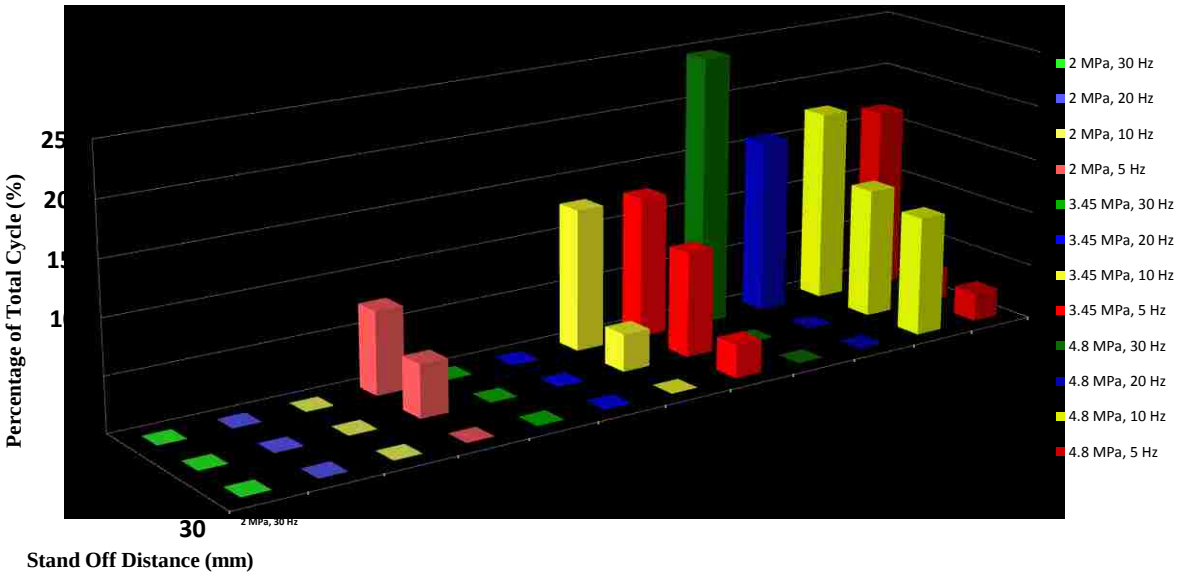

Figure 48 Average Times for Phase 6: Presence of Lasting Bow Shock

How the pressure experienced by the substrate varies with time and how the substrate pressure features correlate with the compressible flow field features is important for a more complete understanding of the SISP. This is considered in the next section.

4.5 Substrate Pressure

The pressure on the substrate was captured for each cycle of every set of operating conditions presented in Table 1. Figure 49 shows an example of the collected pressure data for 5 cycles with an operating supply pressure of 3.45 MPa firing at 5 Hz at a stand off distance of 30 mm. Note that the graphs for the thirty-five remaining sets of operating condition can be found in Appendix E. The graph shows that the cycles within this period are very uniform which indicates that the SISP operation is stable. From this

information the average peak pressure was calculated for all operating conditions and summarized in bar graph format in Figure 50.

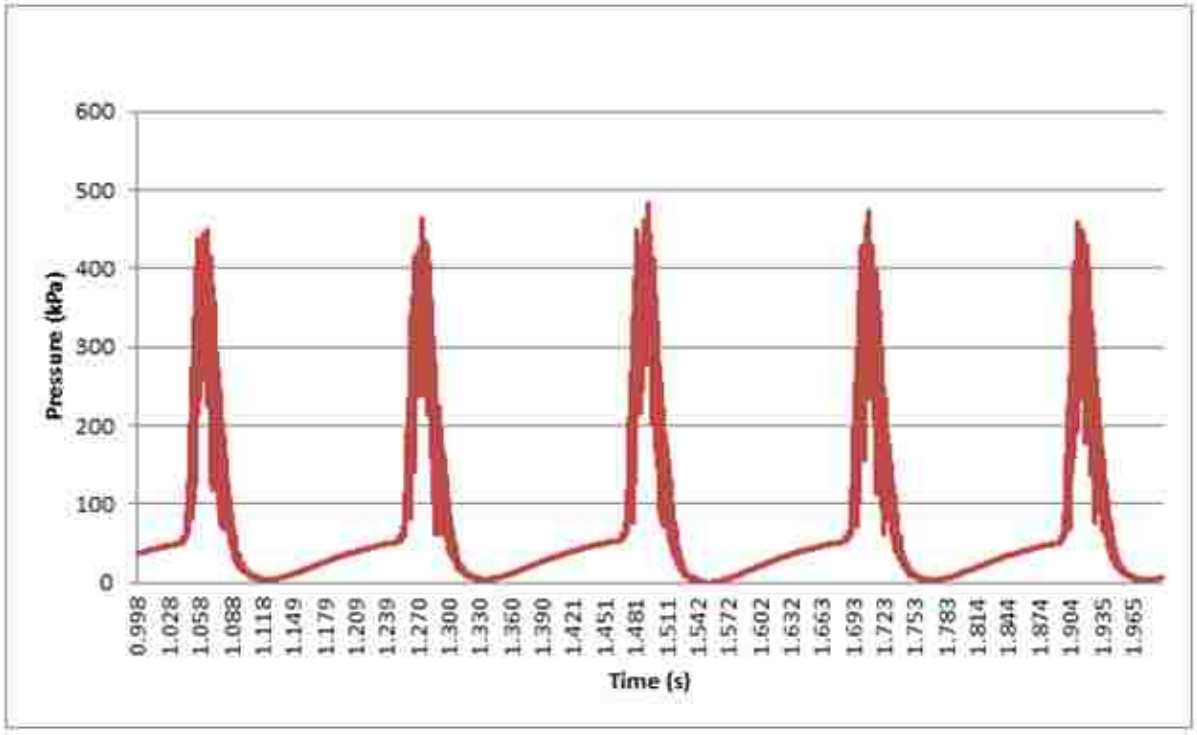

Figure 49 Substrate Pressure Graph

An analysis of Figure 50 reveals some key factors for maximizing the pressure imposed on the substrate. It is quite clear that increasing the initial supply pressure from 2 MPa to 3.45 MPa has a drastic effect of more than doubling the substrate pressure value. However, increasing the pressure to 4.8 MPa, shows only an increase of approximately 50 kPa. When the frequency is decreased from 30 Hz each the pressure experienced on the substrate increases. It is interesting to note that the stand off distance does not seem to have a severe effect on the pressure, as one would have expected, with only slight gains when the space between the exit nozzle and substrate is reduced.

It has been shown in the literature review, Section 2.2.2, that the bow shock wave has a negative effect on the substrate pressure and should be avoided. The ideal case for SISP spraying is therefore taken to be that which produces a flow that is both high in substrate pressure but has no bow shock. This criterion was selected as the high pressure can be translated to the impact strength of the flow onto the substrate as a result of the high velocity of that flow. A comparison of Figures 48 and 50 reveals only 5 such cases. To further optimize the ideal case one can arbitrarily assume a minimum substrate pressure requirement of 222 kPa which is the mean pressure of all cases then the resultant conditions are:

1) A supply pressure of 3.45 MPa firing at 10 Hz at a stand off distance of 30 mm.
2) A supply pressure of 4.8 MPa firing at 20 Hz at a stand off distance of 20 mm.
3) A supply pressure of 4.8 MPa firing at 20 Hz at a stand off distance of 30 mm.
4) A supply pressure of 4.8 MPa firing at 30 Hz at a stand off distance of 20 mm.
5) A supply pressure of 4.8 MPa firing at 30 Hz at a stand off distance of 30 mm.

Therefore, with these assumptions, the most ideal set of spray operating conditions is set 1. This is due to the fact that, not only is the substrate pressure approximately 100 kPa higher than the others, it has a lower supply pressure resulting in a lower cost of operation.

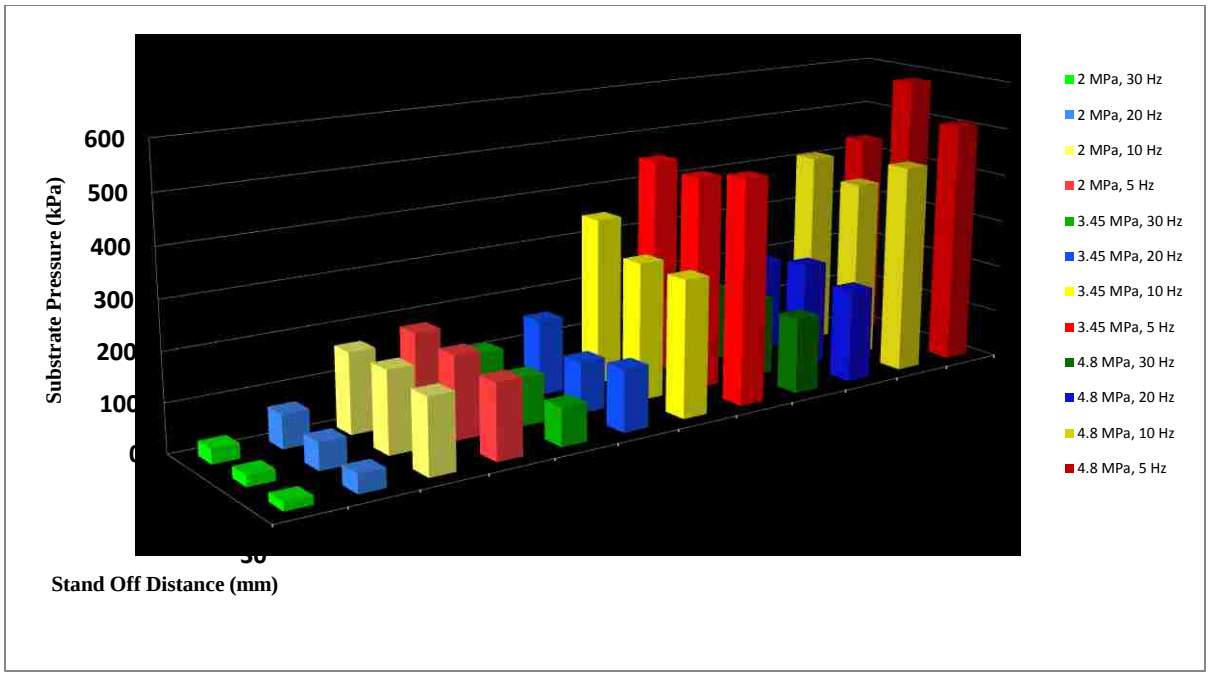

Figure 50 Average Peak Pressures

Chapter 5 Conclusions

In conclusion, an experimental apparatus was designed and constructed to simulate Centerline's Waverider Shock Induced Spray Process device. A series of experiments were conducted with operating pressure ratios of 2, 3.45 and 4.8 MPa, rotary valve firing frequencies of 5, 10, 20 and 30 Hz and stand off distances of 10, 20 and 30 mm. In each of these cases a detailed qualitative analysis was conducted of individual frames of a high speed video taken using a custom Schlieren system. This revealed a total of 12 distinct events that occurred during one cycle of flow. These events were; 1) Appearance of Initial Shock Wave, 2) Initial Shock Wave Impacts Substrate and Reflects, 3) Reflected Shock Impacts Exit Nozzle, 4) Vortex Ring Formation Leaves Exit Nozzle, 5) Vortex Ring Formation Impacts Substrate, 6) Vortex Ring Formation Dissipates, 7) Initial Indication of Accelerated Flow, 8) First Appearance of Shock Diamonds in Flow, 9) Formation of Lasting Bow Shock, 10) Last Appearance of Bow Shock, 11) Last Appearance of Shock Diamonds, 12) Completion of the Cycle.

These events were then divided into six phases defined as; 1) The Duration of the Cycle, Period 2) The Initial Shock Wave and Its Reflection in the Gap, 3) The Existence of a Vortex Ring, 4) The Calmness of Flow, 5) The Supersonic Jet, 6) The Presence of a Lasting Bow Shock.

Comparing all operating conditions for each phase allowed the formulation of the following conclusions:

1) The duration of the cycle period was, as expected, found to be dependent on the firing frequency of the rotary valve with the stand off distance and supply pressure having little to no effect.

2) The initial shock wave appearing and reflecting in the gap was found to make up a tiny portion of the total cycle duration with higher firing frequencies having a larger phase duration percentage due simply to the fact that the cycle period is shorter as frequency increases. The stand off distance and supply pressure seemed to have little effect on this phase.

3) The existence of a vortex ring was influenced by all three operating conditions. For example at the highest firing frequency, 30 Hz, only the trial with a stand off distance of 10 mm produced a vortex that reached the substrate at a supply pressure of 2 MPa. Therefore vortex rings have difficulty forming at higher firing frequencies and stand off distances as well as low supply pressures.

4) When the calm phase existed its duration tended to decrease with increasing supply pressure and firing frequency and be relatively independent of stand off distance.

5) The supersonic jet phase was found to be highly dependent on the supply pressure used. At 2 MPa the supersonic jet only formed at low firing frequencies, 5-10 Hz with one jet forming at 20 Hz at the closest stand off distance of 10 mm. It would

seem that the longest phase duration occurs at high supply pressures, high frequencies and short stand off distances. It is expected that this phase will have the most significant effect on the acceleration of the solid particles in the SISP.

6) The presence of the bow shock phase was found to occur mainly with low firing frequencies and higher supply pressures. These conditions as well as smaller stand off distances produced a longer bow shock duration.

A quantitative analysis was then conducted to investigate the pressure experienced by the pressure transducer mounted within the substrate and to correlate it with the high speed image frames. The result of this showed that the supply pressure and the firing frequency of the rotary valve had the largest effect on the substrate pressure. Conditions which are known to have a detrimental effect on the deposition rate and hence not be desirable in a thermal spray process were considered. This led to the discovery of a set of operating conditions that produced the highest pressure on the substrate while creating no observable bow shock. This was a supply pressure of 3.45 MPa firing at 10 Hz at a stand off distance of 30 mm.

Chapter 6 Future Work

This experimental work has successfully shown how the flow field near the substrate behaves in the Shock Induced Spray Process under certain operating conditions. The effect that this flow field has on particles travelling with the flow has been not been considered. The next step is to inject actual particles into the flow at various times throughout the cycle to observe the fluid-particle interaction, especially that between the bow shock wave and the particles. The Schlieren system can be used to observe the finer details of these interactions which will aid in understanding how the SISP can be fully optimized. In order to accomplish this it will be necessary to move the apparatus to Centerline's Thermal Spray facility.

References

[1] Lefteri C. 2007. *Making it: Manufacturing techniques for product design,* London: Laurence King Pub. 240pp.

[2] Bunshah R.F. 2001. *Handbook of hard coatings: Deposition technologies, properties and applications,* Park Ridge, N.J.: Noyes Publications ; Norwich, N.Y. 550pp.

[3] Berndt C.C., Bernecki T.F.1993. ASM International. *Thermal spray coatings: Research, design, and applications : Proceedings of the 5th national thermal spray conference,* Anaheim, California. 691pp

[4] Ahmad Z. 2006. Institution of Chemical Engineers. *Principles of corrosion engineering and corrosion control,* Boston, MA: Elsevier/BH. 656pp. 1st ed.

[5] Pawlowski L. 2008. *The science and engineering of thermal spray coatings,* The Atrium, Southern Gate, Chichester, West Sussex, England: John Wiley and Sons. 656pp. 2nd. ed.

[6] Fauchais P., Vardelle A., Dussoubs B. 2001. *Quo vadis thermal spraying?* J. Therm. Spray Technol. 10 : 44-66.

[7] Li M., Christofides, P. 2009. *Modeling and control of high-velocity oxygen-fuel (HVOF) thermal spray: A tutorial review.* J. Therm. Spray Technol. 18 : 753-68.

[8] Fauchais P., Joulia A., Goultier S., Chazelas C., Vardelle M., Rossignol S. 2013. *Suspension and solution plasma spraying.* Journal of Physics. D, Applied physics. 46 : 224015.

[9] Karthikeyan J. 2005. *Cold spray technology.* Adv Mater Processes. 163 : 33-5.

[10] Gartner F., Stoltenhoff T., Schmidt T., Kreye, H. 2006. *The cold spray process and its potential for industrial applications.* J. Therm. Spray Technol. 15 : 223-32.

[11] Jodoin B., Richer P., Berube, G., Ajdelsztajn L., Erdi-Betchi A., Yandouzi M. 2007. *Pulsed-gas dynamic spraying: Process analysis, development and selected coating examples.* Surf Coat Technol. 201 : 7544-51.

[12] Yandouzi M., Jodoin B. 2009. *WC-based coating production by the pulsed gas dynamic spraying process: Coatings and process analysis*. Proceedings of the International Thermal Spray Conference, Las Vegas, Nevada. 219-224pp

[13] Karimi M., Jodoin B., Rankin G. 2011. *Shock-wave-induced spraying: Modeling and physics of a new spray process.* J. Therm. Spray Technol. 20 : 866-81.

[14] Yandouzi M., Richer P., Jodoin B. 2009. *SiC particulate reinforced al-12Si alloy composite coatings produced by the pulsed gas dynamic spray process: Microstructure and properties.* Surf Coat Technol. 203 : 3260-70.

[15] Roberson J.A., Crowe C.T. 1993. *Engineering fluid mechanics,* One Beacon Beach, Boston, MA: Houghton Mifflin Company. 5th. ed.

[16] Atcheson, B. 2007. *Schlieren-based flow imaging*. MSc Thesis. University of British Columbia.

[17] Panigrahi P.K., Muralidhar K. 2012. *Schlieren and shadowgraph methods in heat and mass transfer,* Springer.

[18] John J.E., Keith T.G. 2006. *Gas dynamics,* Upper Saddle River, New Jersey: Pearson Education, Inc. 3rd. ed.

[19] Setzman J. 2002. *Under/over expanded nozzles*. Aeronautics slides. Georgia Institute of Technology, Georgia. http://soliton.ae.gatech.edu/people/jseitzma/classes/ae3450/underoverexpanded_two.pdf

[20] Norum, T.D. & Seiner, J.M., *Measurements of mean static pressure and far field acoustics of shock-containing supersonic jets*. NASA TM 84521 http://naca.larc.nasa.gov/search.jsp?R=19820025274&qs=N%3D4294966788%2B4294879153%2B4294747441

[21] Pattison J., Celoto S., Khan A, O'Neill W. 2008. *Standoff distance and bow shock phenomena in the cold spray process.* Surf Coat Technol. 202: 1443-54

[22] Srivatsan V.R, Dolatabadi A. 2006. *Simulation of particle-shock interaction in a high velocity oxygen fuel process.* Proceedings of the International Thermal Spray Conference. Seattle, Washington. 481-7

[23] Morgan R., Fox P., Pattison J., Sutcliffe C., O'Neill W. 2004. *Analysis of cold gas dynamically sprayed aluminium deposits.* Mater Lett. 58 : 1317-20.

[24] Yin S., Wang X., Li W., Xu B. 2010. *Numerical study on the effect of substrate angle on particle impact velocity and normal velocity component in cold gas dynamic spraying based on CFD.* J. Therm. Spray Technol. 19 : 1155-62.

[25] Huynh D. 2013. *Experimental design of a shock tube for the time response study of porous pressure sensitive paint.* MaSc Thesis. University of Ohio, Ohio.

[26] Cadney S., Brochu M., Richer P., Jodoin B. 2008. *Cold gas dynamic spraying as a method for freeforming and joining materials.* Surf Coat Technol. 202 : 2801-6.

[27] Villafuerte J., VAnderzwer D., Yandouzi M., Jodoin B. 2009. *Shockwave induced spraying.* Adv Mater Processes. 167 : 32-4.

[28] Karimi M. 2012**.** *Advancement of shock wave induced spraying process through the study of gas and particle flow fields*. PhD Thesis. University of Windsor. Windsor, Ontario.

[29] Elder F.K. Jr., De Haas N. 1952. *Experimental study of the formation of a vortex ring at the open end of a cylindrical shock tube.* J. Appl. Phys. 23 : 1065-9.

[30] Baird J.P. 1987. *Supersonic vortex rings.* Proceedings of the Royal Society of London.Series A, Mathematical and physical sciences. 409 : 59-65.

[31] Glezer A., Coles D. 1999. *An experimental study of a turbulent vortex ring*. J. Fluid Mech, 211, pp 243-283.

[32] Settles G., Torbe P., Lori J., Miller J.D., Datto J. 2005. *Full-scale high-speed schlieren imaging of explosions and gunshots.* Proceedings of SPIE-International Society for Optical Engineering. 5580 : 60-8.

[33] Ishii R., Fujimoto H., Hatta N., Umeda Y. 1999. *Experimental and numerical analysis of circular pulse jets.* J. Fluid Mech. 392 : 129-53.

[34] Arakeri J.H., Das D., Krothapalli A., Lourenco L. 2004. *Vortex ring formation at the open end of a shock tube: A particle image velocimetry study.* Phys. Fluids. 16 : 1008-19.

[35] Endo M., Iwamoto J. 1999. *A study of pulsatile jet discharged from pipe end.* J. Visualization. 1 : 261-9.

[36] Gaetani P., Guardone A., Persico G. 2008. *Shock tube flows past partially opened diaphragms.* J. Fluid Mech. 602 : 267-86.

[37] Kim H.D., Setoguichi T. 1999. *Study of the discharge of weak shocks from an open end of a duct.* J. Sound Vibrat. 226 : 1011-42.

[38] Endo M., Futagami Y., Iwamoto J. 2000. *Relation between the flow pattern downstream of duct and the noise.* JSAE Rev. 21 : 125-32.

[39] Kimura A., Iwamoto J. 2002. *A study on generation of noise by high-speed pulsating jets.* J. Visualization. 5 : 371-9.

[40] Deardorff D. 2000. *Introduction to measurements and error analysis.* University of North Carolina, North Carolina. http://user.physics.unc.edu/~deardorf/uncertainty/UNCguide.html

Appendices

Appendix A LabVIEW Program

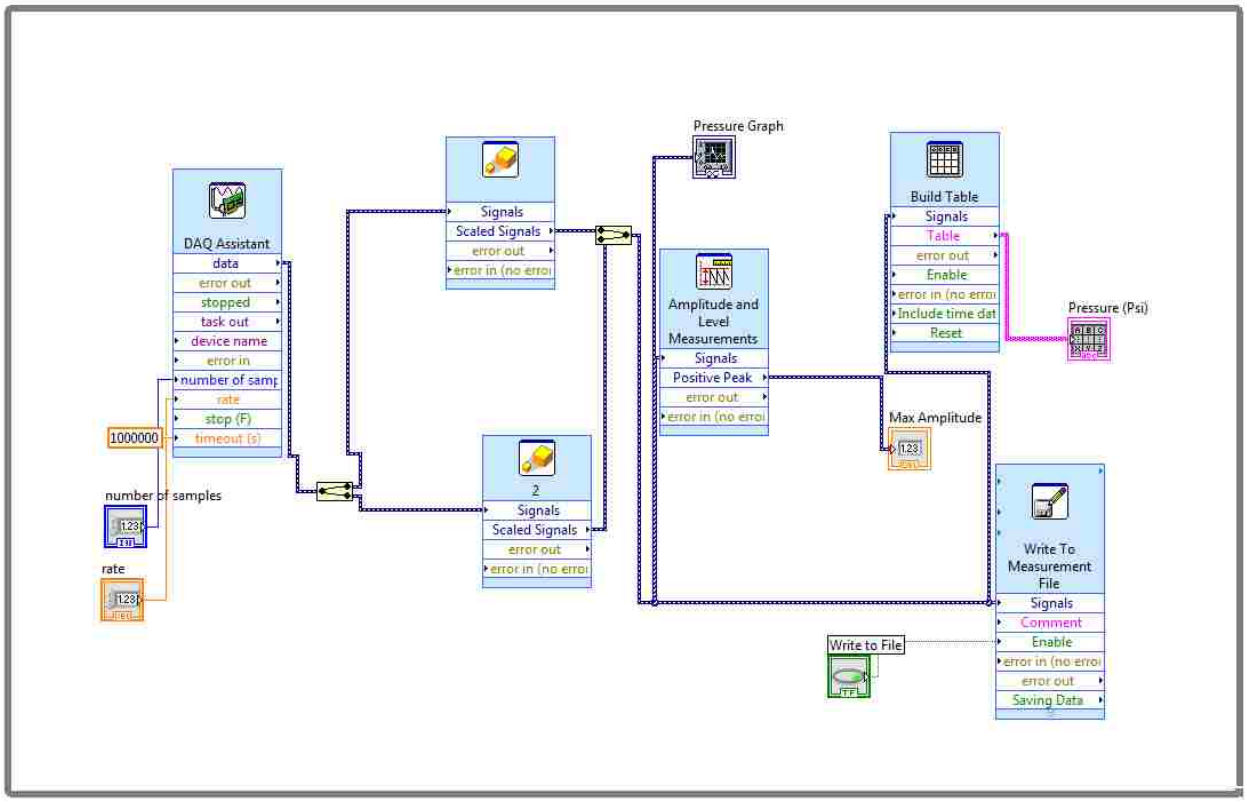

Figure A1 LabVIEW Code for Camera and Pressure Data

Appendix B Single Cycle Pressure Graphs

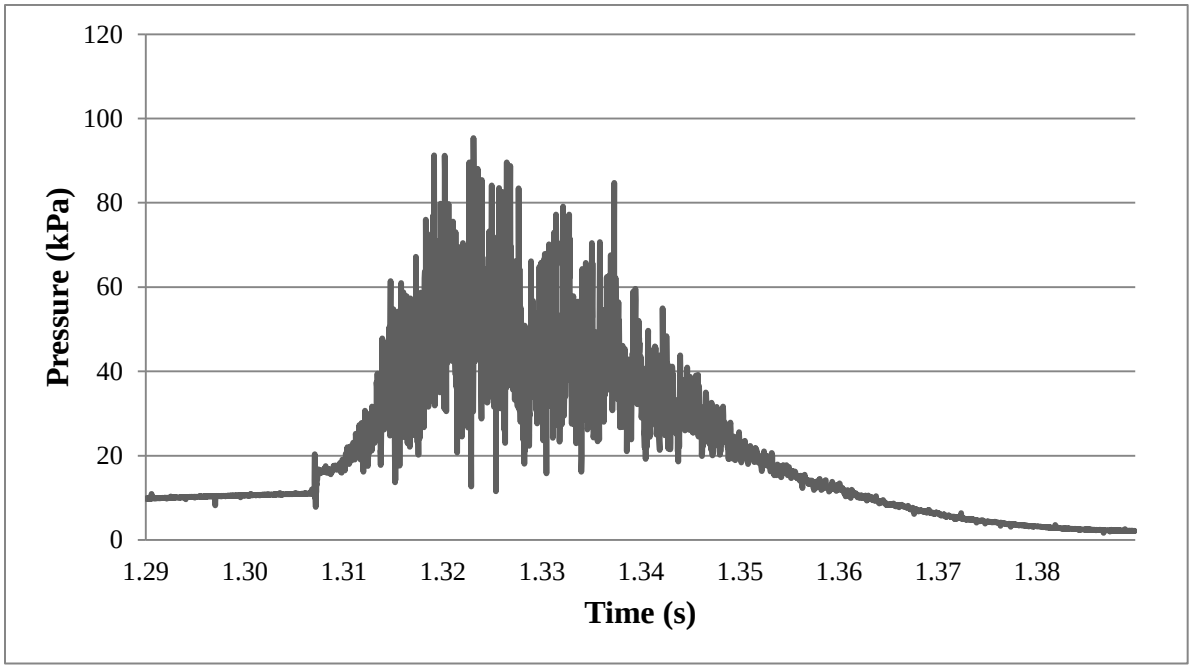

Figure B1 Single Cycle Pressure for a Supply Pressure of 2 MPa Firing at 5 Hz at 10mm SOD

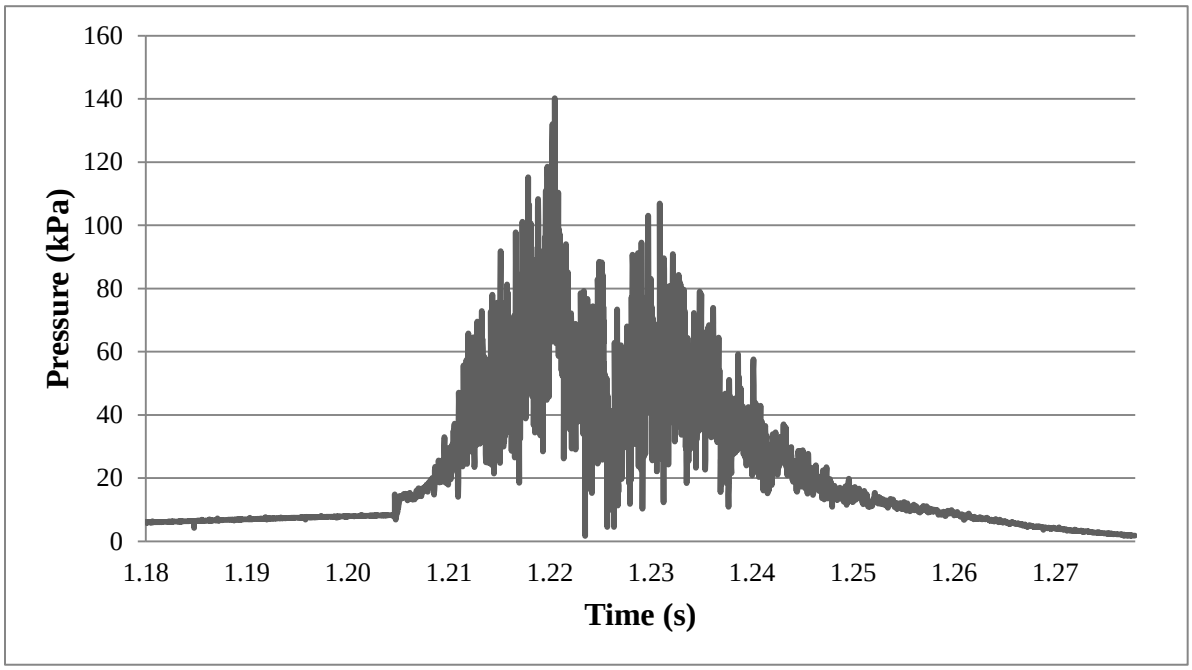

Figure B2 Single Cycle Pressure for a Supply Pressure of 2 MPa Firing at 5 Hz at 20mm SOD

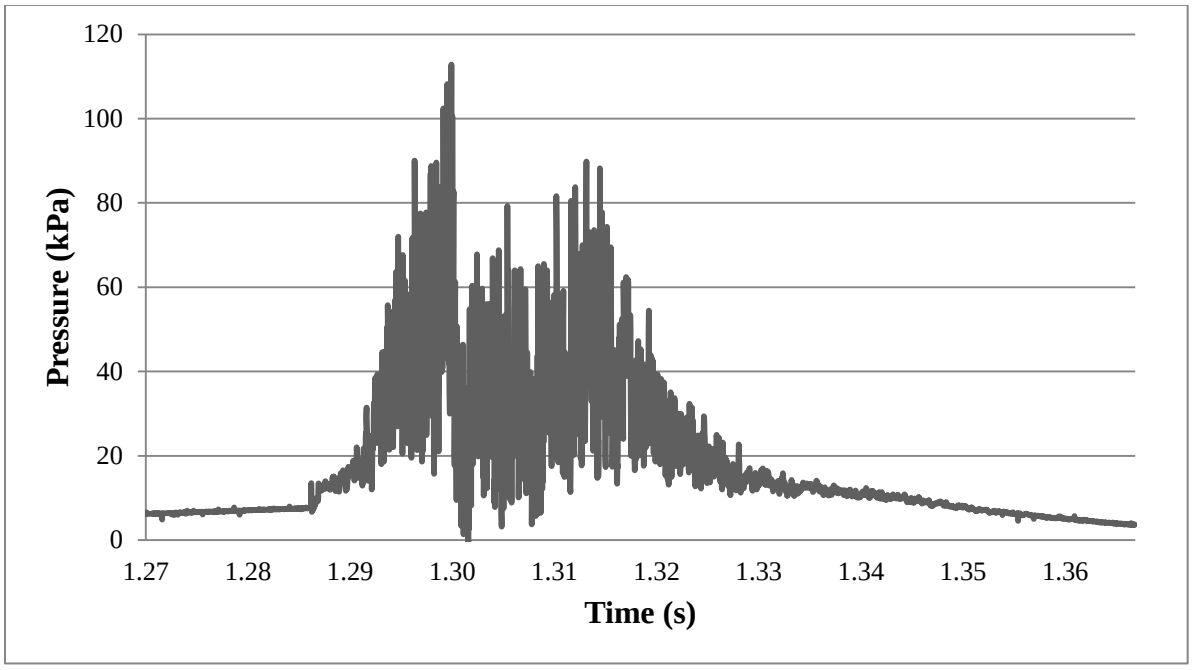

Figure B3 Single Cycle Pressure for a Supply Pressure of 2 MPa Firing at 5 Hz at 30mm SOD

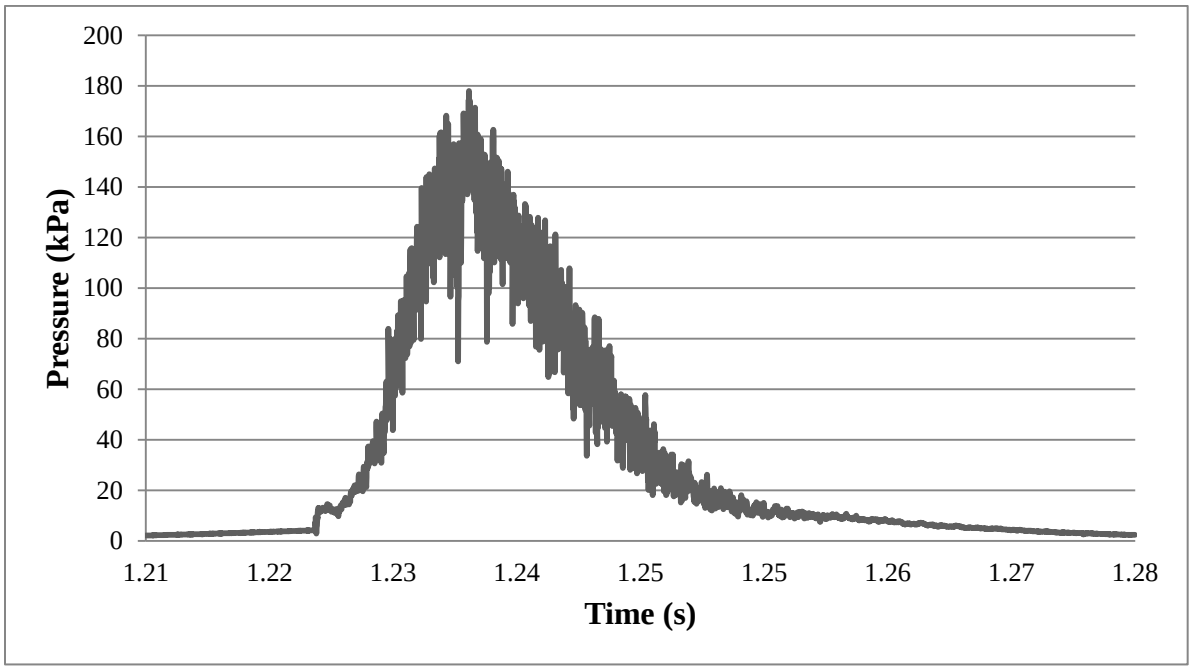

Figure B4 Single Cycle Pressure for a Supply Pressure of 2 MPa Firing at 10 Hz at 10mm SOD

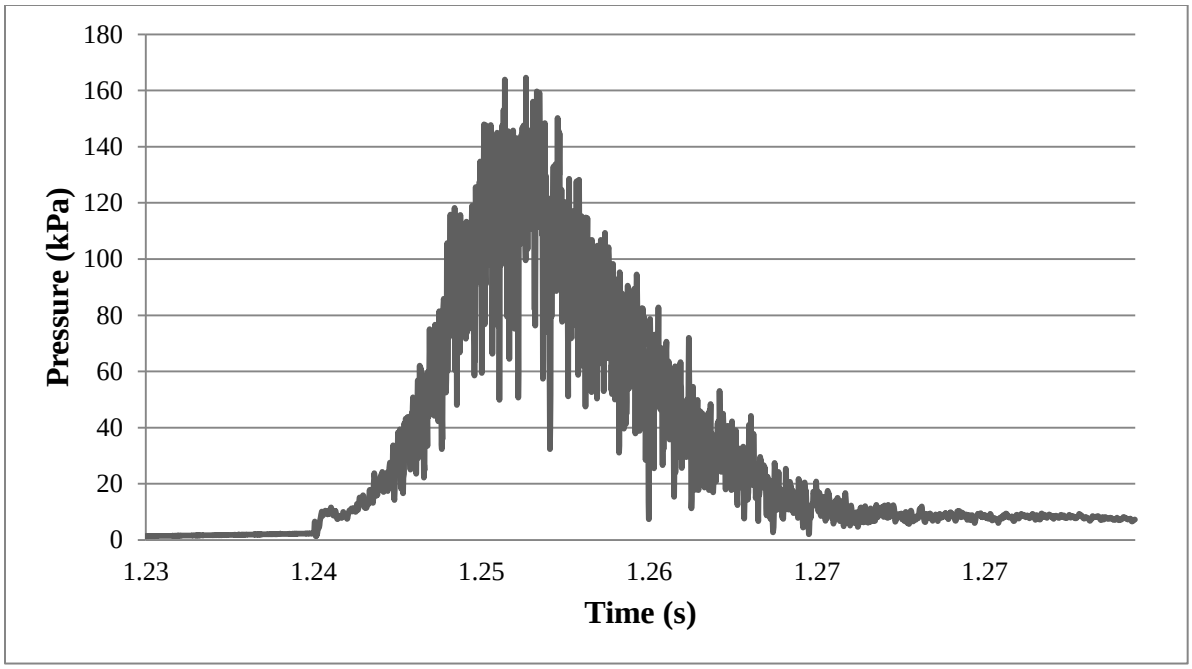

Figure B5 Single Cycle Pressure for a Supply Pressure of 2 MPa Firing at 10 Hz at 20mm SOD

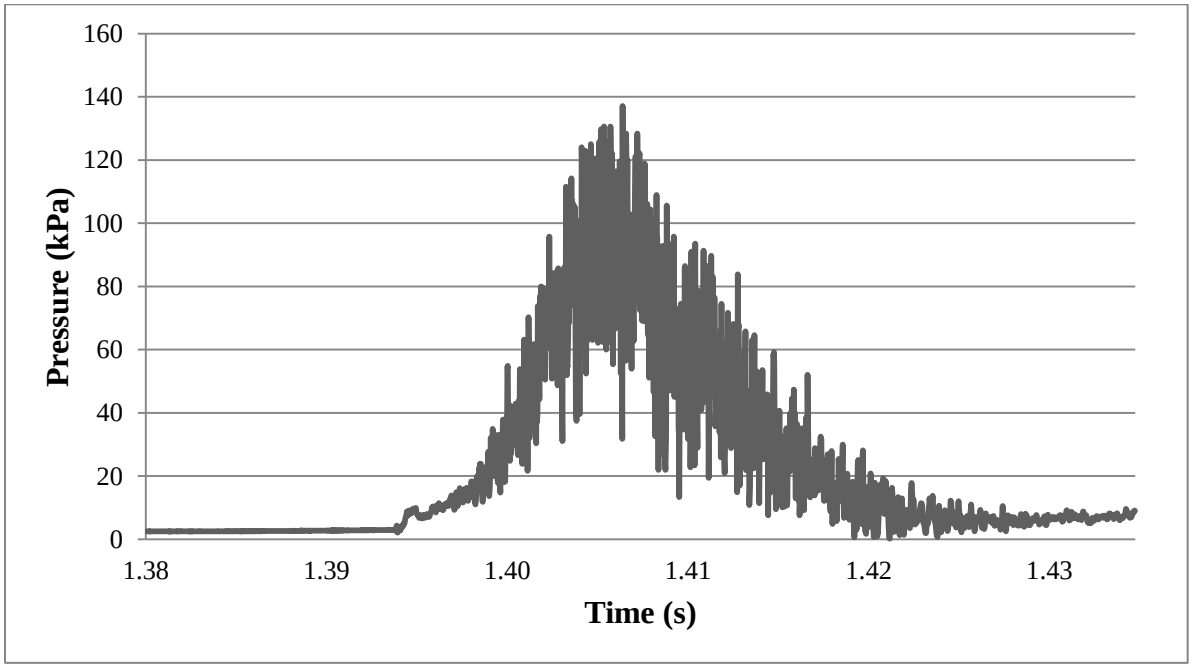

Figure B6 Single Cycle Pressure for a Supply Pressure of 2 MPa Firing at 10 Hz at 30mm SOD

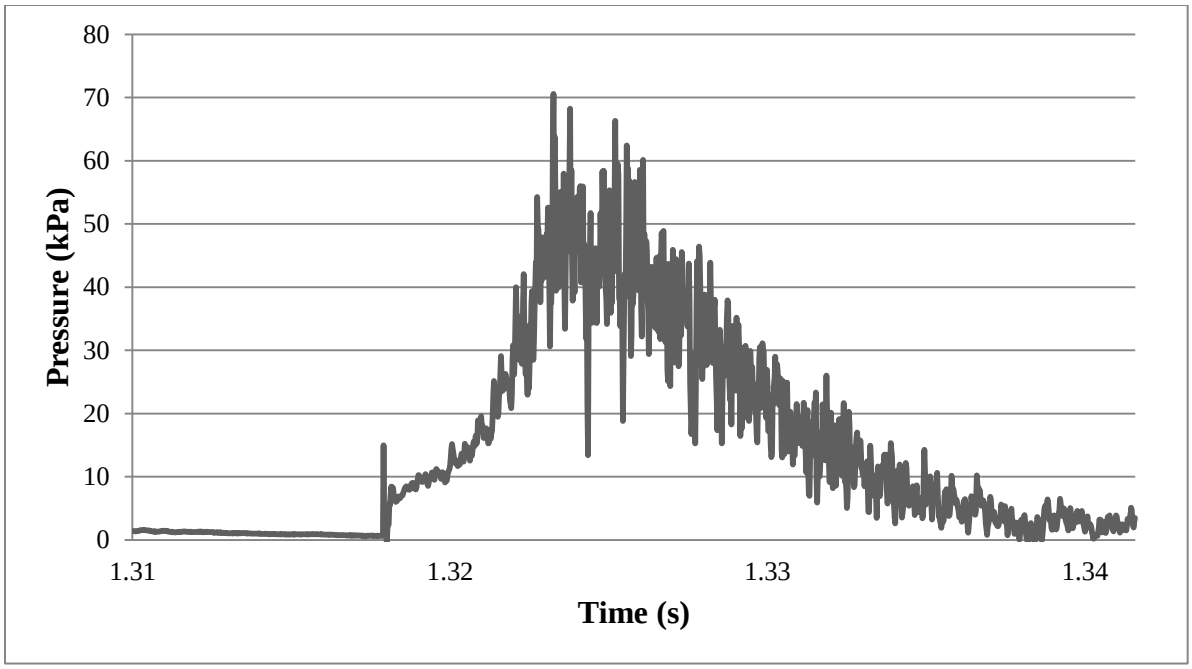

Figure B7 Single Cycle Pressure for a Supply Pressure of 2 MPa Firing at 20 Hz at 10mm SOD

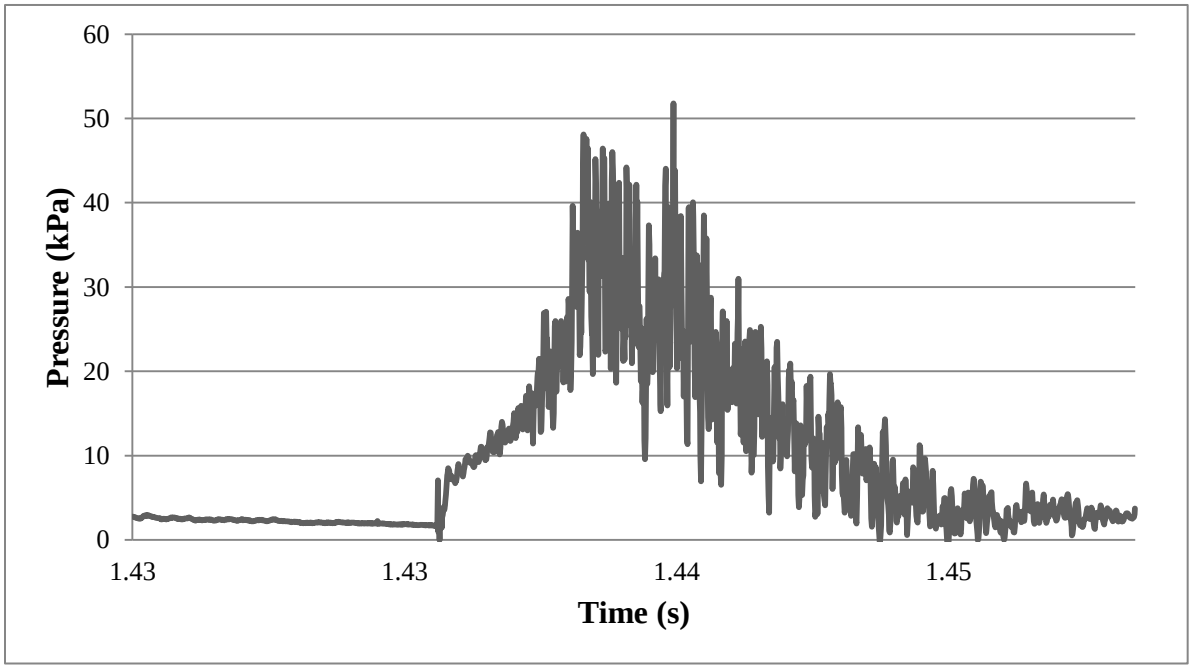

Figure B8 Single Cycle Pressure for a Supply Pressure of 2 MPa Firing at 20 Hz at 20mm SOD

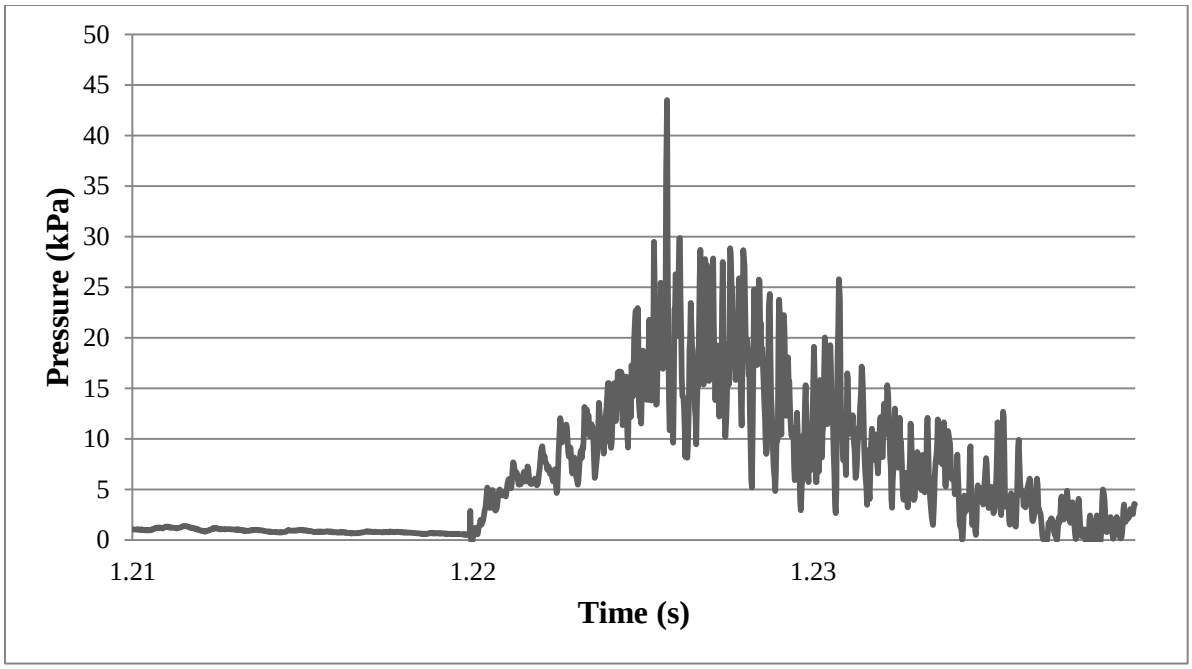

Figure B9 Single Cycle Pressure for a Supply Pressure of 2 MPa Firing at 20 Hz at 30mm SOD

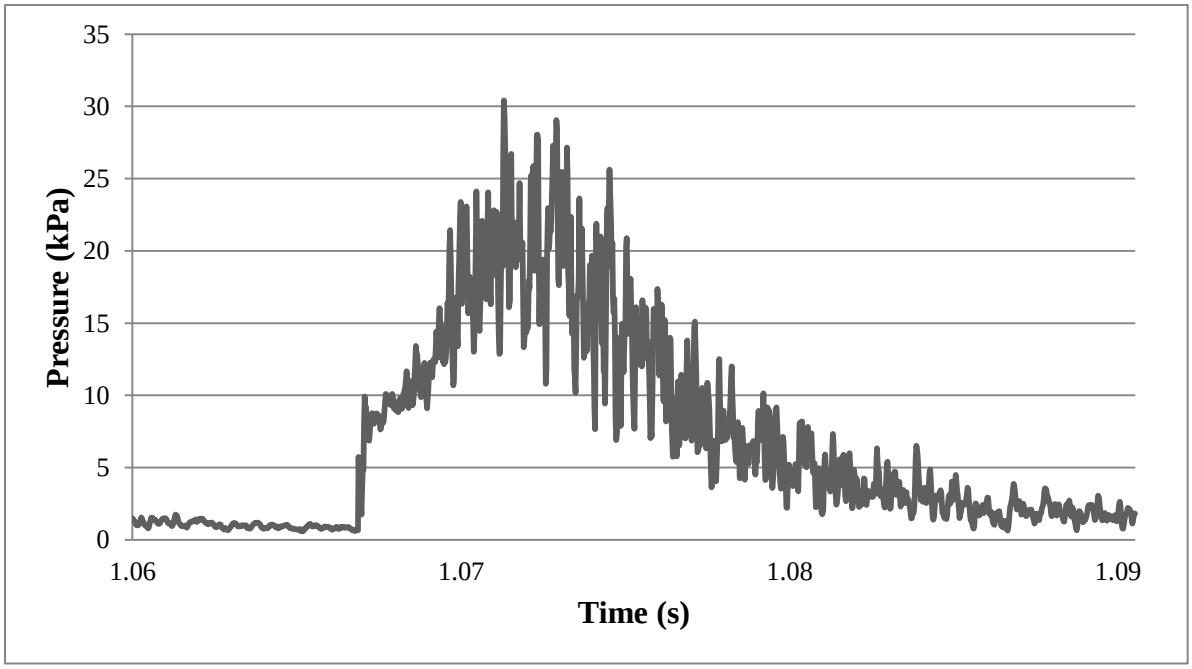

Figure B10 Single Cycle Pressure for a Supply Pressure of 2 MPa Firing at 30 Hz at 10mm SOD

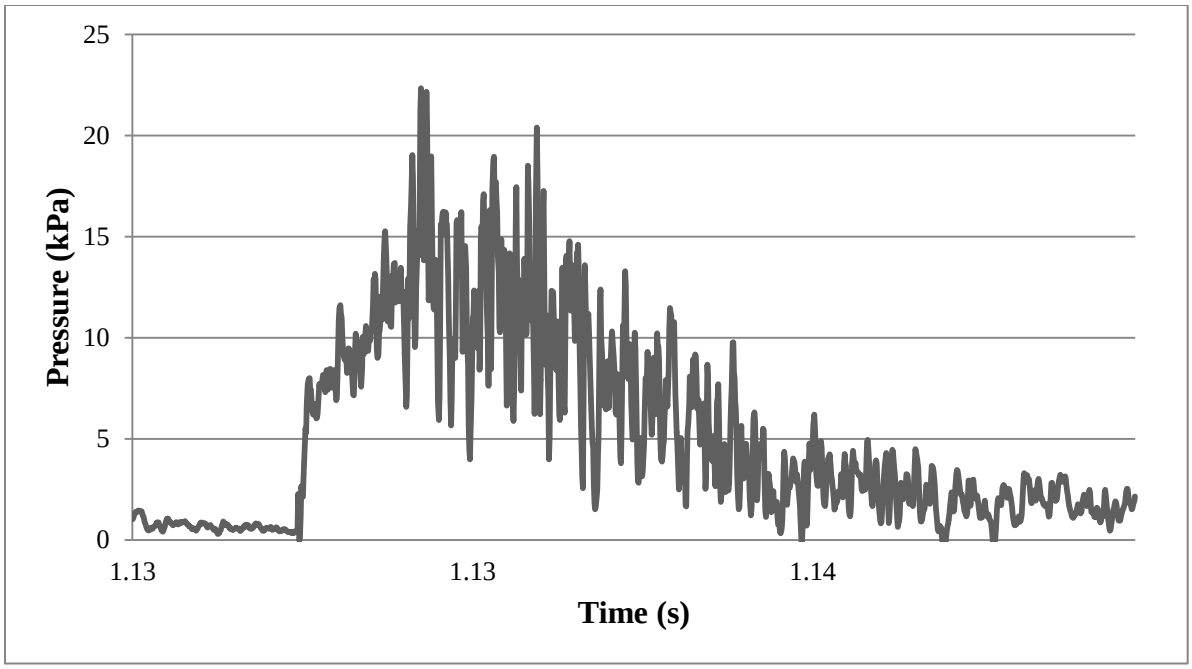

Figure B11 Single Cycle Pressure for a Supply Pressure of 2 MPa Firing at 30 Hz at 20mm SOD

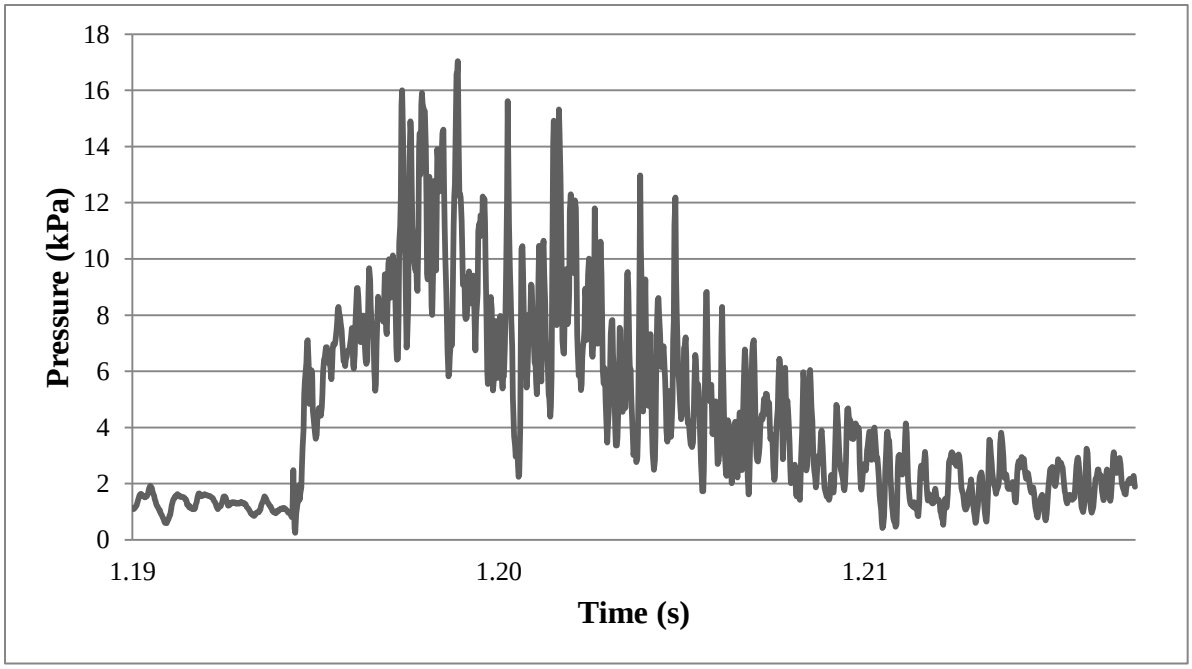

Figure B12 Single Cycle Pressure for a Supply Pressure of 2 MPa Firing at 30 Hz at 30mm SOD

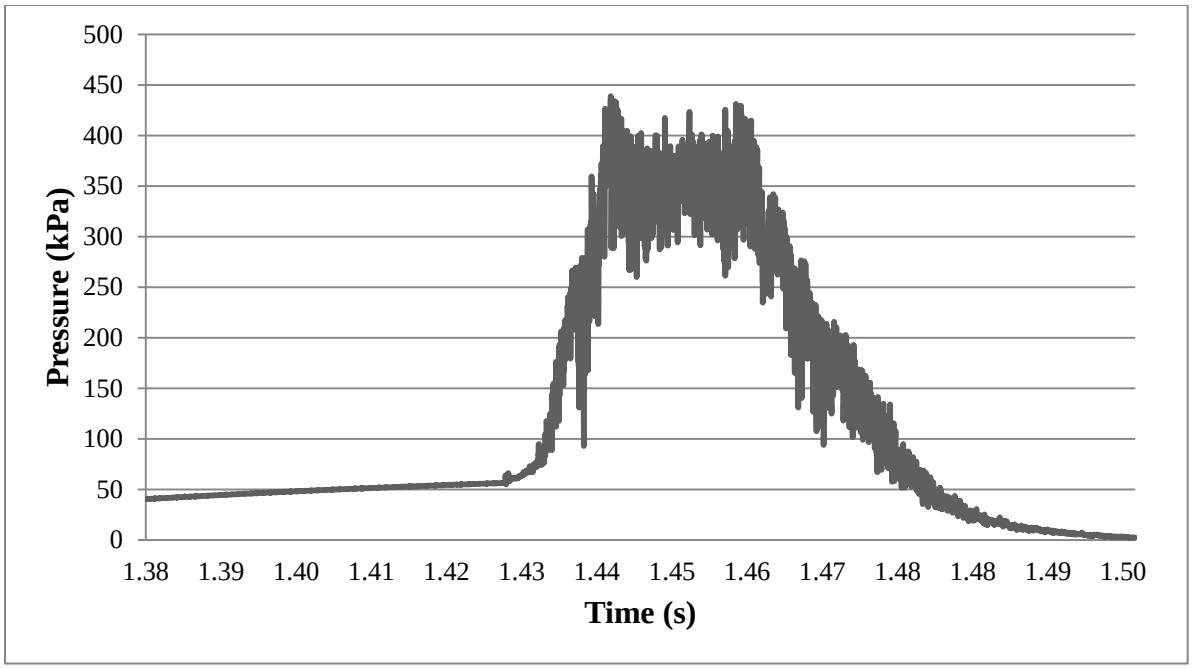

Figure B13 Single Cycle Pressure for a Supply Pressure of 3.45 MPa Firing at 5 Hz at 20mm SOD

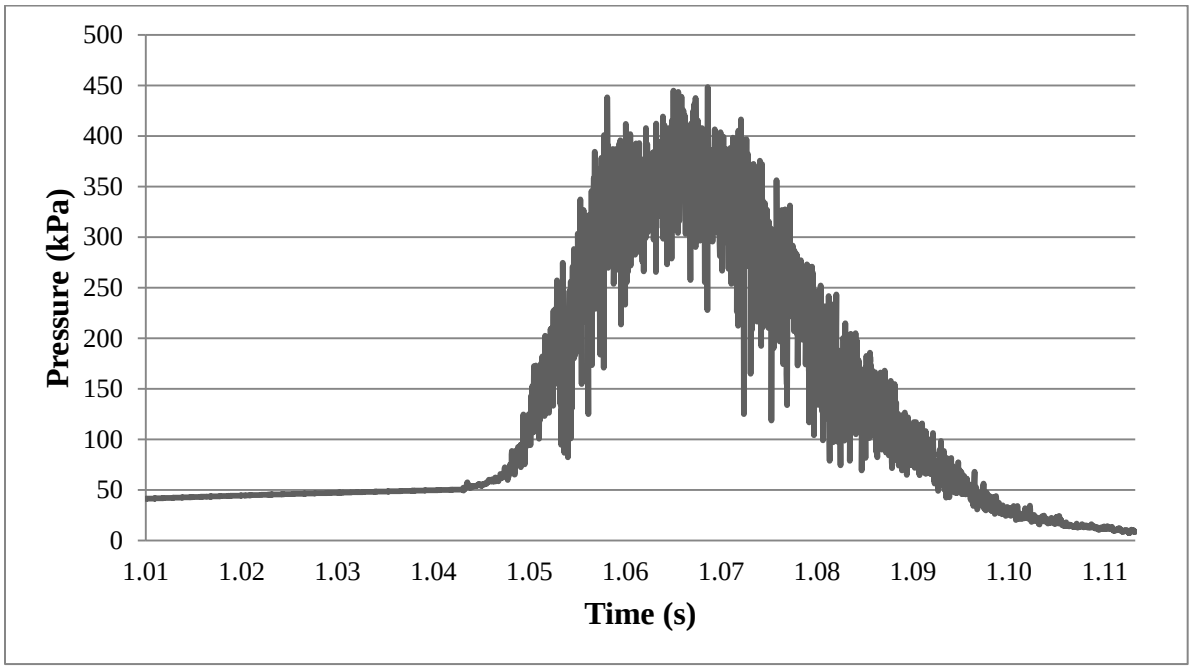

Figure B14 Single Cycle Pressure for a Supply Pressure of 3.45 MPa Firing at 5 Hz at 30mm SOD

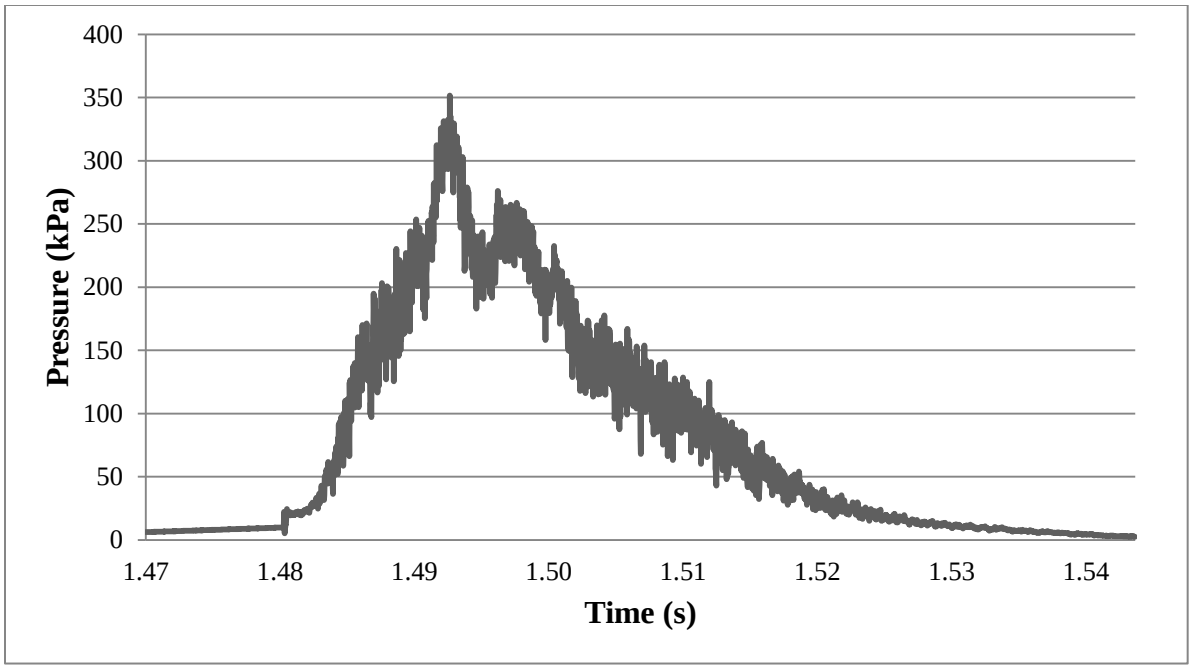

Figure B15 Single Cycle Pressure for a Supply Pressure of 3.45 MPa Firing at 10 Hz at 10mm SOD

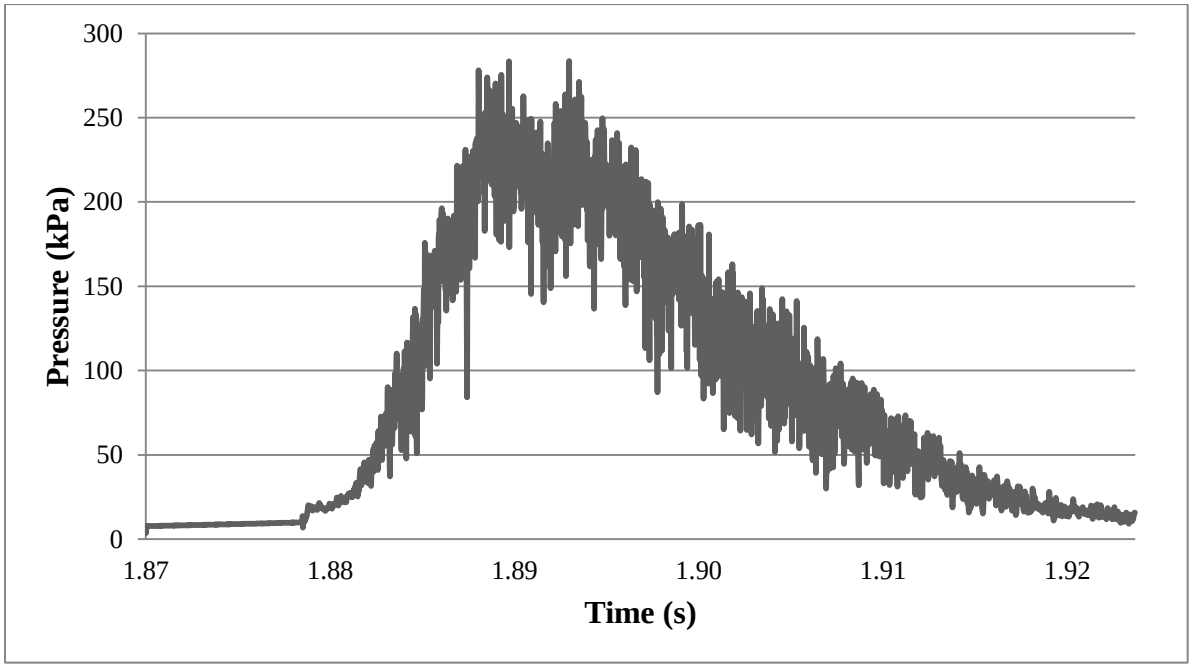

Figure B16 Single Cycle Pressure for a Supply Pressure of 3.45 MPa Firing at 10 Hz at 20mm SOD

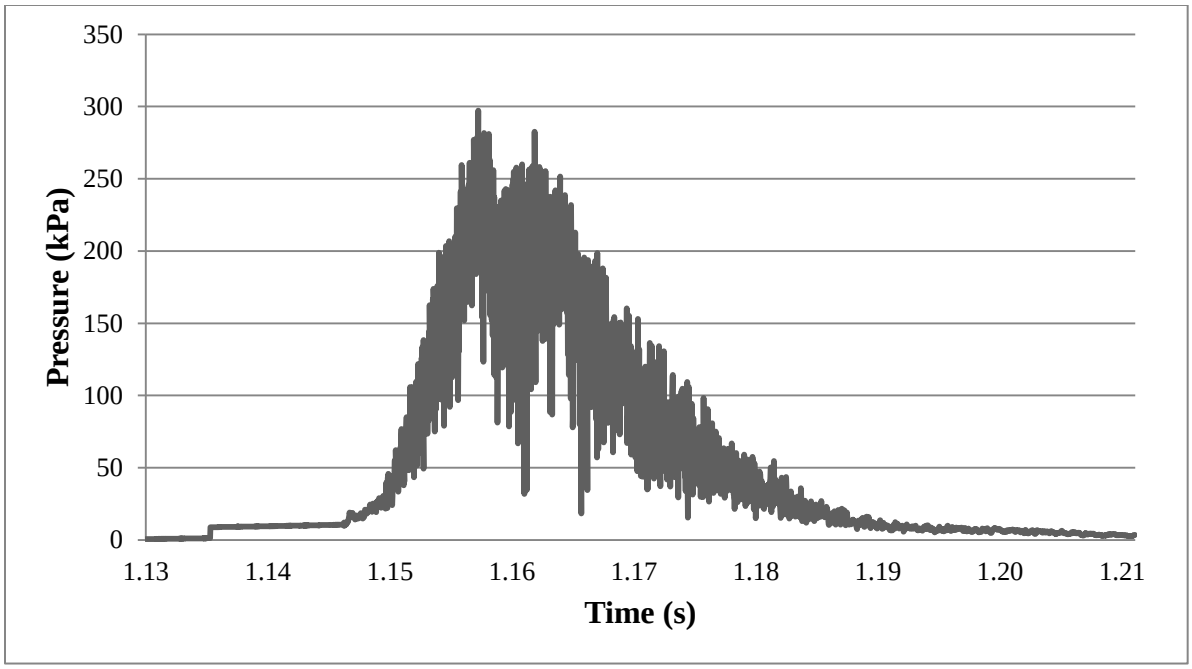

Figure B17 Single Cycle Pressure for a Supply Pressure of 3.45 MPa Firing at 10 Hz at 30mm SOD

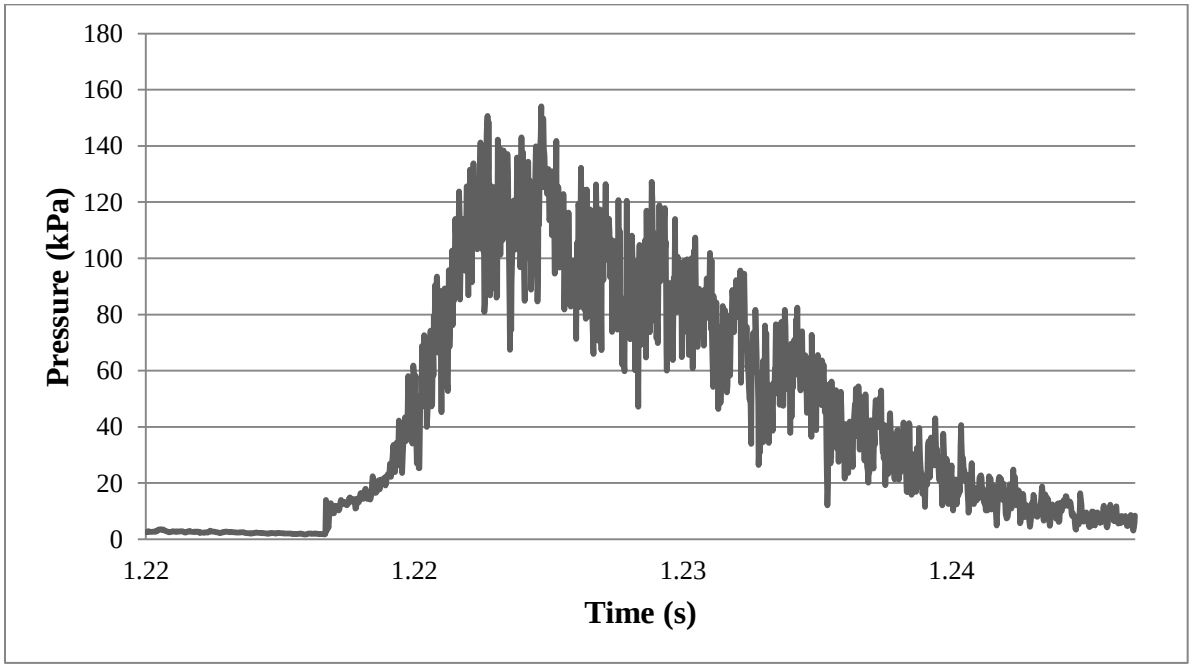

Figure B18 Single Cycle Pressure for a Supply Pressure of 3.45 MPa Firing at 20 Hz at 10mm SOD

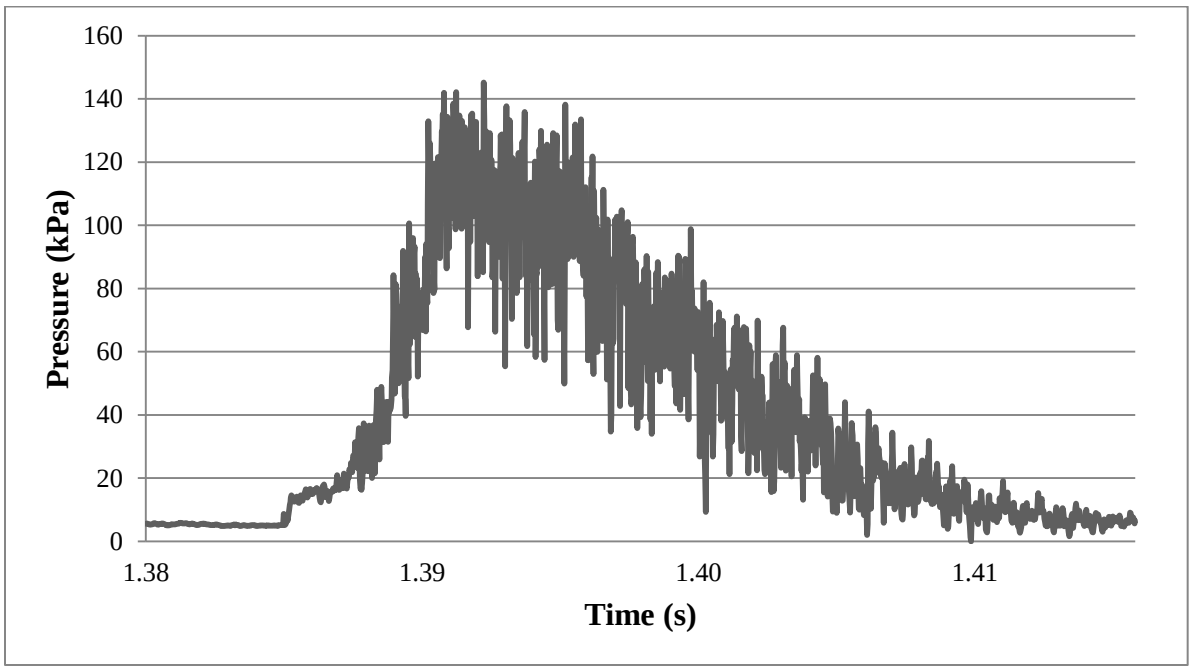

Figure B19 Single Cycle Pressure for a Supply Pressure of 3.45 MPa Firing at 20 Hz at 20mm SOD

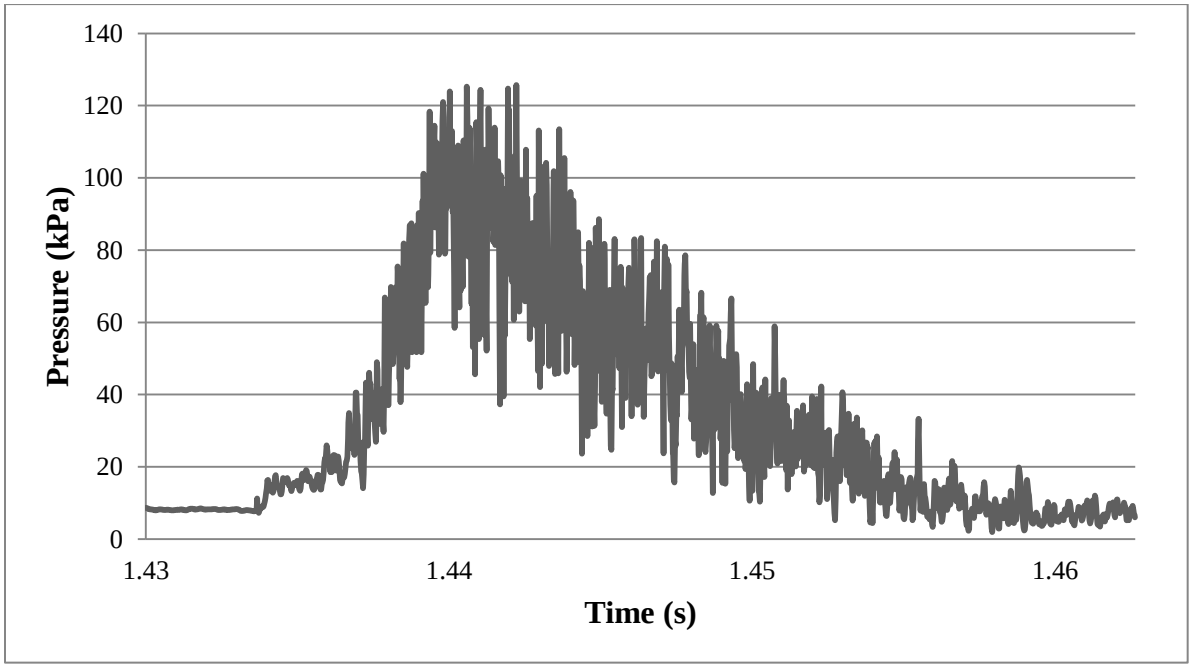

Figure B20 Single Cycle Pressure for a Supply Pressure of 3.45 MPa Firing at 20 Hz at 30mm SOD

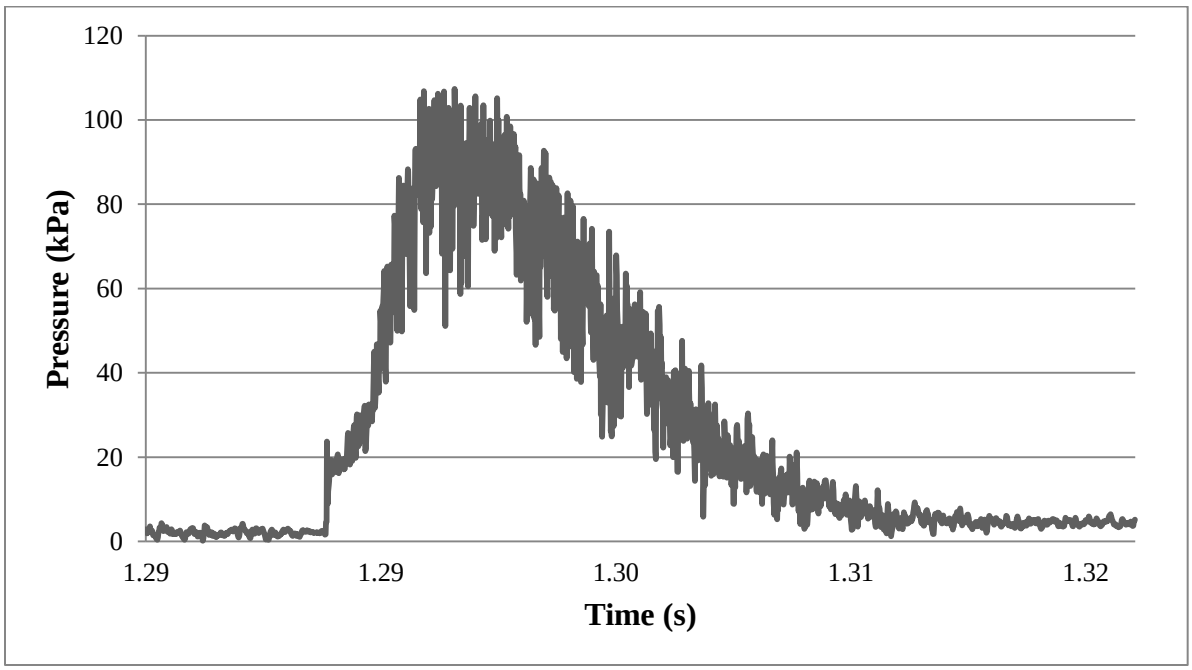

Figure B21 Single Cycle Pressure for a Supply Pressure of 3.45 MPa Firing at 30 Hz at 10mm SOD

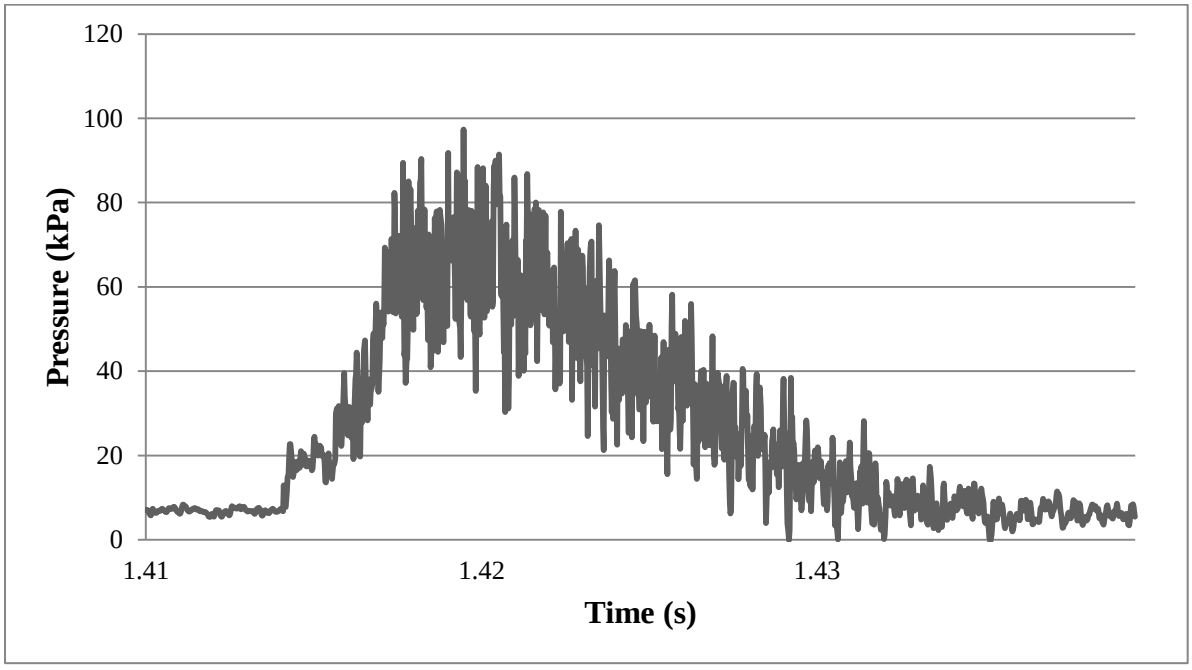

Figure B22 Single Cycle Pressure for a Supply Pressure of 3.45 MPa Firing at 30 Hz at 20mm SOD

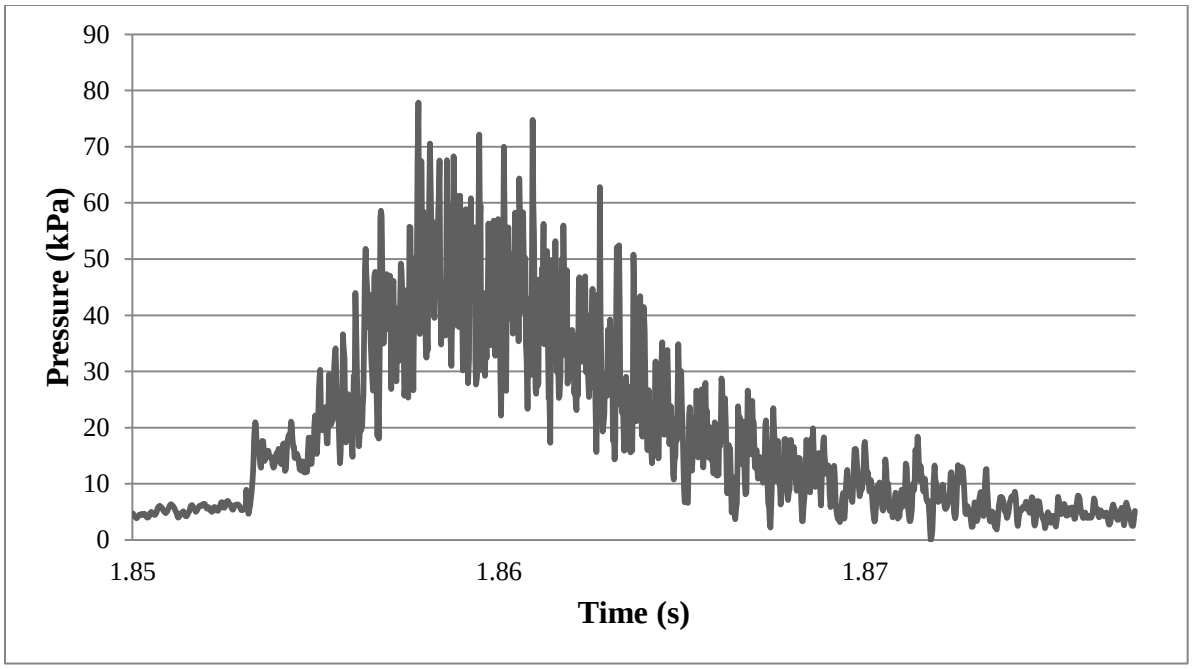

Figure B23 Single Cycle Pressure for a Supply Pressure of 3.45 MPa Firing at 30 Hz at 30mm SOD

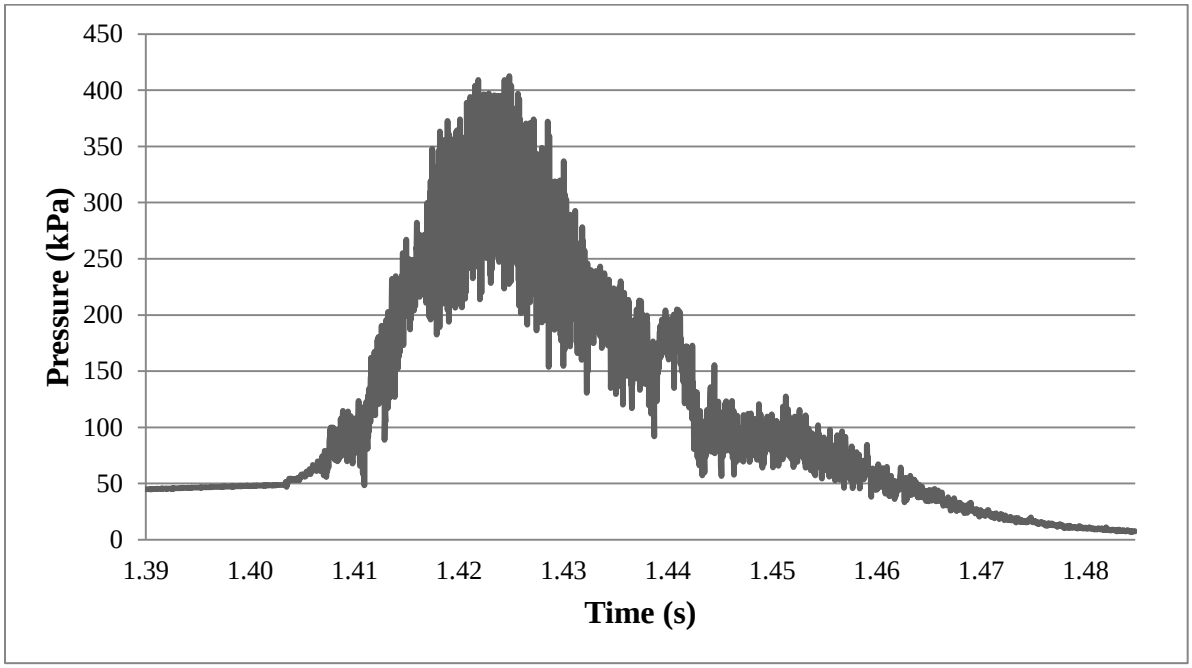

Figure B24 Single Cycle Pressure for a Supply Pressure of 4.8 MPa Firing at 5 Hz at 10mm SOD

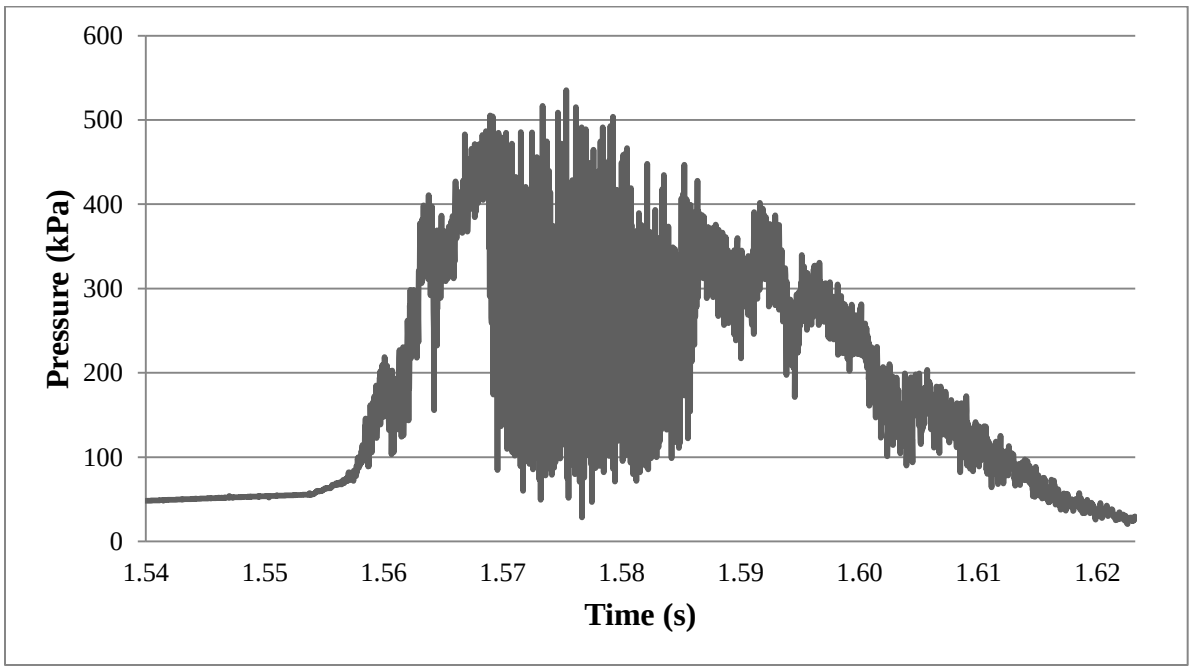

Figure B25 Single Cycle Pressure for a Supply Pressure of 4.8 MPa Firing at 5 Hz at 20mm SOD

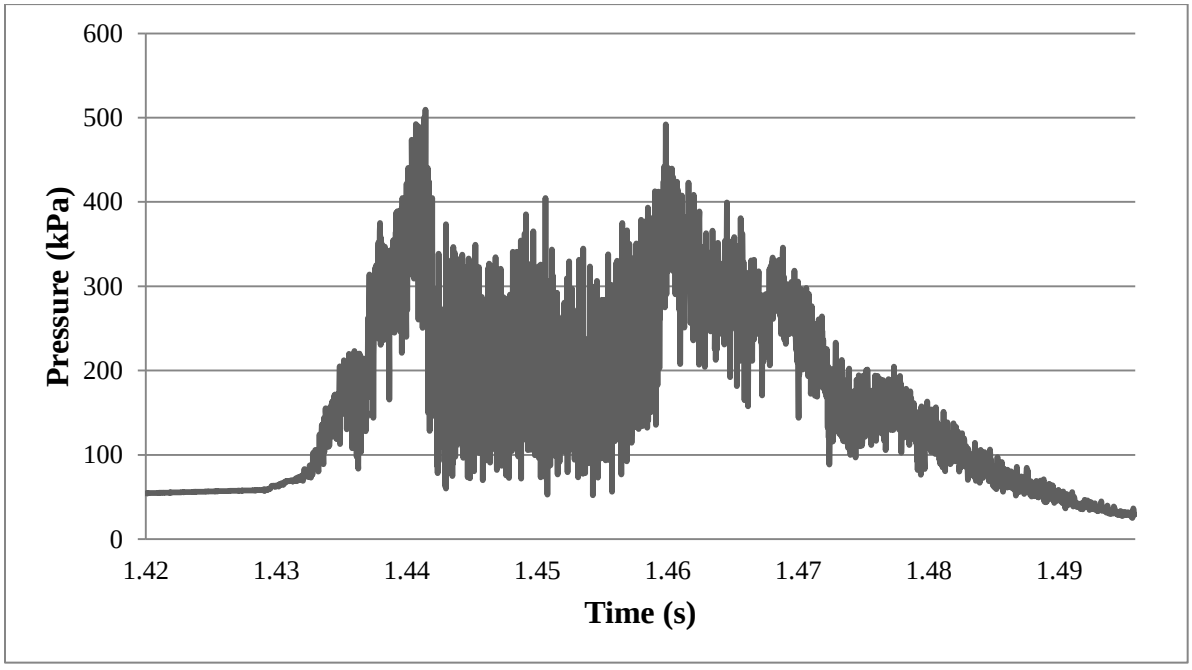

Figure B26 Single Cycle Pressure for a Supply Pressure of 4.8 MPa Firing at 5 Hz at 30mm SOD

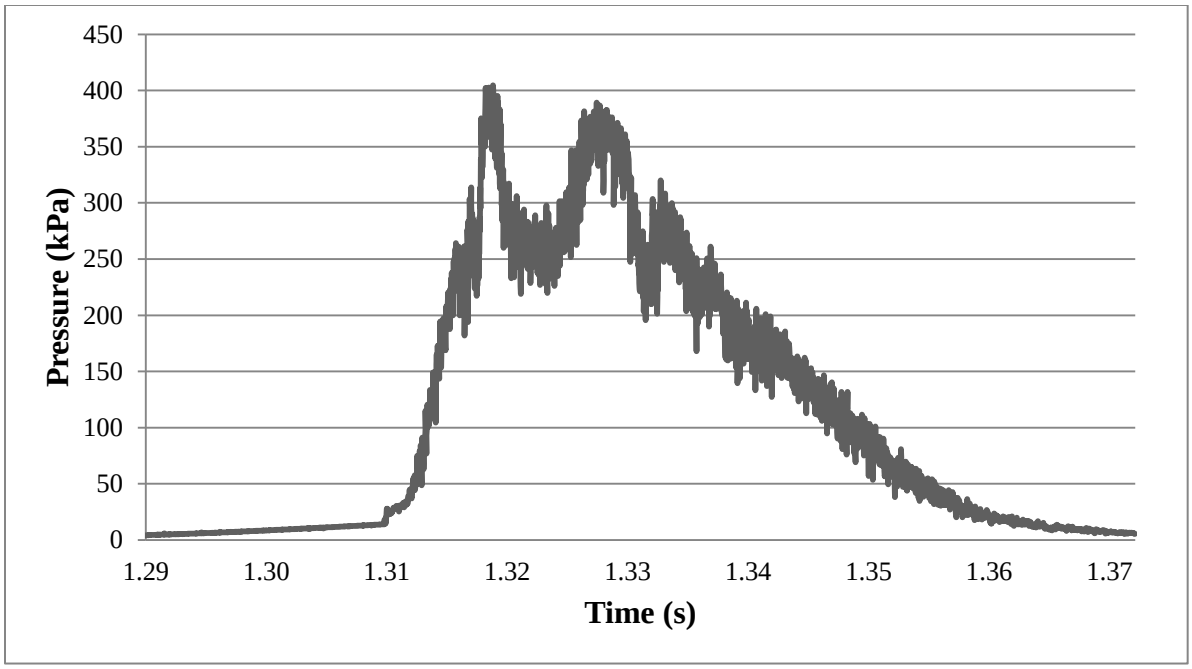

Figure B27 Single Cycle Pressure for a Supply Pressure of 4.8 MPa Firing at 10 Hz at 10mm SOD

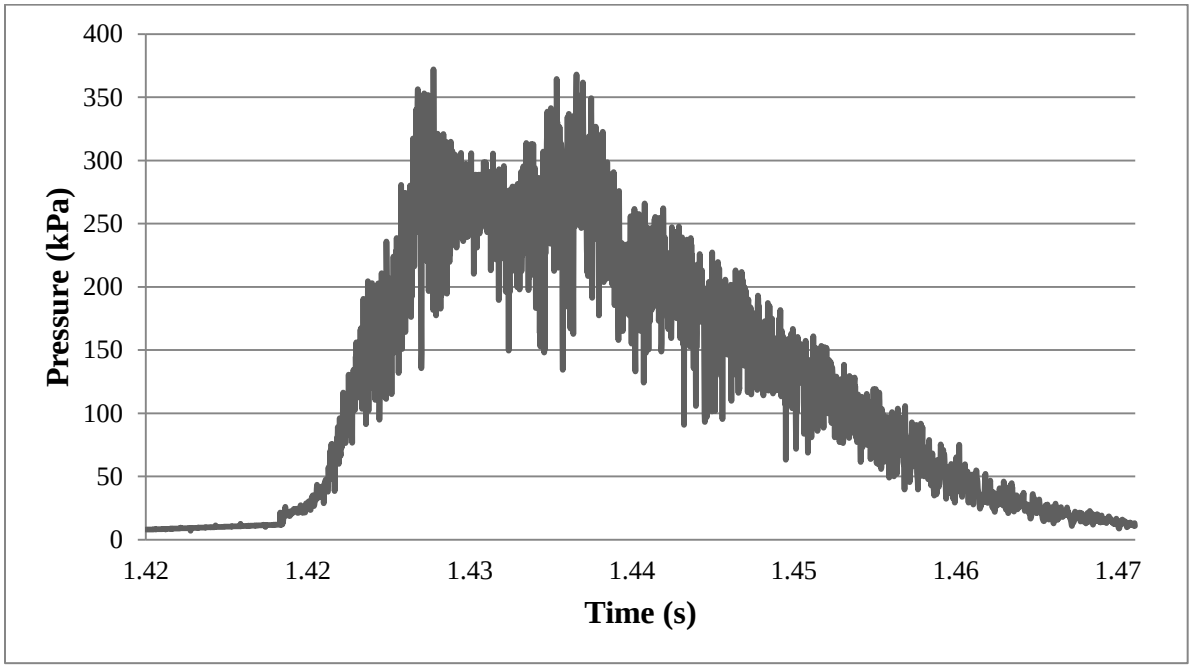

Figure B28 Single Cycle Pressure for a Supply Pressure of 4.8 MPa Firing at 10 Hz at 20mm SOD

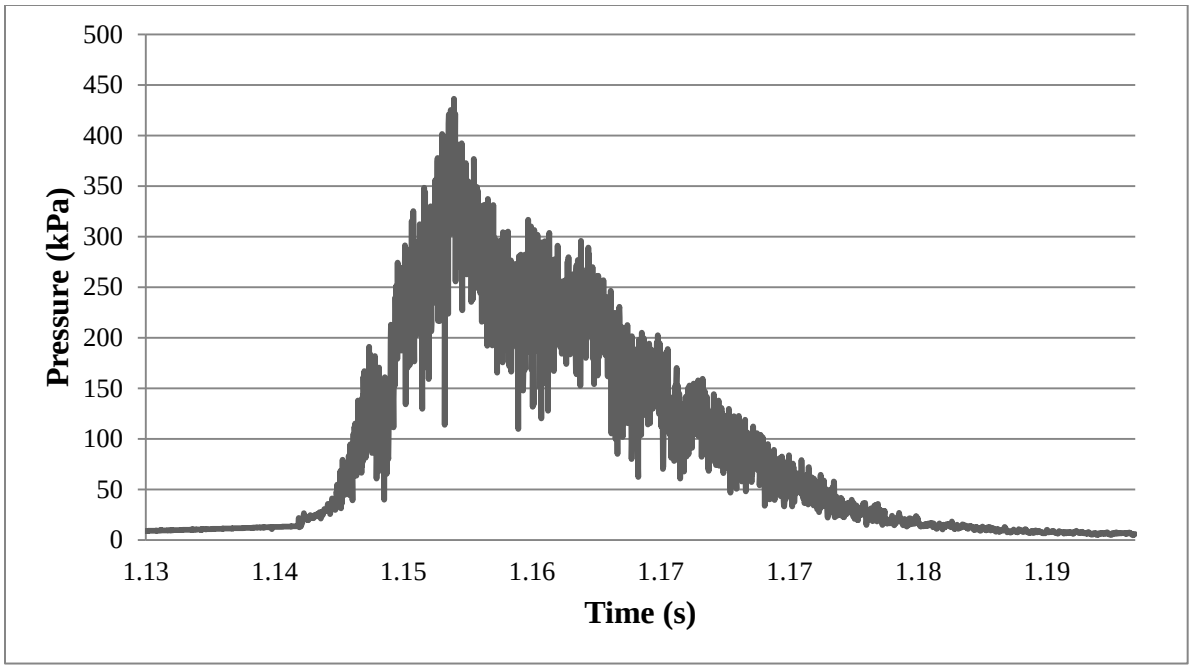

Figure B29 Single Cycle Pressure for a Supply Pressure of 4.8 MPa Firing at 10 Hz at 30mm SOD

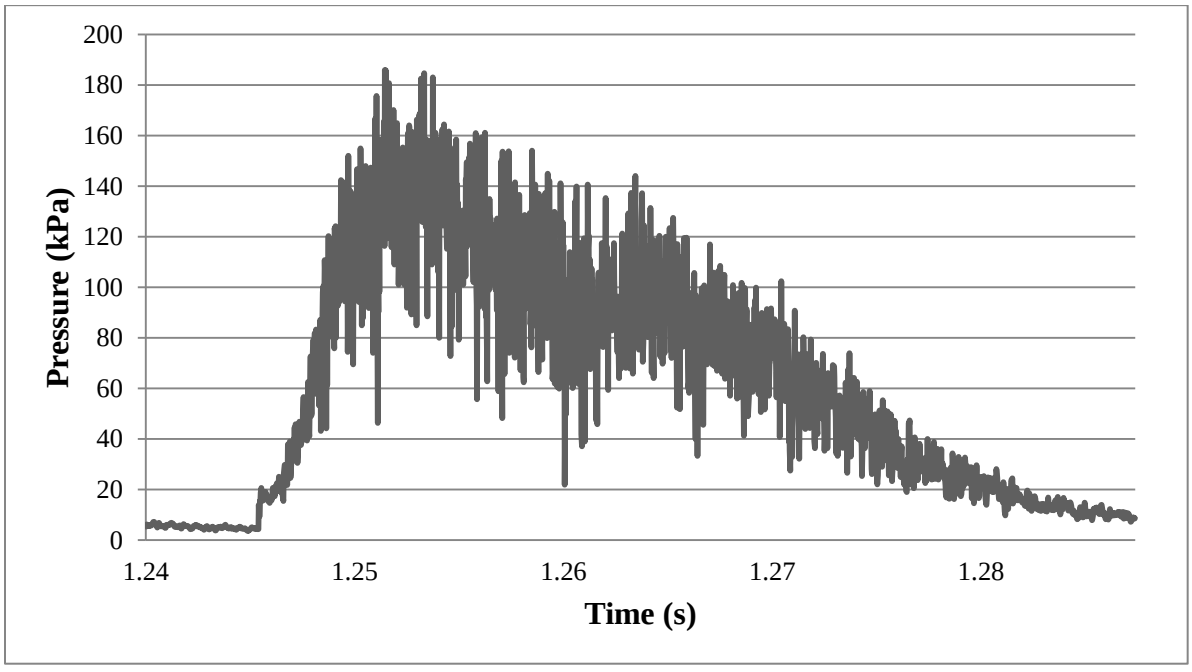

Figure B30 Single Cycle Pressure for a Supply Pressure of 4.8 MPa Firing at 20 Hz at 10mm SOD

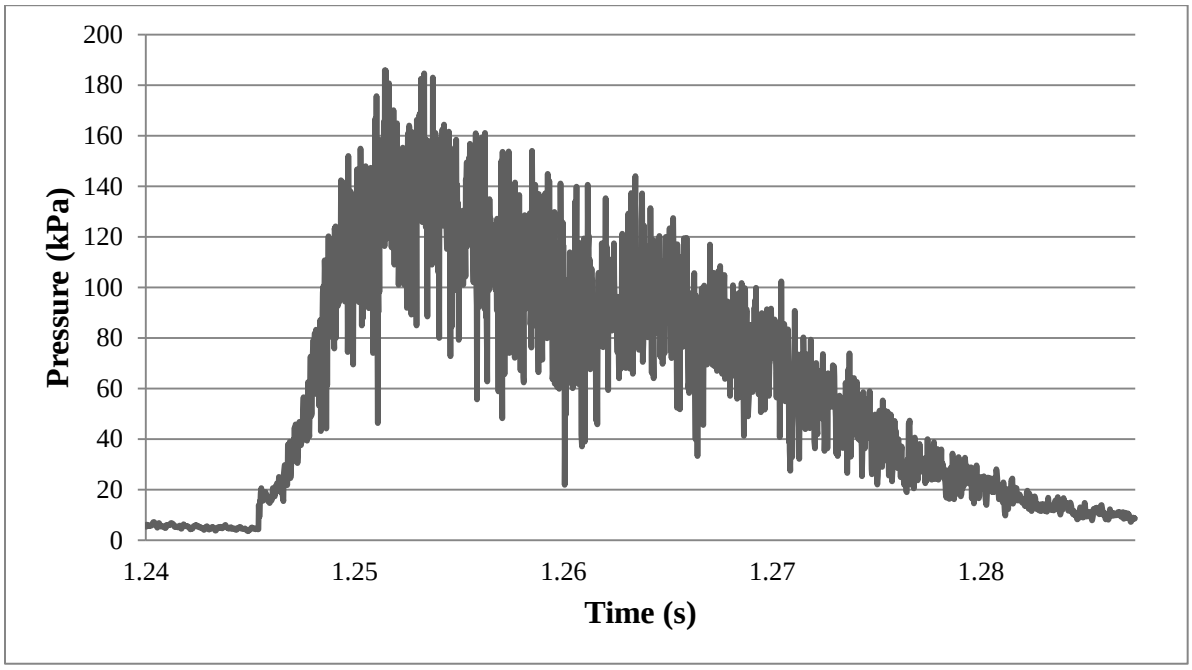

Figure B31 Single Cycle Pressure for a Supply Pressure of 4.8 MPa Firing at 20 Hz at 20mm SOD

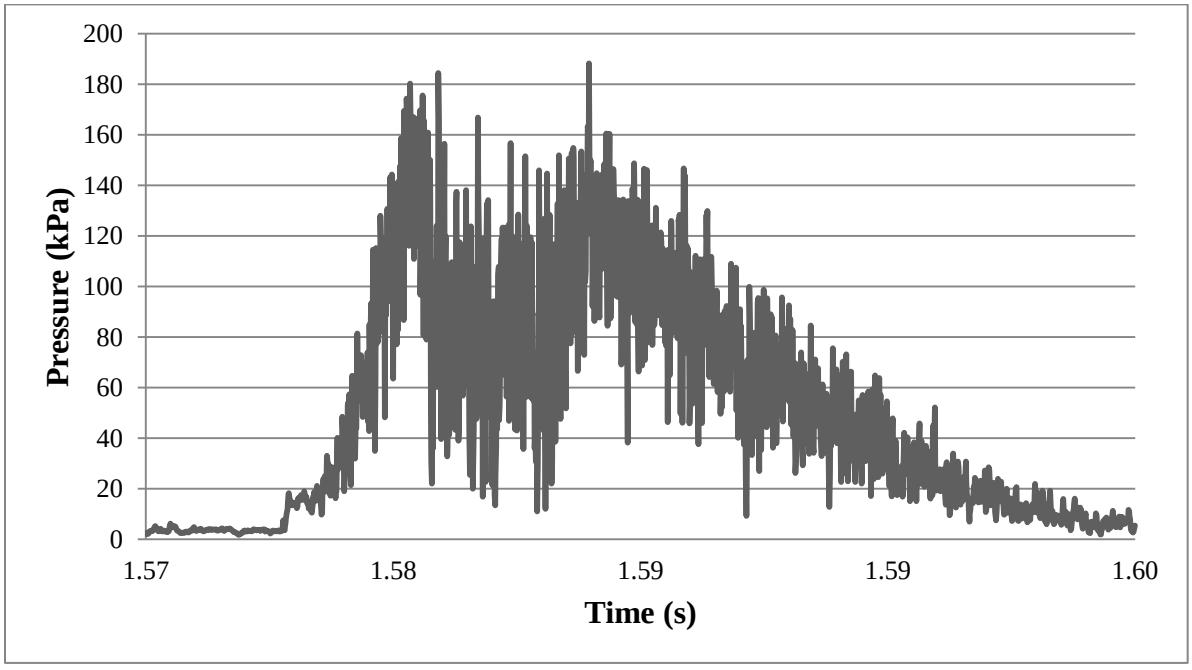

Figure B32 Single Cycle Pressure for a Supply Pressure of 4.8 MPa Firing at 20 Hz at 30mm SOD

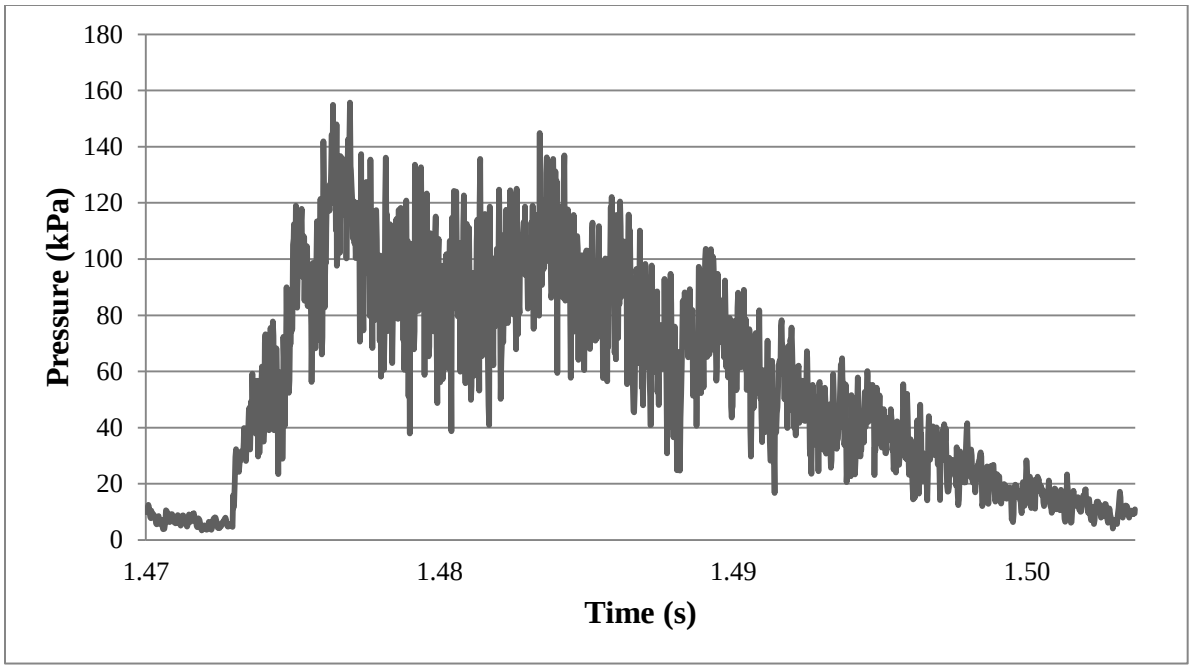

Figure B33 Single Cycle Pressure for a Supply Pressure of 4.8 MPa Firing at 30 Hz at 10mm SOD

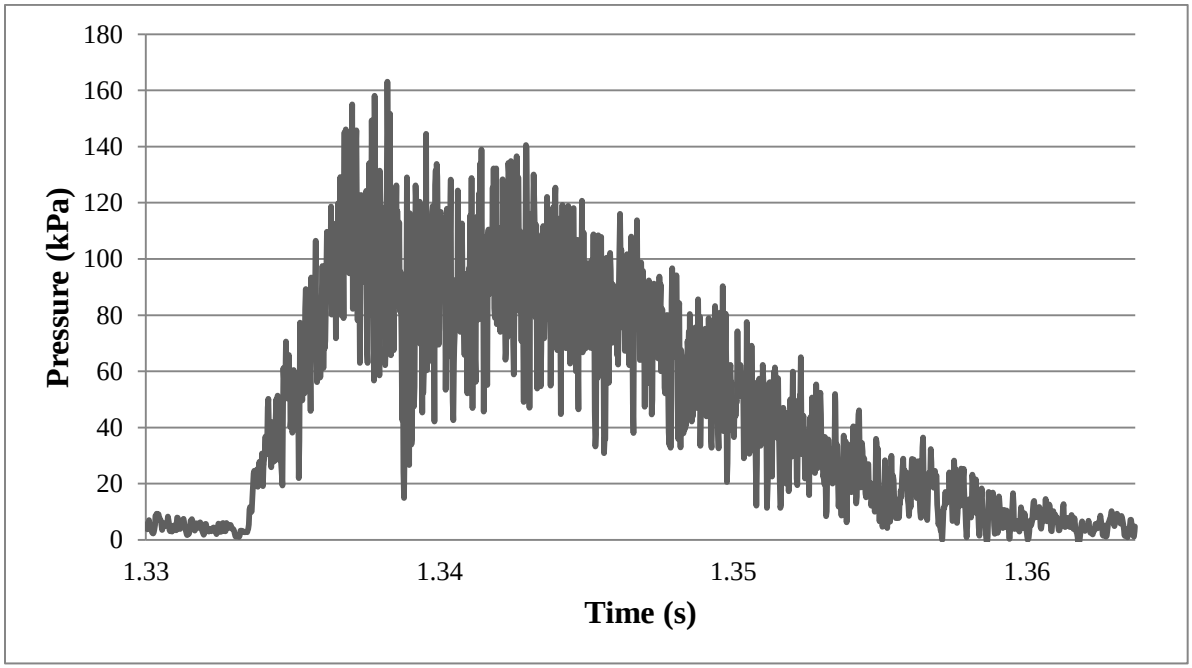

Figure B34 Single Cycle Pressure for a Supply Pressure of 4.8 MPa Firing at 30 Hz at 20mm SOD

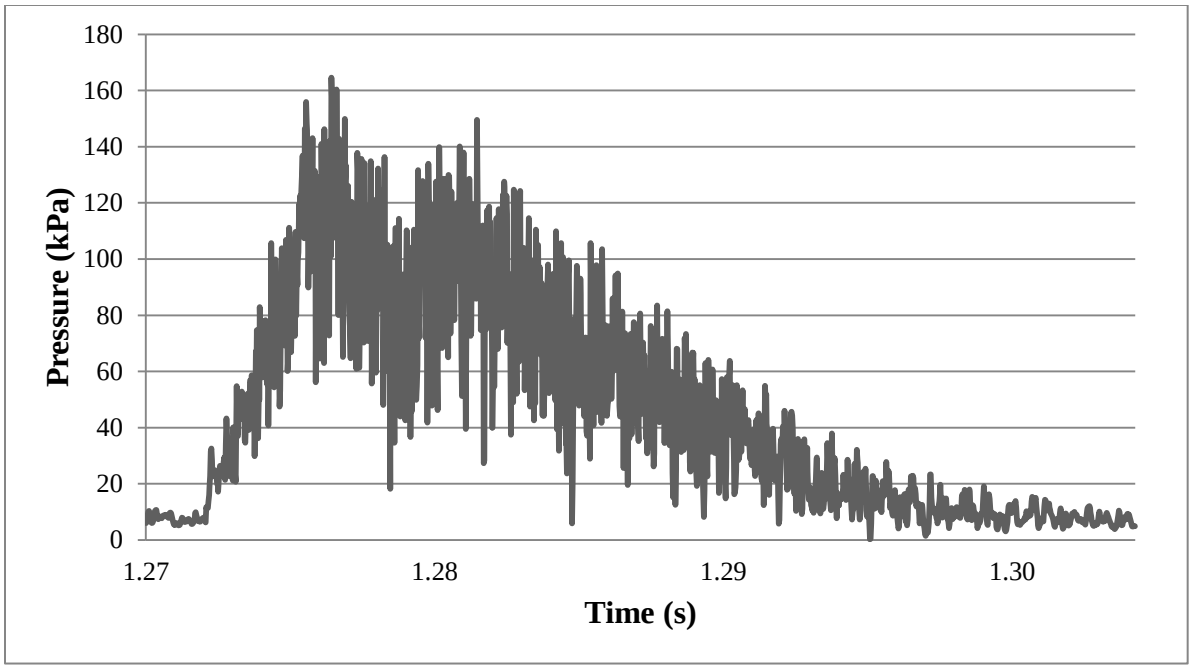

Figure B35 Single Cycle Pressure for a Supply Pressure of 4.8 MPa Firing at 30 Hz at 30mm SOD

Appendix C Frame Tables

***Note 0 = Not Seen**

Table C1 Frame Table for a Supply Pressure of 2 MPa Firing at 5 Hz at 10mm SOD

Event	Cycle 1	Cycle 2	Cycle 3	Cycle 4	Cycle 5
1	59792	68624	77289	85965	94778
2	59796	68627	77293	85969	94782
3	59797	68628	77294	85970	94783
4	59801	68637	77299	85976	94788
5	59813	68645	77310	85987	94798
6	59822	68657	77322	85997	94810
7	60037	68892	77546	86226	95041
8	60210	69031	77689	86369	95174
9	60347	69143	77836	86586	95391
10	61259	69893	78566	87269	96059
11	61543	70307	78966	87468	96291
12	68624	77289	85965	94778	103521

Table C2 Frame Table for a Supply Pressure of 2 MPa Firing at 5 Hz at 20mm SOD

Event	Cycle 1	Cycle 2	Cycle 3	Cycle 4	Cycle 5
1	60837	69541	78190	86937	95733
2	60840	69544	78193	86940	95736
3	60841	69545	78194	86941	95737
4	60845	69549	78198	86945	95742
5	60865	69570	78217	86963	75762
6	60877	69580	78229	86975	95772
7	61047	69786	78420	87195	95988
8	61284	70021	78642	87383	96185
9	61482	70162	78859	87636	96486
10	61985	70666	79351	88096	96870
11	62389	71039	79672	88487	97286
12	69541	78190	86937	95733	104489

Table C3 Frame Table for a Supply Pressure of 2 MPa Firing at 5 Hz at 30mm SOD

Event	Cycle 1	Cycle 2	Cycle 3	Cycle 4	Cycle 5
1	58928	67740	76471	85278	94108
2	58931	67743	76474	85281	94111
3	58932	67744	76475	85282	94112
4	58933	67746	76478	85284	94114
5	58967	67777	76509	85316	94147
6	58976	67787	76517	85325	94156
7	59116	67983	76690	85551	94350
8	59483	68303	77039	85802	94681
9	0	0	0	0	0
10	0	0	0	0	0
11	60316	69140	77705	86621	95469
12	67740	76471	85278	94108	102905

Table C4 Frame Table for a Supply Pressure of 2 MPa Firing at 10 Hz at 10mm SOD

Event	Cycle 1	Cycle 2	Cycle 3	Cycle 4	Cycle 5
1	53184	58654	64124	69596	75057
2	53188	58658	64128	69600	75061
3	53189	58659	64129	69601	75062
4	53193	58663	64132	69605	75065
5	53202	58672	64141	69614	75075
6	53218	58689	64158	69627	75088
7	53366	58863	64347	69815	75262
8	53549	58984	64462	69918	75395
9	0	0	0	0	0
10	0	0	0	0	0
11	54396	59851	65263	70703	76144
12	58654	64124	69596	75057	80542

Table C5 Frame Table for a Supply Pressure of 2 MPa Firing at 10 Hz at 20mm SOD

Event	Cycle 1	Cycle 2	Cycle 3	Cycle 4	Cycle 5
1	54113	59530	64988	70419	75884
2	54117	59534	64992	70423	75888
3	54118	59535	64992	70424	75889
4	54119	59536	64994	70425	75890
5	54139	59556	65015	70444	75909
6	54151	59568	65025	70456	75922
7	54229	59721	65176	70590	76095
8	54560	59981	65389	70810	76292
9	0	0	0	0	0
10	0	0	0	0	0
11	55144	60467	66085	71390	76782
12	59530	64988	70419	75884	81345

Table C6 Frame Table for a Supply Pressure of 2 MPa Firing at 10 Hz at 30mm SOD

Event	Cycle 1	Cycle 2	Cycle 3	Cycle 4	Cycle 5
1	56546	62008	67532	73037	78551
2	56550	62012	67535	73041	78555
3	56551	62013	67536	73042	78556
4	56551	62013	67537	73042	78556
5	56580	62043	67566	73071	78584
6	56588	62048	67571	73078	78590
7	56709	62179	67681	73239	78717
8	57080	62529	68049	73586	79068
9	0	0	0	0	0
10	0	0	0	0	0
11	57284	62860	68263	73802	79411
12	62008	67532	73037	78551	84120

Table C7 Frame Table for a Supply Pressure of 2 MPa Firing at 20 Hz at 10mm SOD

Event	Cycle 1	Cycle 2	Cycle 3	Cycle 4	Cycle 5
1	53328	55978	58622	61277	63927
2	53332	55982	58626	61281	63931
3	53333	55983	58627	61282	63932
4	53337	55987	58631	61286	63936
5	53346	55996	58640	61295	63945
6	53355	56006	58649	61305	63954
7	53509	56176	58804	61457	64128
8	53657	56317	58948	61589	64256
9	0	0	0	0	0
10	0	0	0	0	0
11	53789	56443	59026	61719	64379
12	55978	58622	61277	63927	66502

Table C8 Frame Table for a Supply Pressure of 3 MPa Firing at 20 Hz at 20mm SOD

Event	Cycle 1	Cycle 2	Cycle 3	Cycle 4	Cycle 5
1	54179	56820	59484	62143	64796
2	54183	56824	59488	62147	64800
3	54184	56825	59489	62148	64801
4	54186	56826	59490	62149	64802
5	54205	56845	59504	62168	64826
6	54215	56856	59521	62178	64835
7	54335	56971	59667	62324	64947
8	0	0	0	0	0
9	0	0	0	0	0
10	0	0	0	0	0
11	0	0	0	0	0
12	56820	59484	62143	64796	67459

Table C9 Frame Table for a Supply Pressure of 2 MPa Firing at 20 Hz at 30mm SOD

Event	Cycle 1	Cycle 2	Cycle 3	Cycle 4	Cycle 5
1	53456	56110	58758	61409	64059
2	53460	56114	58762	61413	64062
3	53461	56115	58763	61414	64063
4	53461	56115	58763	61414	64063
5	53663	56329	58965	61636	64289
6	0	0	0	0	0
7	0	0	0	0	0
8	0	0	0	0	0
9	0	0	0	0	0
10	0	0	0	0	0
11	0	0	0	0	0
12	56110	58758	61409	64058	66725

Table C10 Frame Table for a Supply Pressure of 2 MPa Firing at 30 Hz at 10mm SOD

Event	Cycle 1	Cycle 2	Cycle 3	Cycle 4	Cycle 5
1	53426	55219	57016	58814	60616
2	53430	55223	57020	58818	60620
3	53431	55224	57021	58819	60621
4	53434	55227	57024	58822	60624
5	53442	55235	57031	58829	60632
6	53452	55242	57040	58839	60641
7	53596	55383	57191	58988	60794
8	0	0	0	0	0
9	0	0	0	0	0
10	0	0	0	0	0
11	0	0	0	0	0
12	55219	57016	58814	60616	62401

Table C11 Frame Table for a Supply Pressure of 2 MPa Firing at 30 Hz at 20mm SOD

Event	Cycle 1	Cycle 2	Cycle 3	Cycle 4	Cycle 5
1	53739	55535	57329	59131	60930
2	53743	55539	57333	59135	60934
3	53744	55540	57334	59136	60935
4	53745	55541	57335	59137	60936
5	0	0	0	0	0
6	0	0	0	0	0
7	53894	55707	57491	59291	61089
8	0	0	0	0	0
9	0	0	0	0	0
10	0	0	0	0	0
11	0	0	0	0	0
12	55535	57329	58669	60930	62729

Table C12 Frame Table for a Supply Pressure of 2MPa Firing at 30 Hz at 30mm SOD

Event	Cycle 1	Cycle 2	Cycle 3	Cycle 4	Cycle 5
1	53739	55535	57329	59131	60930
2	53743	55539	57333	59135	60934
3	53744	55540	57334	59136	60935
4	53745	55541	57335	59137	60936
5	0	0	0	0	0
6	0	0	0	0	0
7	53894	55707	57491	59291	61089
8	0	0	0	0	0
9	0	0	0	0	0
10	0	0	0	0	0
11	0	0	0	0	0
12	55535	57329	59131	60930	62702

Table C13 Frame Table for a Supply Pressure of 3.45 MPa Firing at 5 Hz at 20mm SOD

Event	Cycle 1	Cycle 2	Cycle 3	Cycle 4	Cycle 5
1	52530	63655	74882	85977	97030
2	52534	63659	74886	85981	97034
3	52535	63660	74887	85982	97035
4	52536	63661	74888	85984	97036
5	52554	63678	74906	86004	97054
6	52569	63692	74918	86015	97065
7	52728	63851	75098	86153	97220
8	52679	64023	75234	86326	97380
9	53068	64416	75482	86571	97645
10	54154	65282	76753	87706	98588
11	55146	66167	77534	88356	99537
12	63655	74882	85977	97030	108255

Table C14 Frame Table for a Supply Pressure of 3.45 MPa Firing at 5 Hz at 30mm SOD

Event	Cycle 1	Cycle 2	Cycle 3	Cycle 4	Cycle 5
1	54729	65830	77147	88618	99546
2	54732	65833	77150	88621	99550
3	54733	65834	77151	88622	99551
4	54734	65835	77156	88623	99552
5	54759	65862	77183	88647	99577
6	54770	65872	77196	88658	99586
7	54934	66023	77376	88820	99746
8	55134	66236	77580	89034	99963
9	55476	66799	78060	89547	100372
10	55897	67174	78215	89891	100754
11	56773	68022	79352	91058	101772
12	65830	77147	88618	99546	110701

Table C15 Frame Table for a Supply Pressure of 3.45 MPa Firing at 10 Hz at 10mm SOD

Event	Cycle 1	Cycle 2	Cycle 3	Cycle 4	Cycle 5
1	55899	61325	66755	72233	77700
2	55902	61328	66758	72236	77703
3	55903	61329	66759	72237	77704
4	55906	61332	66762	72240	77707
5	55914	61340	66771	72248	77715
6	55928	61354	66783	72261	77729
7	55991	61436	66857	72326	77796
8	56117	61557	66982	72461	77920
9	56283	61751	67172	72668	78194
10	56970	62407	67847	73462	78913
11	57645	62977	68455	73934	79308
12	61325	66755	72233	77700	83168

Table C16 Frame Table for a Supply Pressure of 3.45 MPa Firing at 10 Hz at 20mm SOD

Event	Cycle 1	Cycle 2	Cycle 3	Cycle 4	Cycle 5
1	55715	61107	66466	71832	77169
2	55718	61110	66470	71835	77171
3	55719	61111	66471	71836	77173
4	55721	61112	66472	71837	77175
5	55737	61129	66489	71854	77191
6	55750	61143	66503	71866	77204
7	55814	61216	66572	71934	77272
8	55984	61385	66739	72096	77444
9	56281	61657	67031	72381	77724
10	56470	61854	67212	72561	77894
11	57188	62563	67912	73323	78606
12	61107	66466	71832	77169	82585

Table C17 Frame Table for a Supply Pressure of 3.45 MPa Firing at 10 Hz at 30mm SOD

Event	Cycle 1	Cycle 2	Cycle 3	Cycle 4	Cycle 5
1	56263	61677	67045	72501	77882
2	56267	61681	67049	72505	77886
3	56268	61682	67050	72506	77887
4	56267	61681	67049	72505	77886
5	56294	61707	67076	72533	77912
6	56301	61716	67084	72542	77921
7	56380	61783	67193	72623	78008
8	56597	61991	67364	72811	78204
9	0	0	0	0	0
10	0	0	0	0	0
11	57604	62913	68385	73763	79138
12	61677	67045	72501	77882	83289

Table C18 Frame Table for a Supply Pressure of 3.45 MPa Firing at 20 Hz at 10mm SOD

Event	Cycle 1	Cycle 2	Cycle 3	Cycle 4	Cycle 5
1	53446	56121	58797	61472	64148
2	53449	56124	58800	61475	64151
3	53450	56125	58801	61476	64152
4	53454	56128	58804	61479	64155
5	53460	56135	58811	61487	64163
6	53470	56145	58821	61495	64170
7	53544	56218	58899	61573	64244
8	53669	56345	59018	61706	64359
9	0	0	0	0	0
10	0	0	0	0	0
11	54354	57019	59688	62389	65026
12	56121	58797	61472	64148	66845

Table C19 Frame Table for a Supply Pressure of 3.45 MPa Firing at 20 Hz at 20mm SOD

Event	Cycle 1	Cycle 2	Cycle 3	Cycle 4	Cycle 5
1	53606	56277	58952	61625	64300
2	53609	56280	58953	61629	64304
3	53610	56281	58954	61630	64305
4	53612	56282	58958	61631	64306
5	53626	56296	58972	61645	64320
6	53633	56305	58980	61652	64327
7	53705	56388	59064	61725	64401
8	53890	56552	59225	61899	64571
9	0	0	0	0	0
10	0	0	0	0	0
11	54436	57032	59666	62378	65098
12	56277	58952	61625	64300	66968

Table C20 Frame Table for a Supply Pressure of 3.45 MPa Firing at 20 Hz at 30mm SOD

Event	Cycle 1	Cycle 2	Cycle 3	Cycle 4	Cycle 5
1	53700	56371	59043	61711	64381
2	53703	56374	59046	61714	64384
3	53704	56375	59047	61715	64385
4	53703	56375	59047	61715	64385
5	53726	56397	59069	61736	64407
6	53733	56404	59075	61744	64416
7	53807	56487	59149	61834	64499
8	54040	56658	59362	62011	64700
9	0	0	0	0	0
10	0	0	0	0	0
11	54237	56881	59610	62312	65063
12	56371	59043	61711	64381	67085

Table C21 Frame Table for a Supply Pressure of 3.45 MPa Firing at 30 Hz at 10mm SOD

Event	Cycle 1	Cycle 2	Cycle 3	Cycle 4	Cycle 5
1	53837	55579	57317	59053	60794
2	53840	55582	57320	59056	60797
3	53841	55583	57321	59057	60798
4	53843	55585	57323	59059	60800
5	53848	55589	57328	9064	60804
6	53856	55597	57336	59068	60810
7	53912	55663	57392	59129	60878
8	54022	55749	57495	59217	60968
9	0	0	0	0	0
10	0	0	0	0	0
11	54486	56174	57905	59661	61450
12	55579	57317	59053	60794	62539

Table C22 Frame Table for a Supply Pressure of 3.45 MPa Firing at 30 Hz at 20mm SOD

Event	Cycle 1	Cycle 2	Cycle 3	Cycle 4	Cycle 5
1	53455	55187	56922	58669	60419
2	53458	55190	56925	58672	60422
3	53459	55191	56926	58673	60423
4	53459	55191	56926	58673	60423
5	53469	55201	56935	58683	60433
6	53475	55208	56941	58690	60439
7	53541	55275	57014	58754	60506
8	53681	55406	57120	58868	60649
9	0	0	0	0	0
10	0	0	0	0	0
11	54013	55698	57421	59144	60949
12	55187	56922	58669	60419	62168

Table C23 Frame Table for a Supply Pressure of 3.45 MPa Firing at 30 Hz at 30mm SOD

Event	Cycle 1	Cycle 2	Cycle 3	Cycle 4	Cycle 5
1	52918	54638	56363	58084	59803
2	52921	54641	56366	58087	59806
3	52922	54642	56367	58088	59807
4	52921	54641	56366	58087	59806
5	0	0	0	0	0
6	0	0	0	0	0
7	54047	55787	57551	59287	61028
8	0	0	0	0	0
9	0	0	0	0	0
10	0	0	0	0	0
11	0	0	0	0	0
12	54638	56363	58084	59803	61526

Table C24 Frame Table for a Supply Pressure of 3.45 MPa Firing at 5 Hz at 10mm SOD

Event	Cycle 1	Cycle 2	Cycle 3	Cycle 4	Cycle 5
1	58912	68119	77389	86667	96013
2	58916	68122	77392	86671	96017
3	58919	68125	77393	86672	96018
4	58922	68129	77398	86675	96022
5	58934	68140	77412	86688	96035
6	58947	68151	77427	86704	96051
7	59075	68274	77557	86834	96179
8	59323	68339	77623	86905	96246
9	59401	68530	77749	87129	96375
10	60862	70126	79362	88602	97976
11	61455	70776	80083	89334	98672
12	68119	77389	86667	96013	105287

Table C25 Frame Table for a Supply Pressure of 4.8 MPa Firing at 5 Hz at 20mm SOD

Event	Cycle 1	Cycle 2	Cycle 3	Cycle 4	Cycle 5
1	54570	63550	72553	81513	90536
2	54573	63553	72556	81517	90540
3	54574	63554	72557	81518	90541
4	54577	63556	72560	81521	90544
5	54601	63578	72585	81545	90564
6	54617	63595	72600	81559	90577
7	54709	63698	72710	81678	90698
8	54846	63786	72805	81764	90791
9	55055	64007	73000	81977	90941
10	55348	64305	73282	82256	91286
11	57228	66131	75195	84201	93259
12	63550	72553	81513	90536	99589

Table C26 Frame Table for a Supply Pressure of 4.8 MPa Firing at 5 Hz at 30mm SOD

Event	Cycle 1	Cycle 2	Cycle 3	Cycle 4	Cycle 5
1	57511	66197	75039	84000	92761
2	57514	66200	75042	84003	92764
3	57515	66201	75043	84004	92765
4	57515	66202	75047	84006	92767
5	57546	66232	75078	84036	92797
6	57560	66251	75097	84048	92807
7	57674	66369	75195	84177	92906
8	57780	66490	75326	84274	93029
9	59034	67732	76611	85519	94350
10	59285	67975	76860	85831	94568
11	60138	68841	77643	86642	95359
12	66197	75039	84000	92761	101523

Table C27 Frame Table for a Supply Pressure of 4.8 MPa Firing at 10 Hz at 10mm SOD

Event	Cycle 1	Cycle 2	Cycle 3	Cycle 4	Cycle 5
1	53898	58978	64048	69119	74208
2	53901	58981	64051	69122	74211
3	53902	58982	64052	69123	74212
4	53904	58984	64054	69125	74214
5	53913	58993	64063	69134	74223
6	53929	59008	64079	69148	74237
7	53993	59079	64159	69220	74310
8	54097	59179	64246	69319	74423
9	54277	59348	64370	69450	74592
10	55127	60263	65279	70312	75496
11	55988	61110	66234	71236	76366
12	58975	64048	69119	74208	79205

Table C28 Frame Table for a Supply Pressure of 4.8 MPa Firing at 10 Hz at 20mm SOD

Event	Cycle 1	Cycle 2	Cycle 3	Cycle 4	Cycle 5
1	53230	58435	63639	68886	74087
2	53233	58438	63642	68889	74090
3	53234	58439	63643	68890	74091
4	53235	58440	63644	68891	74092
5	53250	58456	63660	68906	74108
6	53264	58471	63675	68920	74121
7	53340	58545	63754	68994	74199
8	53442	58658	63884	69124	74329
9	53623	58826	64027	69294	74513
10	54312	59496	64754	69820	74981
11	55197	60304	65622	70730	75956
12	58435	63639	68886	74087	79301

Table C29 Frame Table for a Supply Pressure of 4.8 MPa Firing at 10 Hz at 30mm SOD

Event	Cycle 1	Cycle 2	Cycle 3	Cycle 4	Cycle 5
1	54508	59796	65117	70401	75681
2	54511	59799	65120	70404	75684
3	54512	59800	65121	70405	75685
4	54512	59800	65121	70405	75685
5	54534	59821	65140	70427	75706
6	54544	59831	65152	70436	75716
7	54608	59910	65259	70542	75800
8	54757	60047	65368	70640	75937
9	55036	60280	65810	70862	76164
10	55710	60797	66158	71557	76814
11	56206	61621	67021	72278	77527
12	59796	65117	70401	75681	80968

Table C30 Frame Table for a Supply Pressure of 4.8 MPa Firing at 20 Hz at 10mm SOD

Event	Cycle 1	Cycle 2	Cycle 3	Cycle 4	Cycle 5
1	52675	55239	57799	60353	62915
2	52677	55241	57802	60356	62918
3	52678	55242	57803	60357	62919
4	52679	55243	57804	60358	62920
5	52684	55248	57810	60363	62926
6	52690	55256	57817	60369	62932
7	52756	55313	57884	60438	62998
8	52821	55383	57950	60506	63067
9	52941	55510	58091	60641	63201
10	53489	55992	58445	60971	63520
11	54123	56657	59156	61677	64272
12	55238	57799	60353	62915	65476

Table C31 Frame Table for a Supply Pressure of 4.8 MPa Firing at 20 Hz at 20mm SOD

Event	Cycle 1	Cycle 2	Cycle 3	Cycle 4	Cycle 5
1	53536	56077	58616	61144	63684
2	53539	56080	58619	61147	63687
3	53540	56081	58620	61148	63688
4	53541	56082	58621	61149	63689
5	53550	56091	58629	61158	63698
6	53558	56099	58636	61165	63706
7	53623	56161	58709	61239	63778
8	53710	56269	58803	61344	63882
9	0	0	0	0	0
10	0	0	0	0	0
11	54655	57352	59804	62369	64836
12	56077	58616	61144	63684	66242

Table C32 Frame Table for a Supply Pressure of 4.8 MPa Firing at 20 Hz at 30mm SOD

Event	Cycle 1	Cycle 2	Cycle 3	Cycle 4	Cycle 5
1	54491	57034	59586	62136	64678
2	54494	57037	59589	62139	64681
3	54495	57038	59590	62140	64682
4	54495	57038	59590	62140	64682
5	54507	57051	59603	62152	64694
6	54513	57058	59611	62158	64702
7	54587	57117	59675	62234	64777
8	54700	57234	59770	62342	64887
9	0	0	0	0	0
10	0	0	0	0	0
11	55685	58160	60661	63107	65411
12	57034	59586	62136	64678	67227

Table C33 Frame Table for a Supply Pressure of 4.8 MPa Firing at 30 Hz at 10mm SOD

Event	Cycle 1	Cycle 2	Cycle 3	Cycle 4	Cycle 5
1	53000	54728	56454	58186	59920
2	53002	54731	56457	58189	59923
3	53003	54732	56458	58190	59924
4	53004	54733	56459	58191	59925
5	53007	54737	56462	58194	59928
6	53012	54746	56469	58204	59938
7	53037	54772	56493	58230	59974
8	53084	54799	56524	58266	60009
9	53132	54864	56656	58353	60130
10	53601	55396	57055	58847	60376
11	53999	55809	57528	59271	61001
12	54728	56454	58186	59920	61658

Table C34 Frame Table for a Supply Pressure of 4.8 MPa Firing at 30 Hz at 20mm SOD

Event	Cycle 1	Cycle 2	Cycle 3	Cycle 4	Cycle 5
1	53003	54728	56457	58184	59904
2	53006	54731	56460	58187	59907
3	53007	54732	56461	58188	59908
4	53006	54731	56460	58187	59907
5	0	0	0	0	0
6	0	0	0	0	0
7	53052	54803	56503	58244	59969
8	53133	54871	56596	58306	60040
9	0	0	0	0	0
10	0	0	0	0	0
11	53934	55570	57098	58948	60564
12	54728	56457	58184	59904	61641

Table C35 Frame Table for a Supply Pressure of 4.8 MPa Firing at 30 Hz at 30mm SOD

Event	Cycle 1	Cycle 2	Cycle 3	Cycle 4	Cycle 5
1	52913	54638	56363	58084	59803
2	52916	54641	56366	58087	59806
3	52917	54642	56367	58088	59807
4	52916	54641	56366	58087	59806
5	0	0	0	0	0
6	0	0	0	0	0
7	52991	54703	56429	58142	59868
8	53062	54793	56426	58231	59965
9	0	0	0	0	0
10	0	0	0	0	0
11	53670	55246	56978	58786	60505
12	54638	56363	58084	59803	61535

Appendix D Phase Tables

Table D1 Phase Table for a Supply Pressure of 2 MPa Firing at 5 Hz at 10mm SOD

Phase #	Time Average (ms)	Standard Deviation (ms)
1	166.59	1.46
2	0.09	0.01
3	0.41	0.02
4	4.32	0.15
5	23.25	2.01
6	14.26	1.85

Table D2 Phase Table for a Supply Pressure of 2 MPa Firing at 5 Hz at 20mm SOD

Phase #	Time Average (ms)	Standard Deviation (ms)
1	166.29	1.07
2	0.08	0.00
3	0.59	0.02
4	3.82	0.39
5	20.41	0.83
6	8.93	0.96

Table D3 Phase Table for a Supply Pressure of 2 MPa Firing at 5 Hz at 30mm SOD

Phase #	Time Average (ms)	Standard Deviation (ms)
1	167.53	0.72
2	0.08	0.00
3	0.79	0.03
4	3.54	0.61
5	15.02	1.36
6	0.00	0.00

Table D4 Phase Table for a Supply Pressure of 2 MPa Firing at 10 Hz at 10mm SOD

Phase #	Time Average (ms)	Standard Deviation (ms)
1	104.22	0.16
2	0.10	0.00
3	0.47	0.04
4	3.33	0.32
5	15.43	0.91
6	0.00	0.00

Table D5 Phase Table for a Supply Pressure of 2 MPa Firing at 10 Hz at 20mm SOD

Phase #	Time Average (ms)	Standard Deviation (ms)
1	103.74	0.40
2	0.09	0.01
3	0.60	0.01
4	2.63	0.69
5	10.80	1.64
6	0.00	0.00

Table D6 Phase Table for a Supply Pressure of 2 MPa Firing at 10 Hz at 30mm SOD

Phase #	Time Average (ms)	Standard Deviation (ms)
1	105.04	0.73
2	0.09	0.01
3	0.67	0.03
4	2.48	0.36
5	4.98	1.32
6	0.00	0.00

Table D7 Phase Table for a Supply Pressure of 2 MPa Firing at 20 Hz at 10mm SOD

Phase #	Time Average (ms)	Standard Deviation (ms)
1	50.19	0.64
2	0.10	0.00
3	0.35	0.01
4	3.07	0.19
5	2.24	0.43
6	0.00	0.00

Table D8 Phase Table for a Supply Pressure of 2 MPa Firing at 20 Hz at 20mm SOD

Phase #	Time Average (ms)	Standard Deviation (ms)
1	50.59	0.18
2	0.10	0.00
3	0.58	0.03
4	2.43	0.32
5	0.00	0.00
6	0.00	0.00

Table D9 Phase Table for a Supply Pressure of 2 MPa Firing at 20 Hz at 30mm SOD

Phase #	Time Average (ms)	Standard Deviation (ms)
1	50.55	0.14
2	0.09	0.01
3	0.00	0.00
4	0.00	0.00
5	0.00	0.00
6	0.00	0.00

Table D10 Phase Table for a Supply Pressure of 2 MPa Firing at 30 Hz at 10mm SOD

Phase #	Time Average (ms)	Standard Deviation (ms)
1	34.19	0.12
2	0.10	0.00
3	0.32	0.02
4	2.81	0.10
5	0.00	0.00
6	0.00	0.00

Table D11 Phase Table for a Supply Pressure of 2 MPa Firing at 30 Hz at 20mm SOD

Phase #	Time Average (ms)	Standard Deviation (ms)
1	32.49	3.89
2	0.10	0.00
3	0.00	0.00
4	2.98	0.12
5	0.00	0.00
6	0.00	0.00

Table D12 Phase Table for a Supply Pressure of 2 MPa Firing at 30 Hz at 30mm SOD

Phase #	Time Average (ms)	Standard Deviation (ms)
1	34.15	0.23
2	0.10	0.00
3	0.00	0.00
4	2.96	0.12
5	0.00	0.00
6	0.00	0.00

Table D13 Phase Table for a Supply Pressure of 3.45 MPa Firing at 5 Hz at 20mm SOD

Phase #	Time Average (ms)	Standard Deviation (ms)
1	212.29	1.49
2	0.10	0.00
3	0.59	0.03
4	3.01	0.29
5	42.28	3.21
6	20.19	3.04

Table D14 Phase Table for a Supply Pressure of 3.45 MPa Firing at 5 Hz at 30mm SOD

Phase #	Time Average (ms)	Standard Deviation (ms)
1	213.23	3.96
2	0.08	0.01
3	0.69	0.04
4	3.11	0.20
5	34.40	2.64
6	6.39	1.99

Table D15 Phase Table for a Supply Pressure of 3.45 MPa Firing at 10 Hz at 10mm SOD

Phase #	Time Average (ms)	Standard Deviation (ms)
1	103.88	0.46
2	0.08	0.00
3	0.41	0.01
4	1.34	0.15
5	27.74	1.03
6	13.45	1.03

Table D16 Phase Table for a Supply Pressure of 3.45 MPa Firing at 10 Hz at 20mm SOD

Phase #	Time Average (ms)	Standard Deviation (ms)
1	102.36	0.58
2	0.08	0.01
3	0.57	0.02
4	1.30	0.06
5	22.64	0.50
6	3.49	0.19

Table D17 Phase Table for a Supply Pressure of 3.45 MPa Firing at 10 Hz at 30mm SOD

Phase #	Time Average (ms)	Standard Deviation (ms)
1	102.96	0.65
2	0.10	0.00
3	0.67	0.02
4	1.61	0.29
5	18.42	0.84
6	0.00	0.00

Table D18 Phase Table for a Supply Pressure of 3.45 MPa Firing at 20 Hz at 10mm SOD

Phase #	Time Average (ms)	Standard Deviation (ms)
1	51.04	0.18
2	0.08	0.00
3	0.31	0.02
4	1.44	0.05
5	12.87	0.15
6	0.00	0.00

Table D19 Phase Table for a Supply Pressure of 3.45 MPa Firing at 20 Hz at 20mm SOD

Phase #	Time Average (ms)	Standard Deviation (ms)
1	50.90	0.06
2	0.08	0.02
3	0.41	0.02
4	1.47	0.11
5	9.42	0.80
6	0.00	0.00

Table D20 Phase Table for a Supply Pressure of 3.45 MPa Firing at 20 Hz at 30mm SOD

Phase #	Time Average (ms)	Standard Deviation (ms)
1	50.99	0.29
2	0.08	0.00
3	0.56	0.02
4	1.54	0.13
5	5.07	1.26
6	0.00	0.00

Table D21 Phase Table for a Supply Pressure of 3.45 MPa Firing at 30 Hz at 10mm SOD

Phase #	Time Average (ms)	Standard Deviation (ms)
1	33.15	0.07
2	0.08	0.00
3	0.22	0.04
4	1.17	0.11
5	8.48	0.55
6	0.00	0.00

Table D22 Phase Table for a Supply Pressure of 3.45 MPa Firing at 30 Hz at 20mm SOD

Phase #	Time Average (ms)	Standard Deviation (ms)
1	33.19	0.16
2	0.08	0.00
3	0.31	0.02
4	1.28	0.06
5	5.72	0.39
6	0.00	0.00

Table D23 Phase Table for a Supply Pressure of 3.45 MPa Firing at 30 Hz at 30mm SOD

Phase #	Time Average (ms)	Standard Deviation (ms)
1	32.79	0.05
2	0.08	0.00
3	0.00	0.00
4	22.38	0.75
5	0.00	0.00
6	0.00	0.00

Table D24 Phase Table for a Supply Pressure of 4.8 MPa Firing at 5 Hz at 10mm SOD

Phase #	Time Average (ms)	Standard Deviation (ms)
1	176.67	0.94
2	0.10	0.02
3	0.51	0.06
4	2.43	0.06
5	45.27	2.62
6	29.50	1.43

Table D25 Phase Table for a Supply Pressure of 4.8 MPa Firing at 5 Hz at 20mm SOD

Phase #	Time Average (ms)	Standard Deviation (ms)
1	171.50	0.69
2	0.08	0.01
3	0.72	0.06
4	2.08	0.23
5	45.80	0.92
6	5.70	0.51

Table D26 Phase Table for a Supply Pressure of 4.8 MPa Firing at 5 Hz at 30mm SOD

Phase #	Time Average (ms)	Standard Deviation (ms)
1	167.67	1.99
2	0.08	0.00
3	0.86	0.08
4	2.13	0.25
5	44.66	0.40
6	4.85	0.66

Table D27 Phase Table for a Supply Pressure of 4.8 MPa Firing at 10 Hz at 10mm SOD

Phase #	Time Average (ms)	Standard Deviation (ms)
1	96.40	0.69
2	0.08	0.00
3	0.46	0.02
4	1.37	0.11
5	36.84	0.68
6	16.91	0.57

Table D28 Phase Table for a Supply Pressure of 4.8 MPa Firing at 10 Hz at 20mm SOD

Phase #	Time Average (ms)	Standard Deviation (ms)
1	99.32	0.36
2	0.08	0.00
3	0.57	0.02
4	1.45	0.04
5	31.89	1.29
6	11.73	2.14

Table D29 Phase Table for a Supply Pressure of 4.8 MPa Firing at 10 Hz at 30mm SOD

Phase #	Time Average (ms)	Standard Deviation (ms)
1	100.80	0.31
2	0.08	0.00
3	0.59	0.01
4	1.68	0.35
5	30.11	1.54
6	10.99	2.77

Table D30 Phase Table for a Supply Pressure of 4.8 MPa Firing at 20 Hz at 10mm SOD

Phase #	Time Average (ms)	Standard Deviation (ms)
1	48.76	0.07
2	0.07	0.01
3	0.23	0.02
4	1.24	0.09
5	23.46	1.03
6	7.75	1.95

Table D31 Phase Table for a Supply Pressure of 4.8 MPa Firing at 20 Hz at 20mm SOD

Phase #	Time Average (ms)	Standard Deviation (ms)
1	48.40	0.21
2	0.08	0.00
3	0.31	0.02
4	1.32	0.10
5	19.08	1.07
6	0.00	0.00

Table D32 Phase Table for a Supply Pressure of 4.8 MPa Firing at 20 Hz at 30mm SOD

Phase #	Time Average (ms)	Standard Deviation (ms)
1	48.52	0.09
2	0.08	0.00
3	0.37	0.03
4	1.33	0.15
5	15.59	3.49
6	0.00	0.00

Table D33 Phase Table for a Supply Pressure of 4.8 MPa Firing at 30 Hz at 10mm SOD

Phase #	Time Average (ms)	Standard Deviation (ms)
1	32.98	0.09
2	0.07	0.01
3	0.22	0.04
4	0.52	0.09
5	18.77	0.76
6	8.15	2.15

Table D34 Phase Table for a Supply Pressure of 4.8 MPa Firing at 30 Hz at 20mm SOD

Phase #	Time Average (ms)	Standard Deviation (ms)
1	32.91	0.12
2	0.08	0.00
3	0.00	0.00
4	1.05	0.23
5	12.07	2.37
6	0.00	0.00

Table D35 Phase Table for a Supply Pressure of 4.8 MPa Firing at 30 Hz at 30mm SOD

Phase #	Time Average (ms)	Standard Deviation (ms)
1	32.85	0.10
2	0.08	0.00
3	0.00	0.00
4	1.19	0.14
5	10.32	1.07
6	0.00	0.00

Appendix E Substrate Pressure Graphs

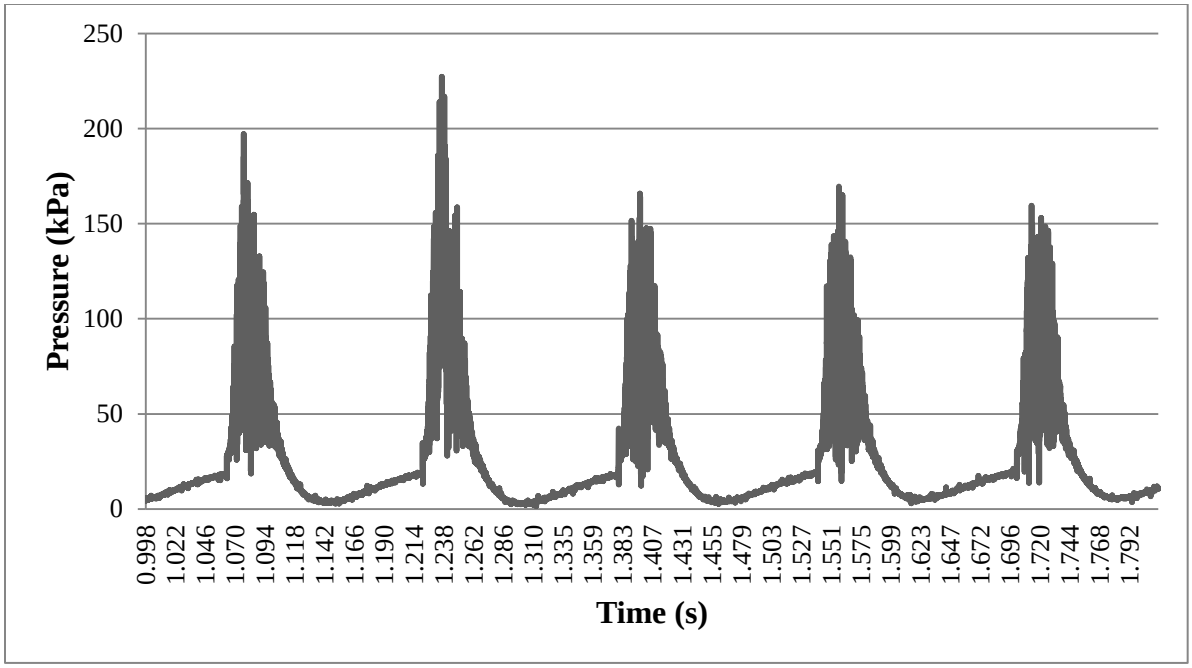

Figure E1 Substrate Pressure Graph for a Supply Pressure of 2MPa Firing at 5 Hz at 10mm SOD

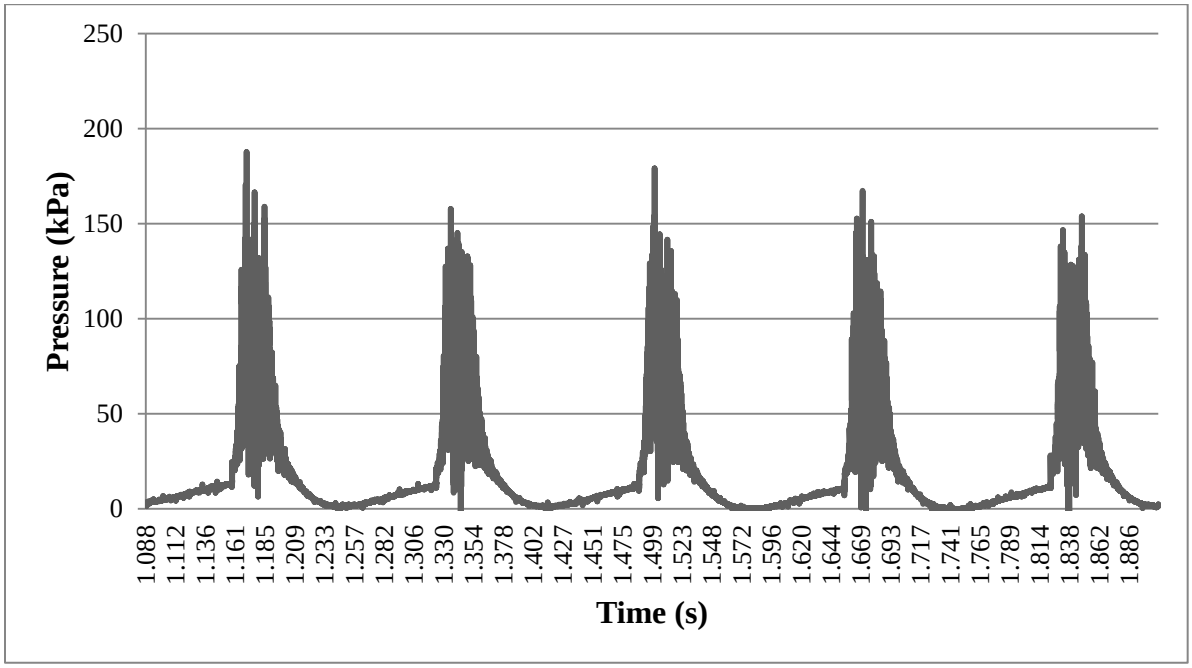

Figure E2 Substrate Pressure Graph for a Supply Pressure of 2 MPa Firing at 5 Hz at 20mm SOD

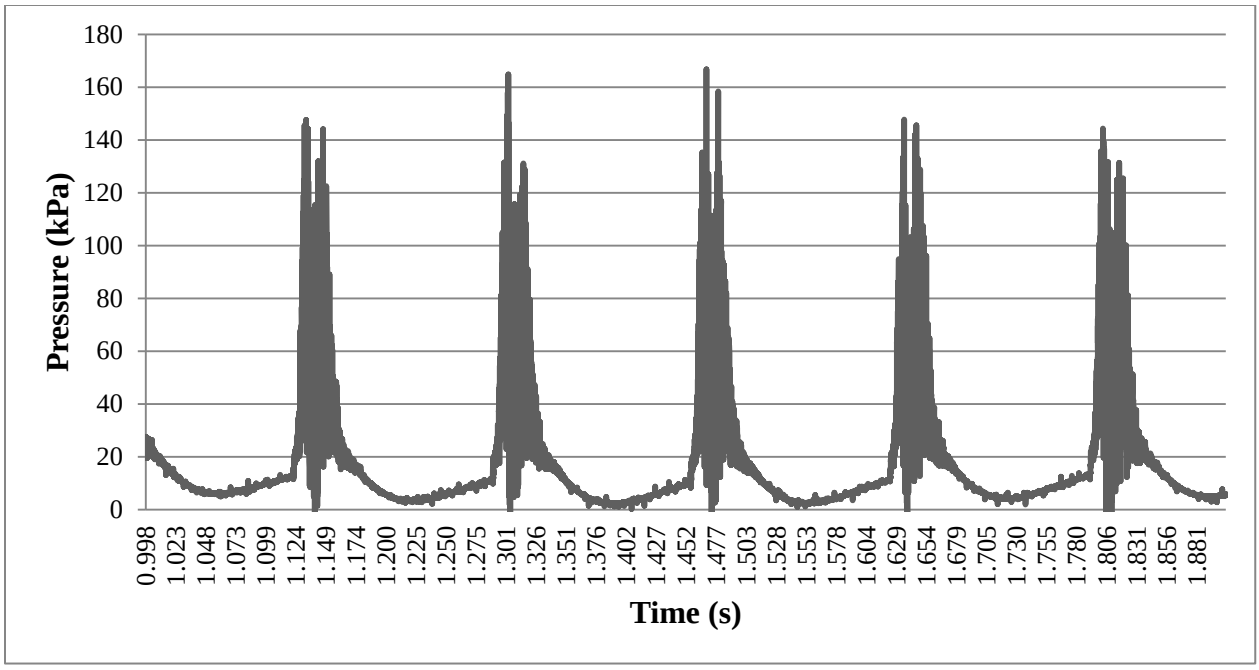

Figure E3 Substrate Pressure Graph for a Supply Pressure of 2 MPa Firing at 5 Hz at 30mm SOD

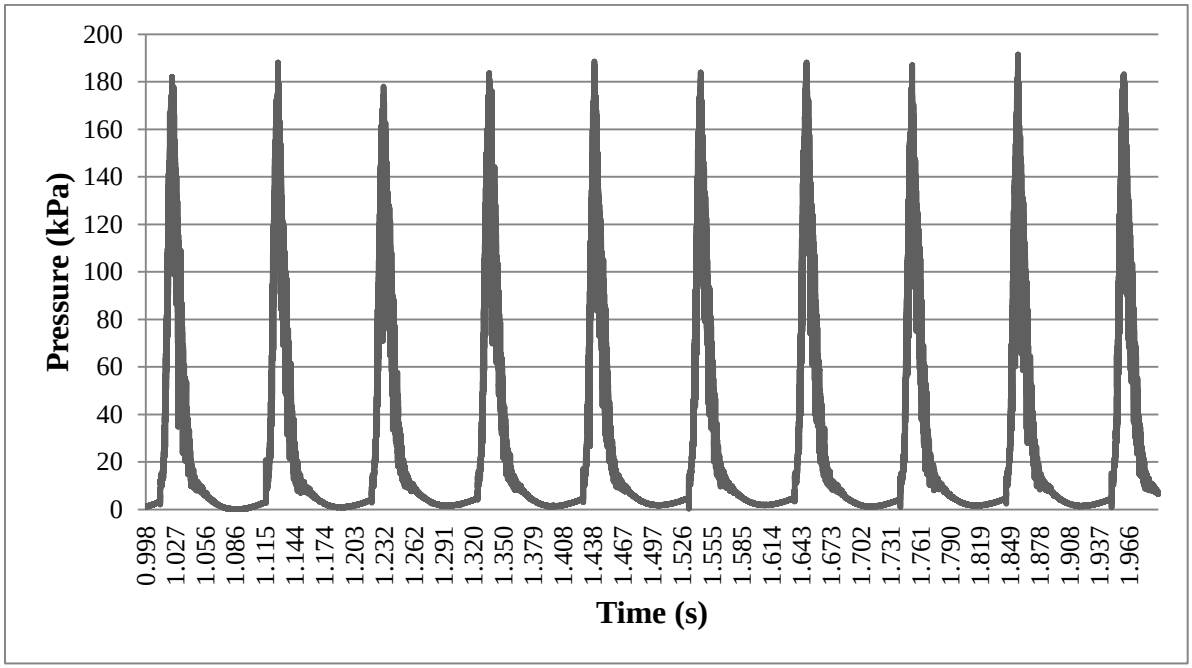

Figure E4 Substrate Pressure Graph for a Supply Pressure of 2 MPa Firing at 10 Hz at 10mm SOD

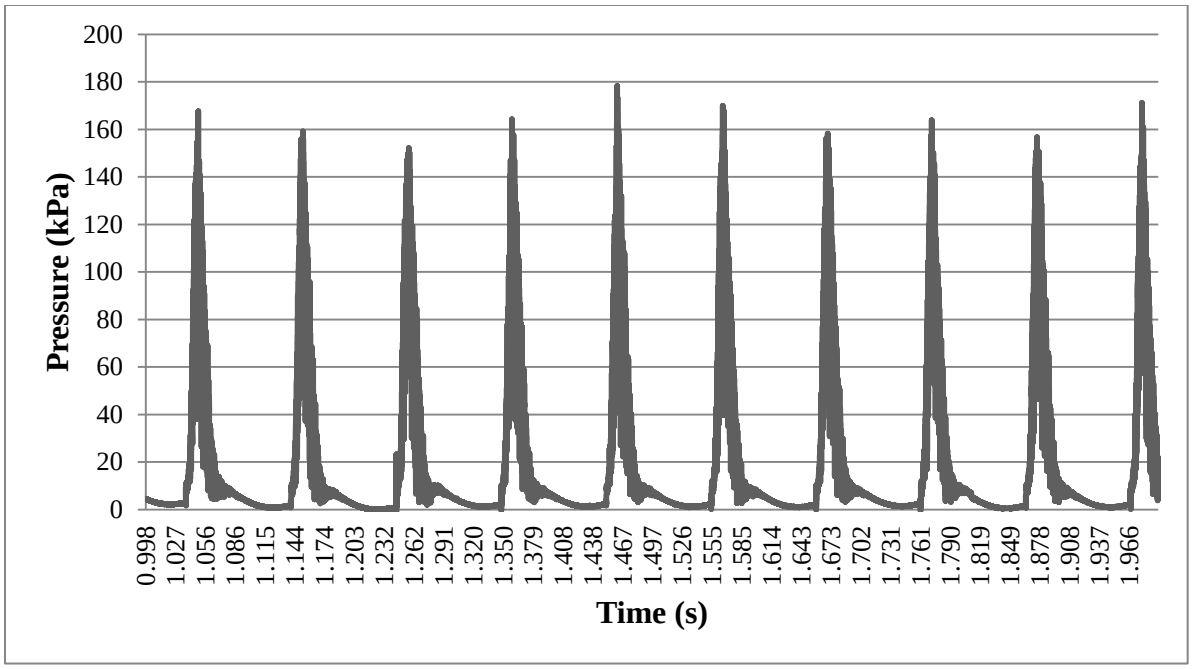

Figure E5 Substrate Pressure Graph for a Supply Pressure of 2 MPa Firing at 10 Hz at 20mm SOD

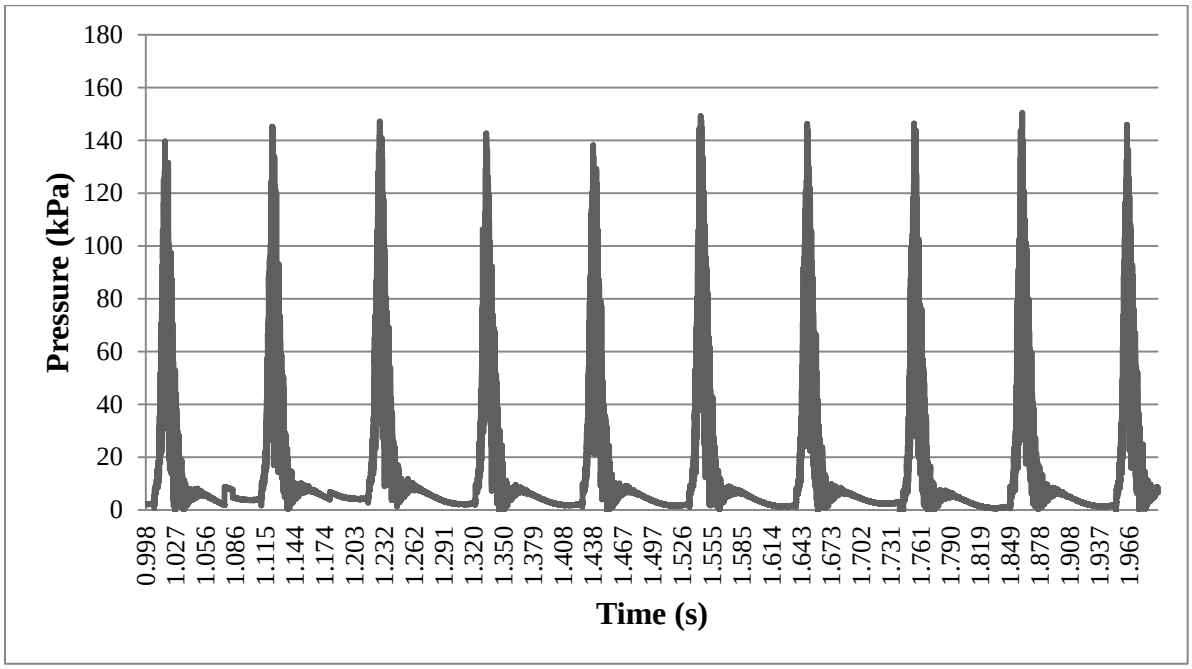

Figure E6 Substrate Pressure Graph for a Supply Pressure of 2 MPa Firing at 10 Hz at 30mm SOD

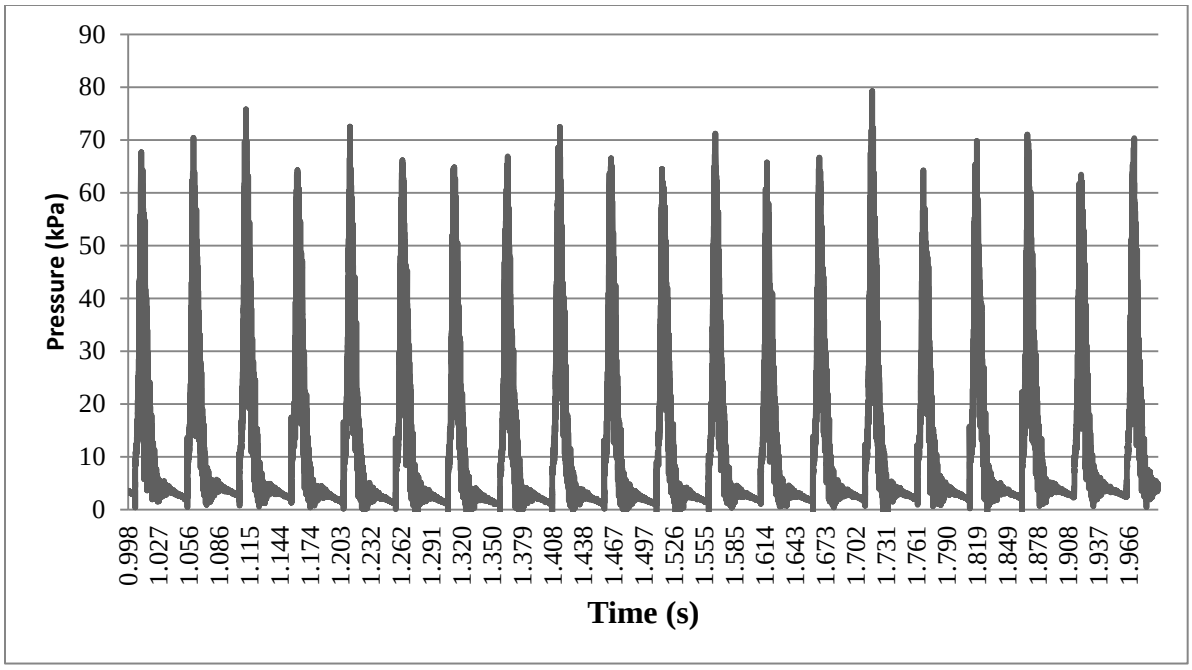

Figure E7 Substrate Pressure Graph for a Supply Pressure of 2 MPa Firing at 20 Hz at 10mm SOD

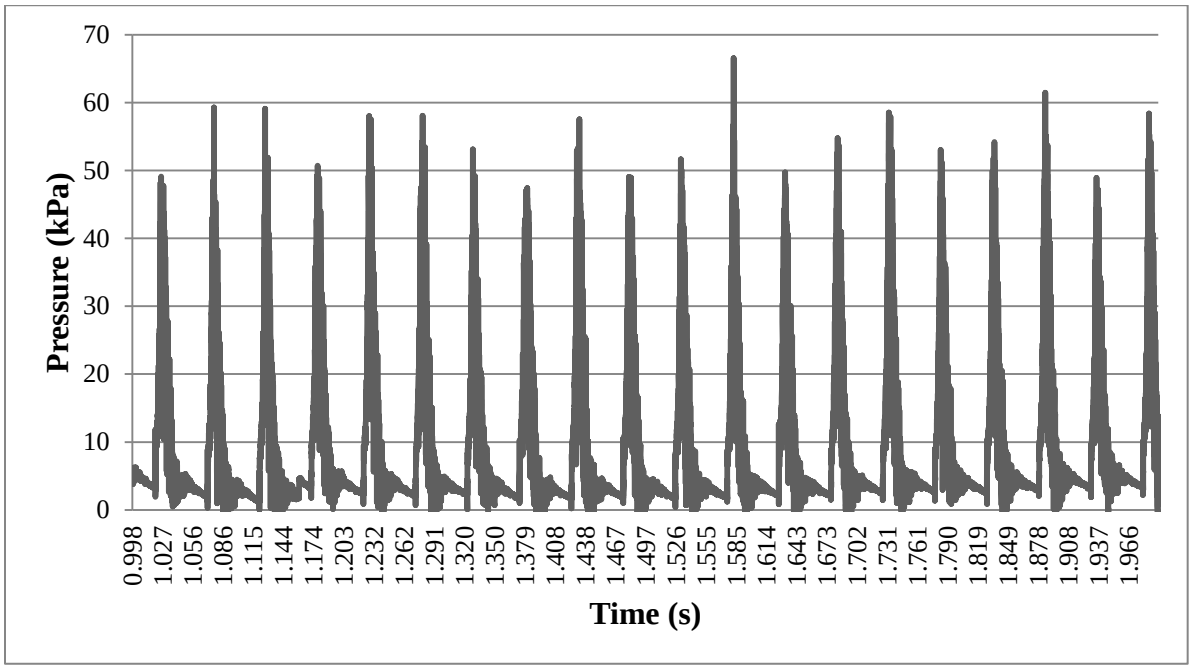

Figure E8 Substrate Pressure Graph for a Supply Pressure of 2 MPa Firing at 20 Hz at 20mm SOD

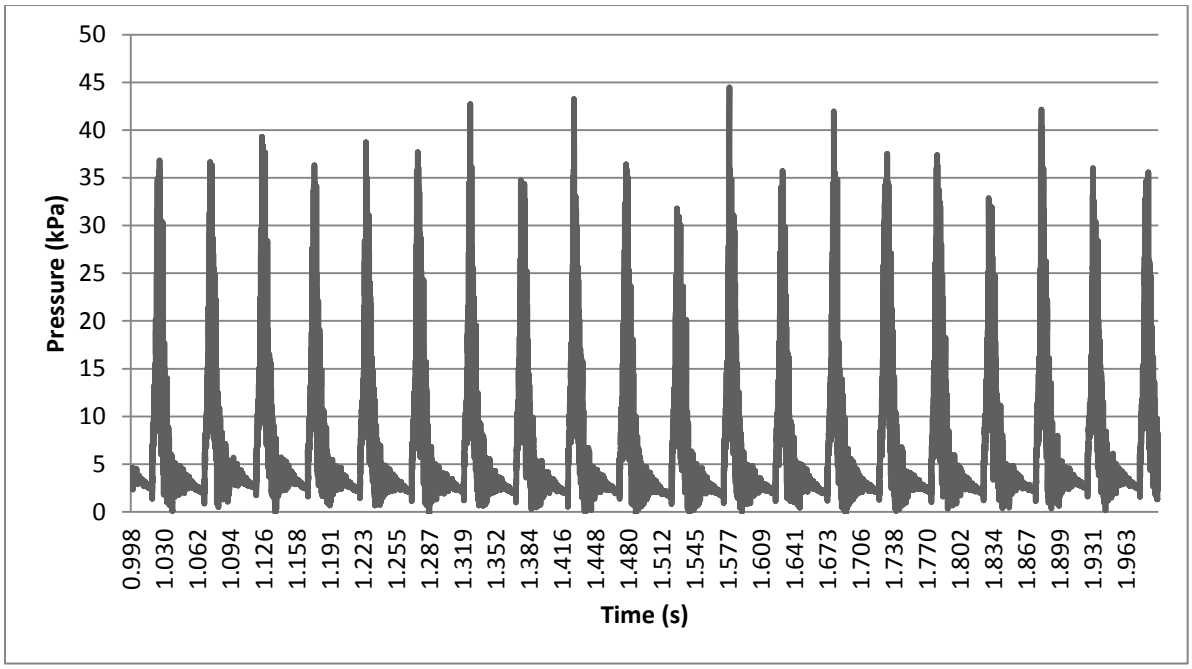

Figure E9 Substrate Pressure Graph for a Supply Pressure of 2 MPa Firing at 20 Hz at 30mm SOD

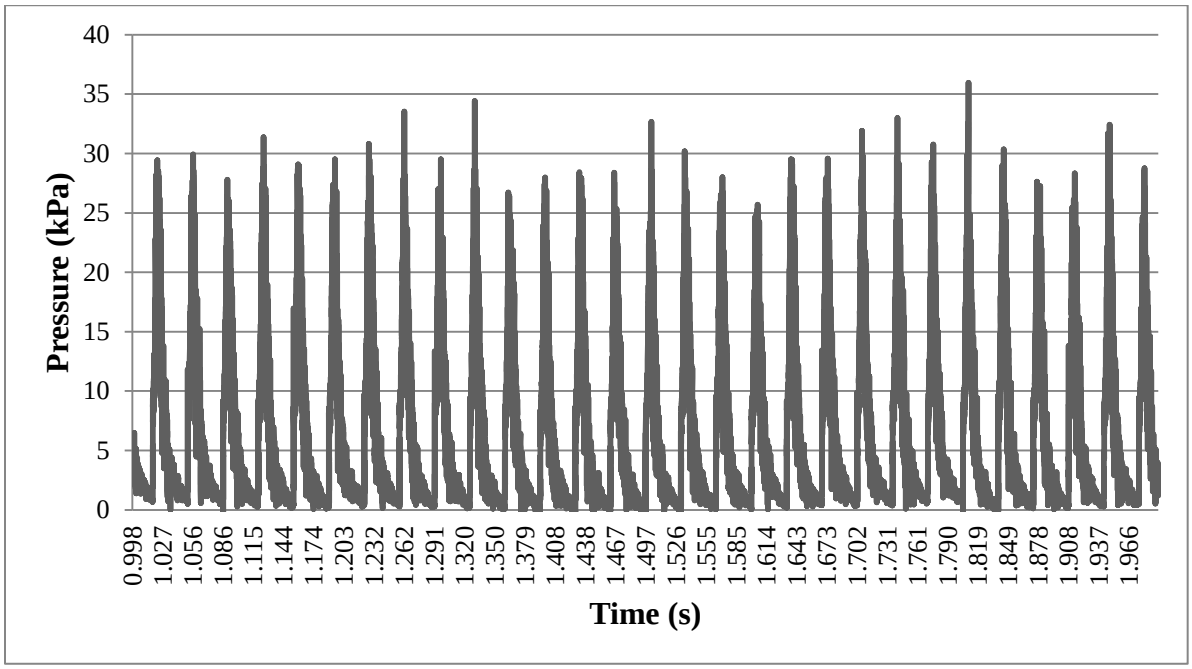

Figure E10 Substrate Pressure Graph for a Supply Pressure of 2 MPa Firing at 30 Hz at 10mm SOD

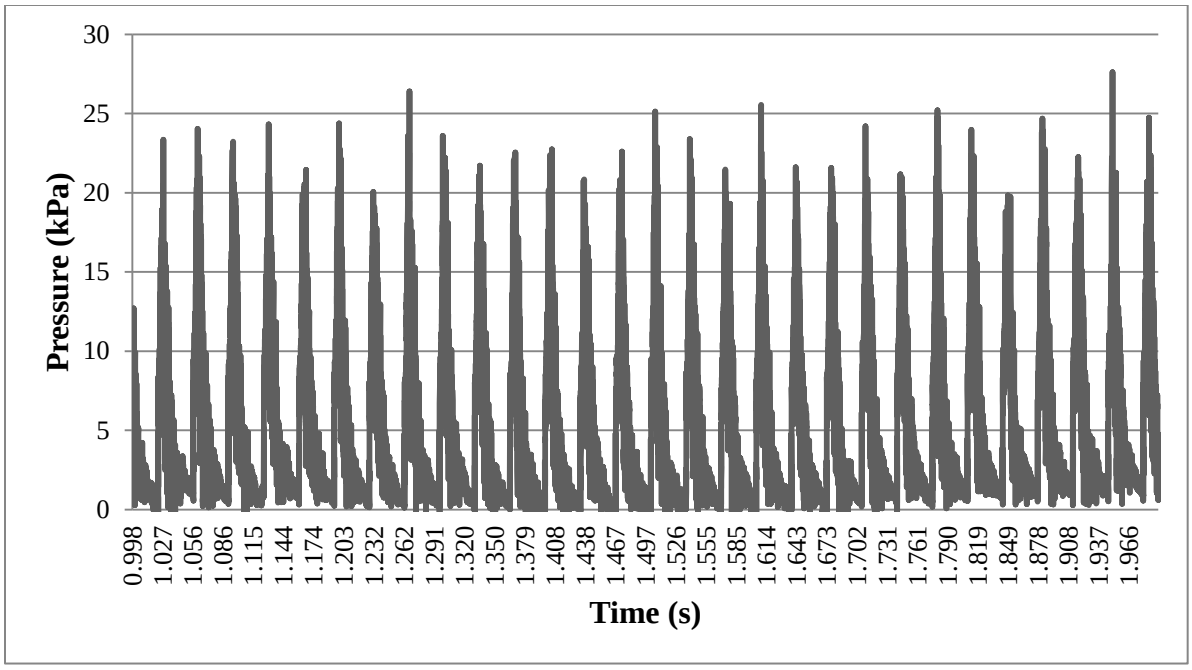

Figure D11 Substrate Pressure Graph for a Supply Pressure of 2 MPa Firing at 30 Hz at 20mm SOD

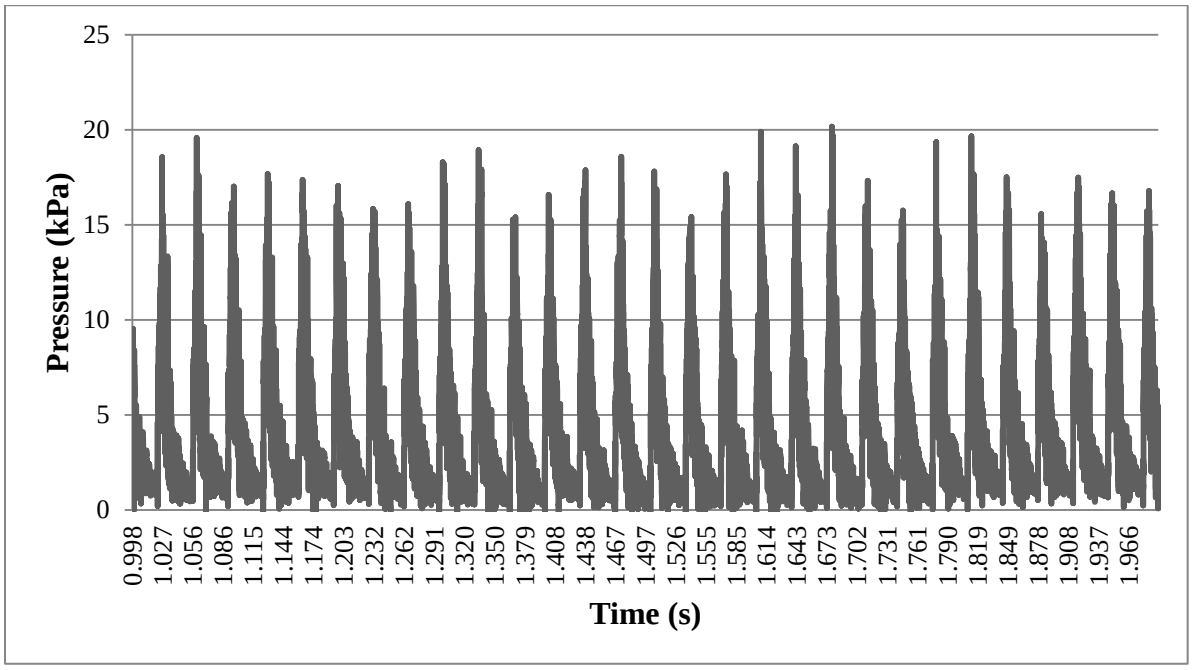

Figure E12 Substrate Pressure Graph for a Supply Pressure of 2 MPa Firing at 30 Hz at 30mm SOD

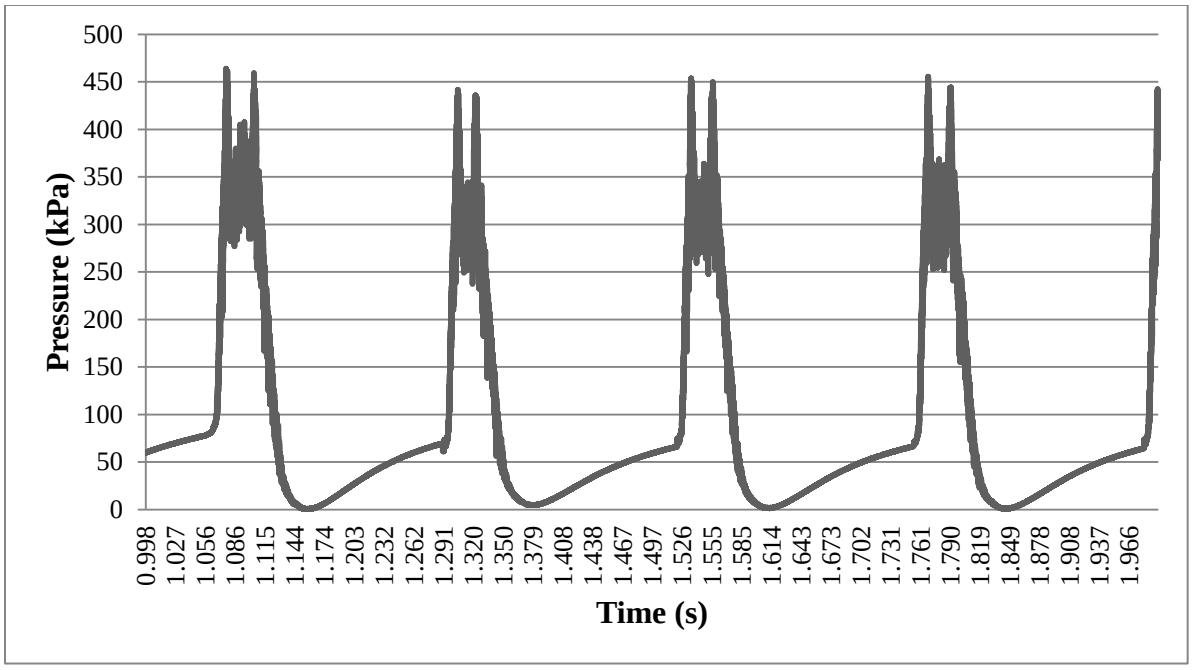

Figure E13 Substrate Pressure Graph for a Supply Pressure of 3.45 MPa Firing at 5 Hz at 10mm SOD

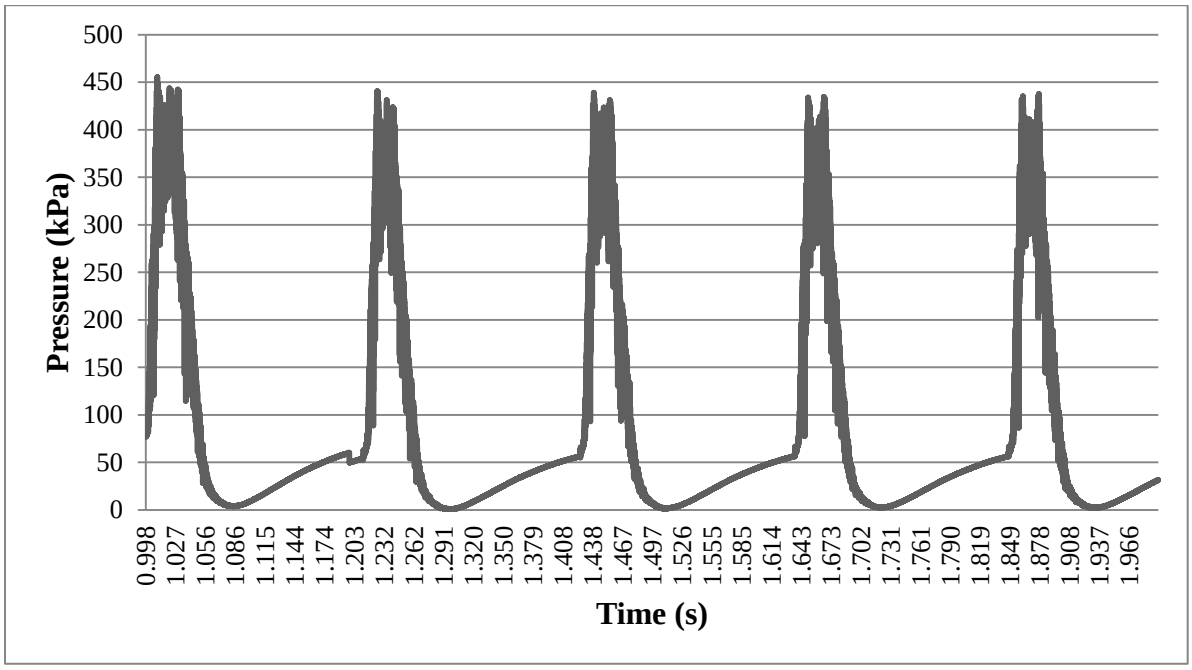

Figure E14 Substrate Pressure Graph for a Supply Pressure of 3.45 MPa Firing at 5 Hz at 20mm SOD

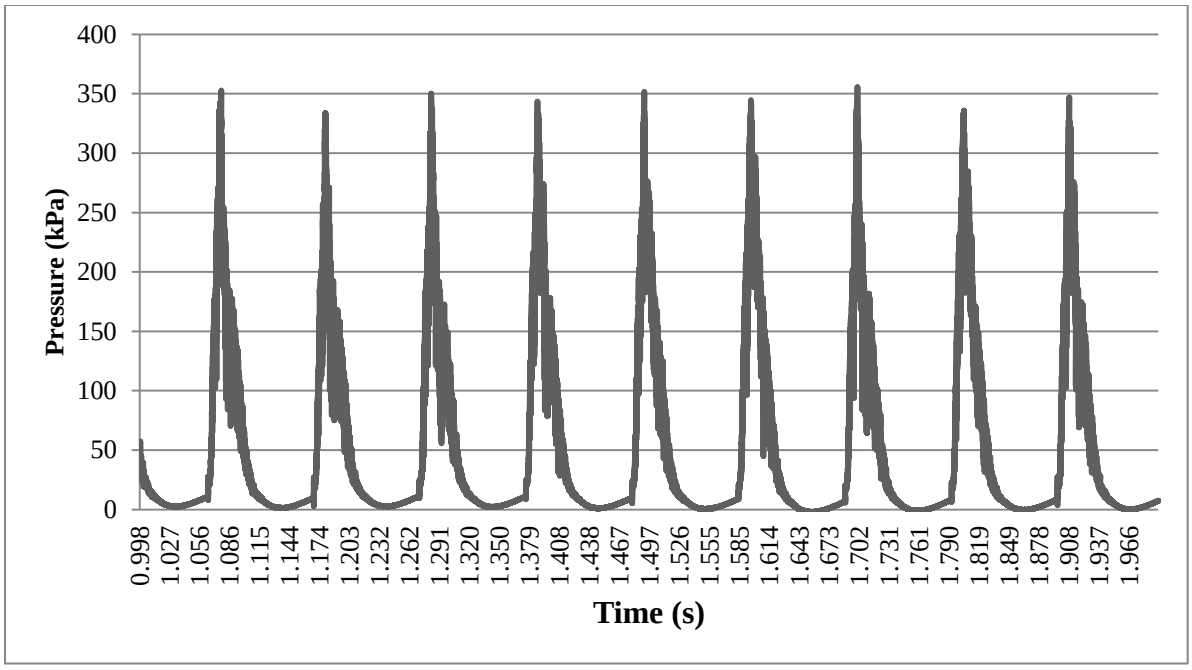

Figure E15 Substrate Pressure Graph for a Supply Pressure of 3.45 MPa Firing at 10 Hz at 10mm SOD

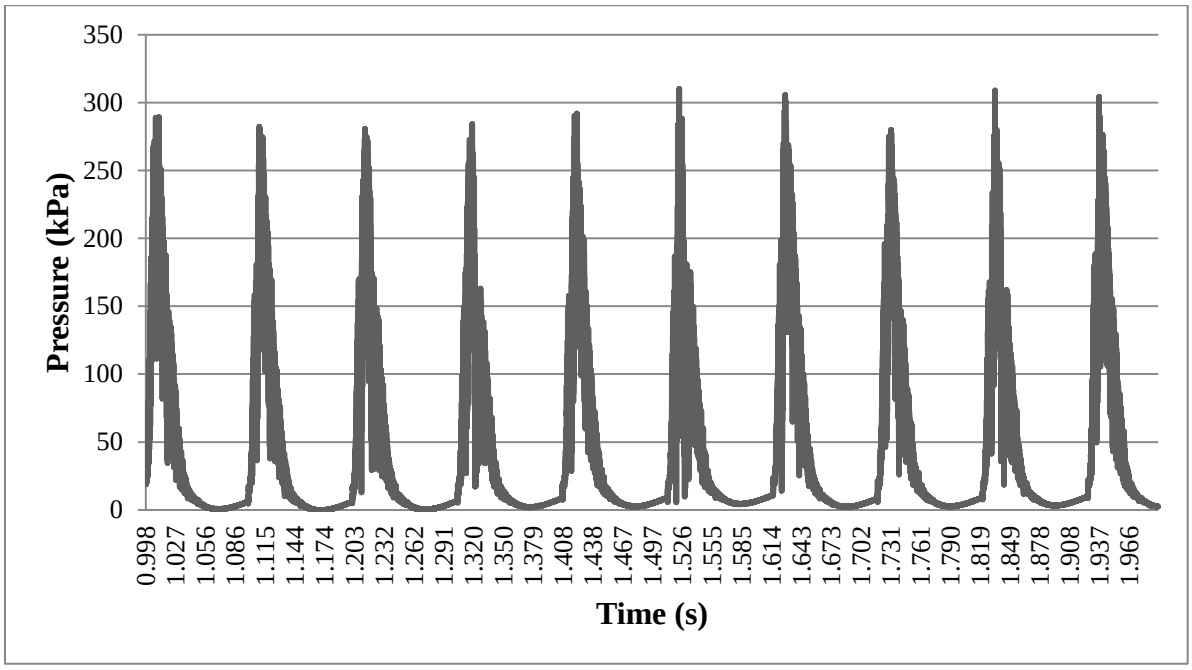

Figure E16 Substrate Pressure Graph for a Supply Pressure of 3.45 MPa Firing at 10 Hz at 20mm SOD

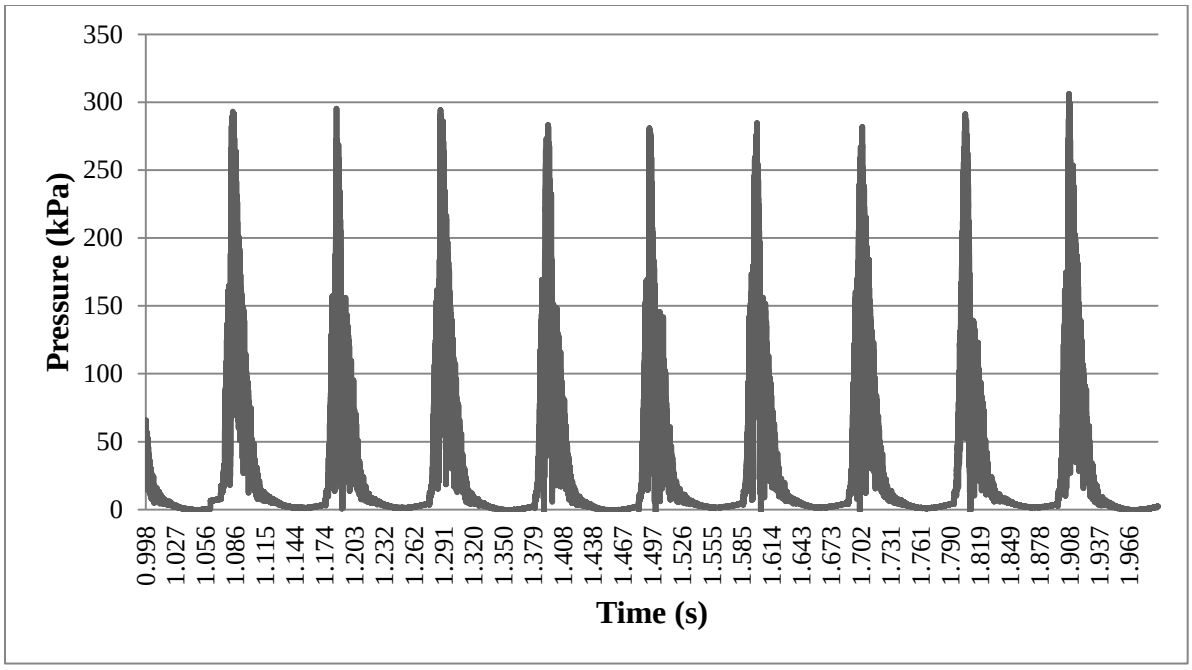

Figure E17 Substrate Pressure Graph for a Supply Pressure of 3.45 MPa Firing at 10 Hz at 30mm SOD

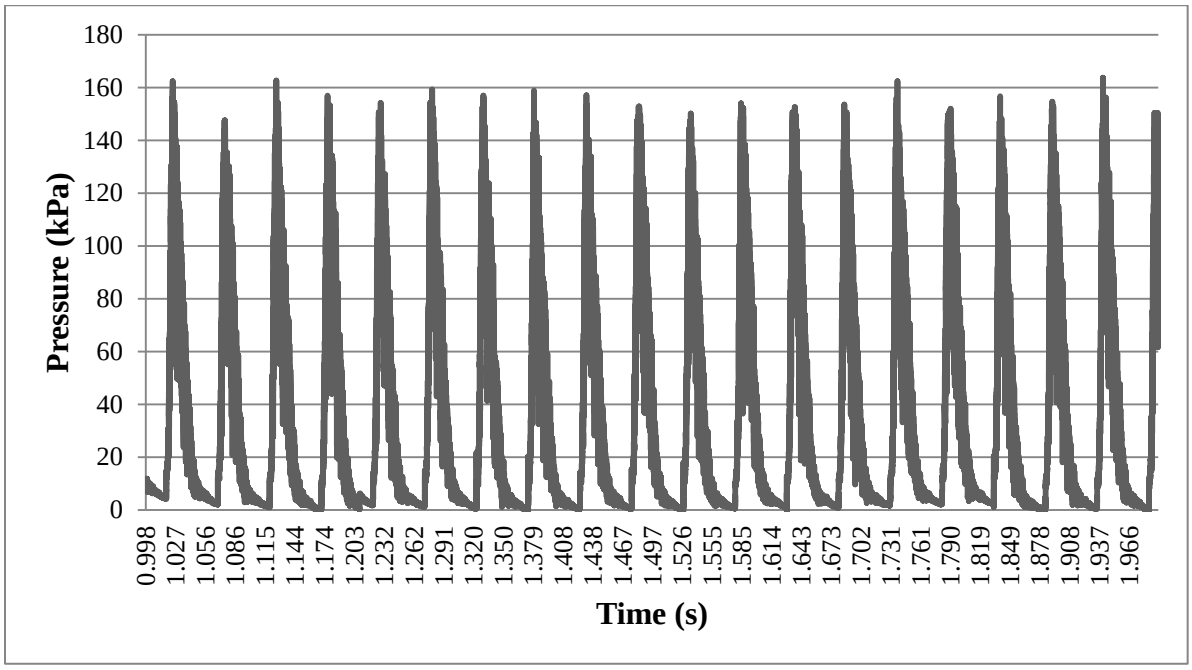

Figure E18 Substrate Pressure Graph for a Supply Pressure of 3.45 MPa Firing at 20 Hz at 10mm SOD

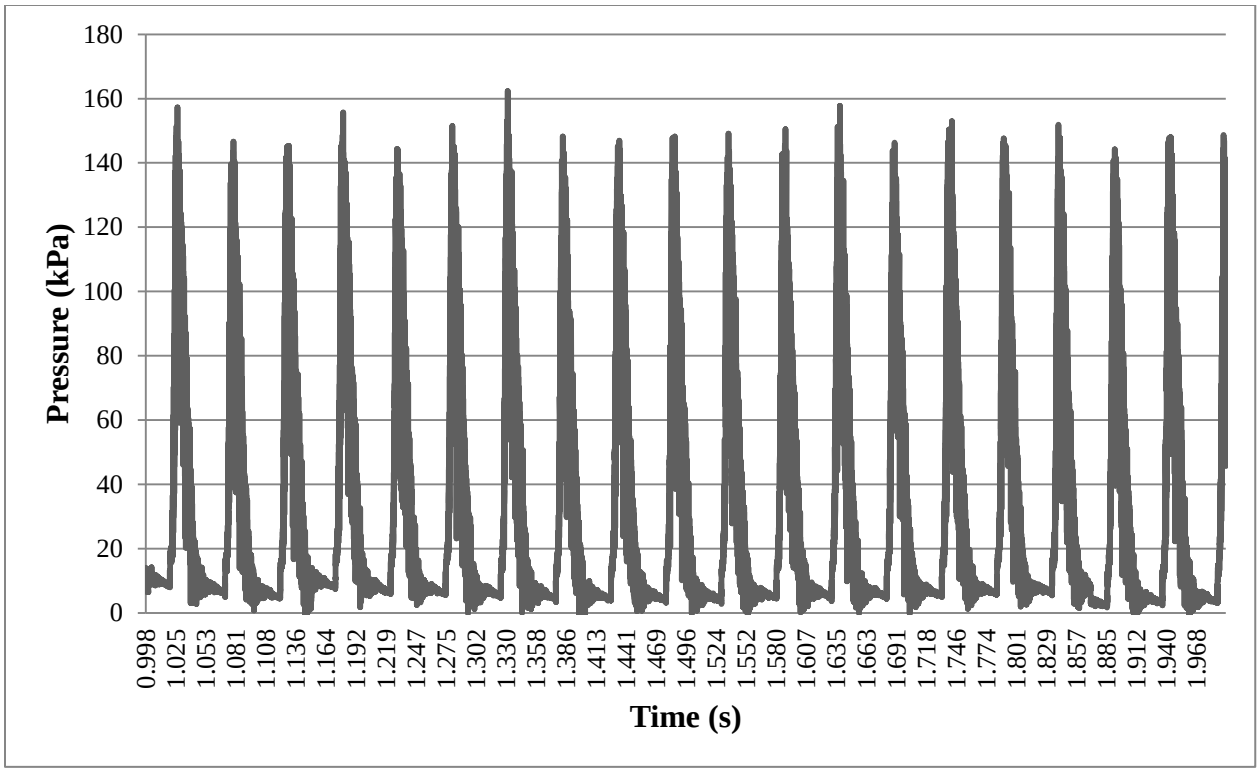

Figure E19 Substrate Pressure Graph for a Supply Pressure of 3.45 MPa Firing at 20 Hz at 20mm SOD

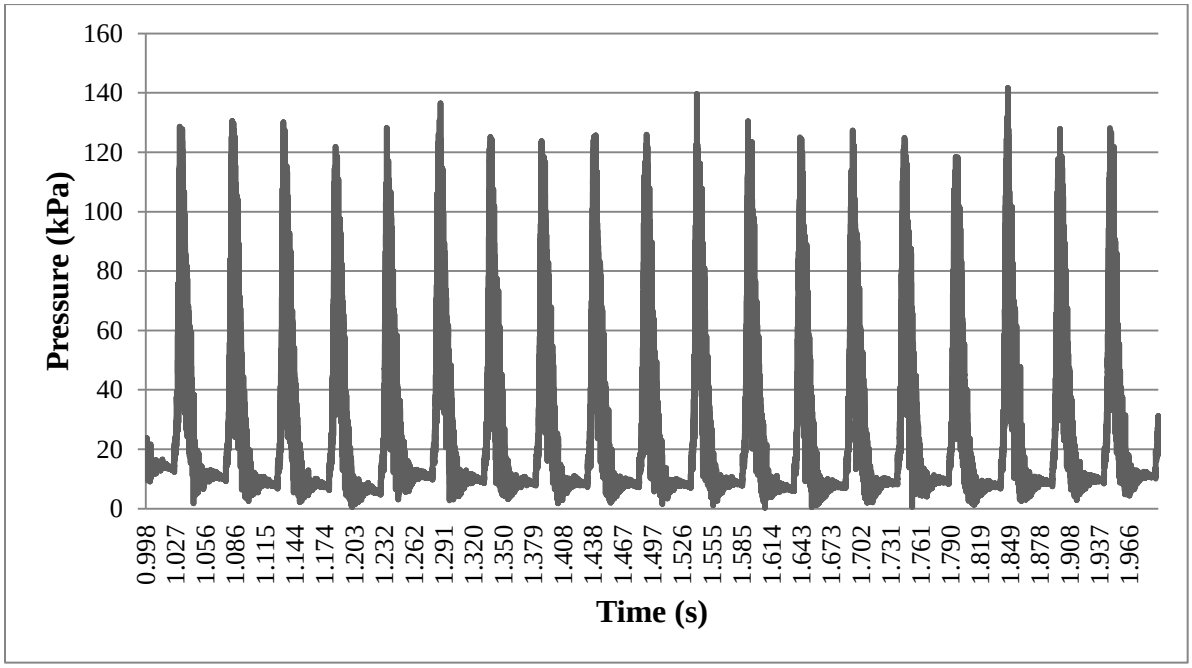

Figure E20 Substrate Pressure Graph for a Supply Pressure of 3.45 MPa Firing at 20 Hz at 30mm SOD

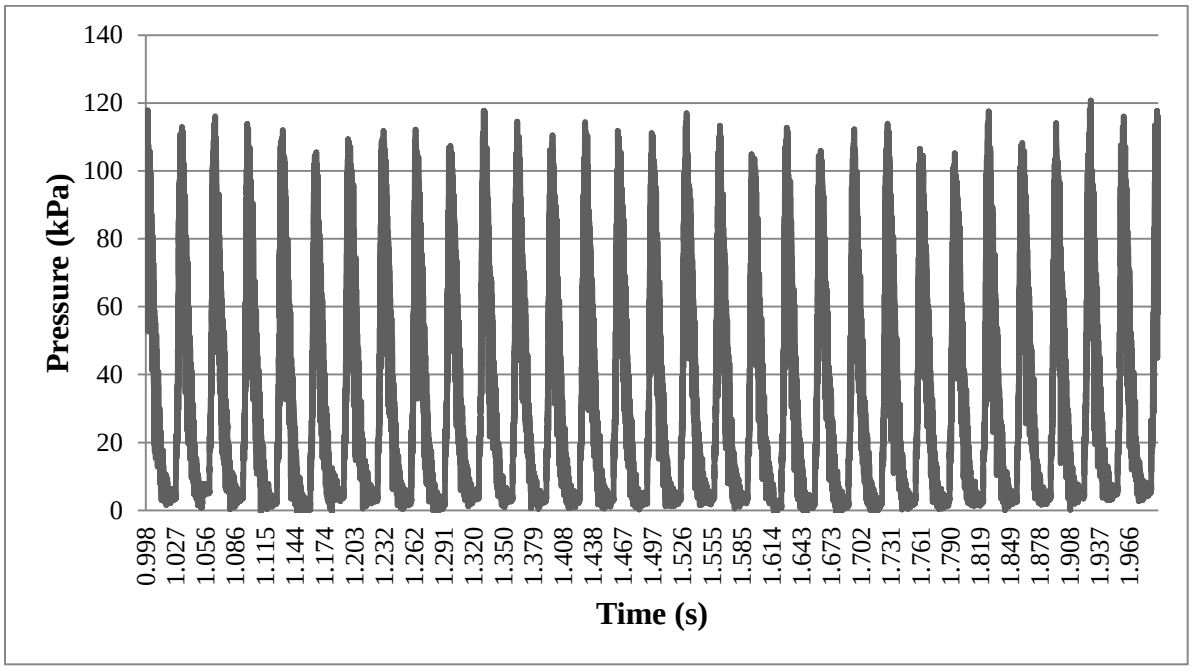

Figure E21 Substrate Pressure Graph for a Supply Pressure of 3.45 MPa Firing at 30 Hz at 10mm SOD

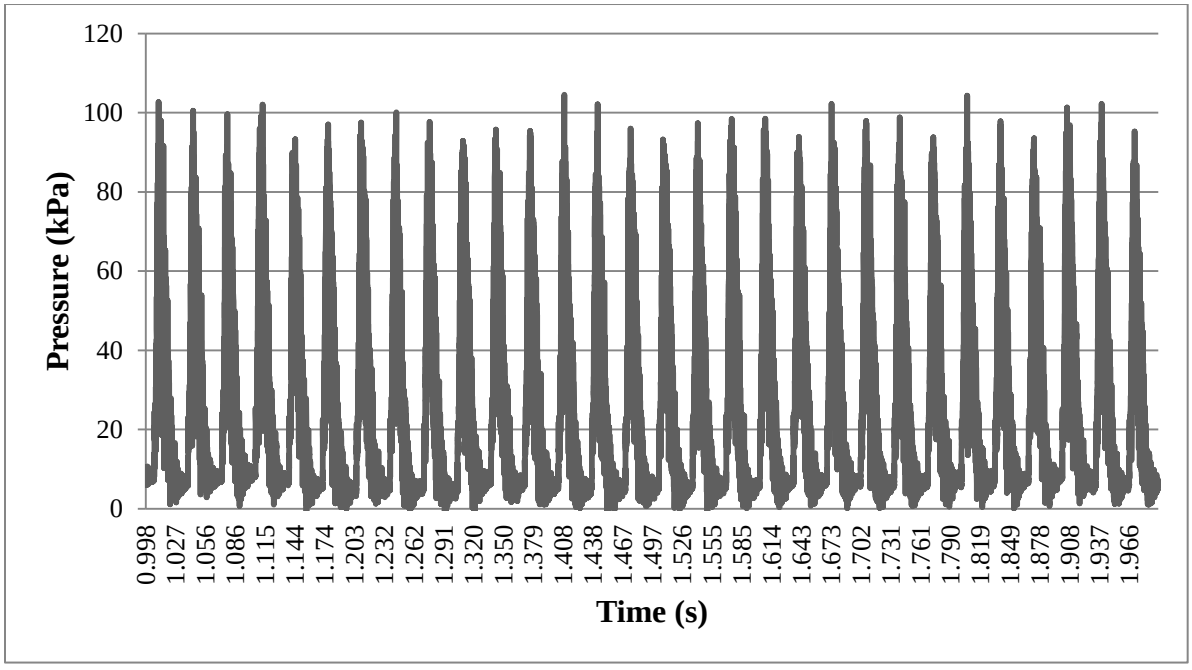

Figure E22 Substrate Pressure Graph for a Supply Pressure of 3.45 MPa Firing at 30 Hz at 20mm SOD

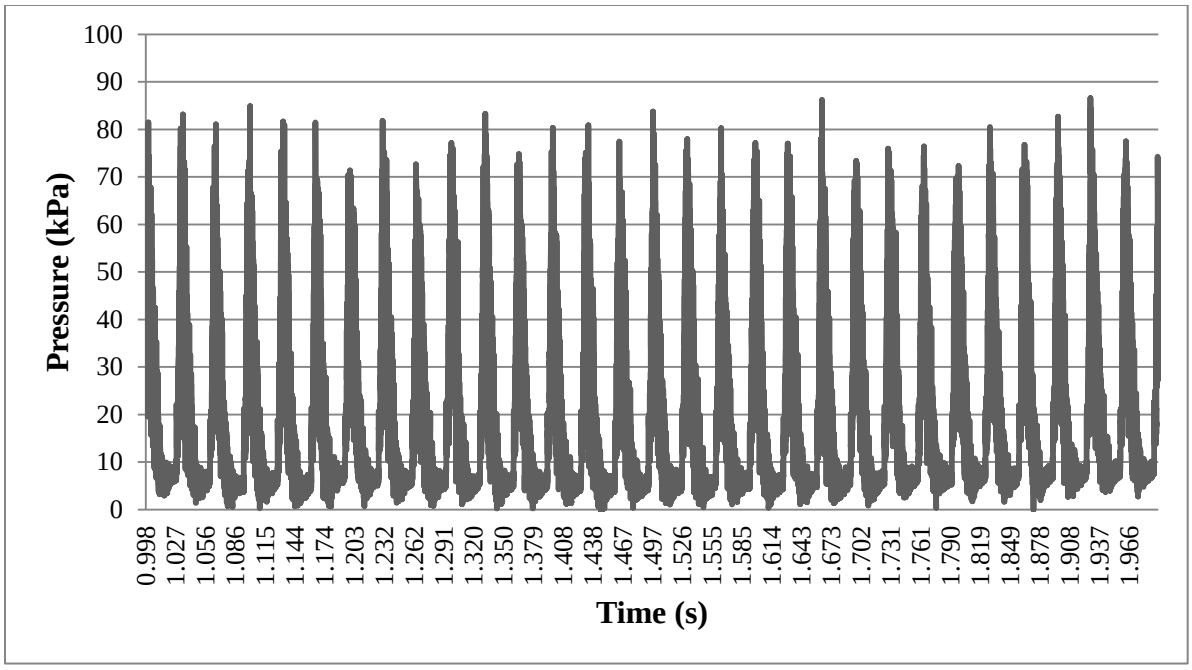

Figure E23 Substrate Pressure Graph for a Supply Pressure of 3.45 MPa Firing at 30 Hz at 30mm SOD

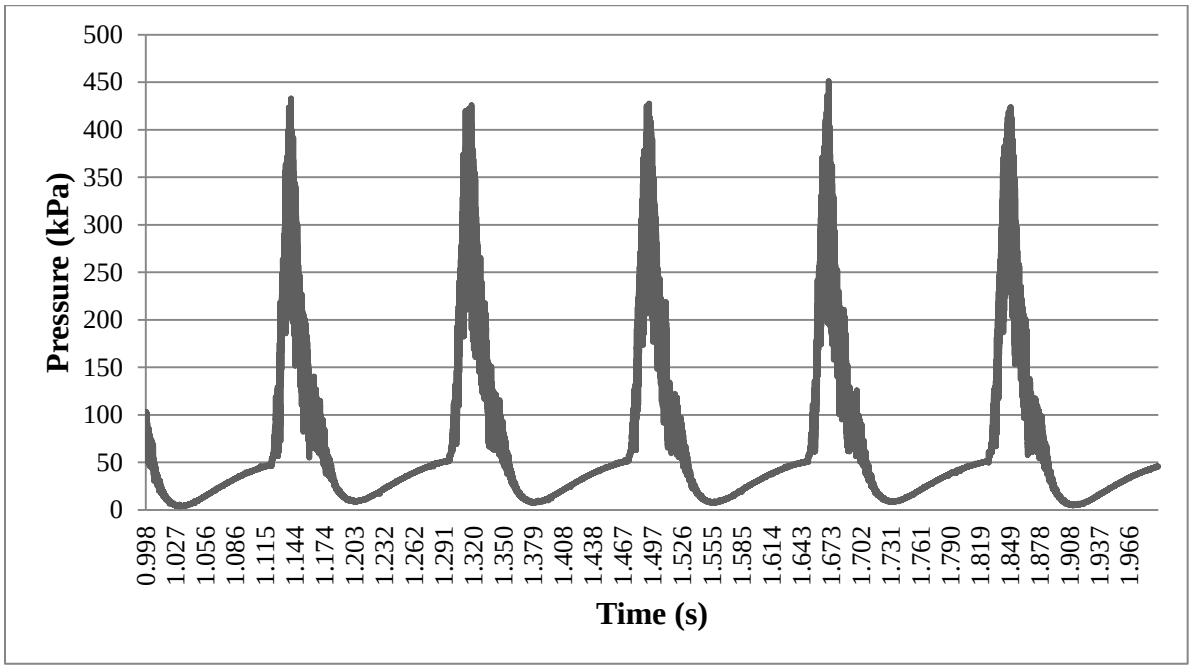

Figure E24 Substrate Pressure Graph for a Supply Pressure of 4.8 MPa Firing at 5 Hz at 10mm SOD

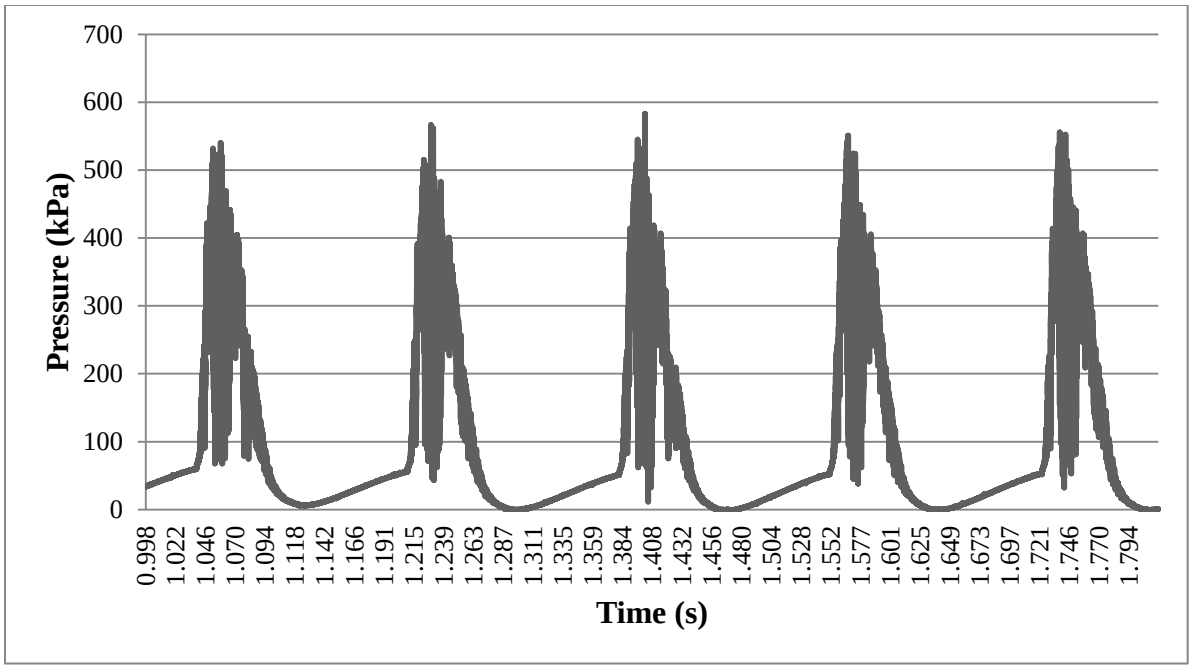

Figure E25 Substrate Pressure Graph for a Supply Pressure of 4.8 MPa Firing at 5 Hz at 20mm SOD

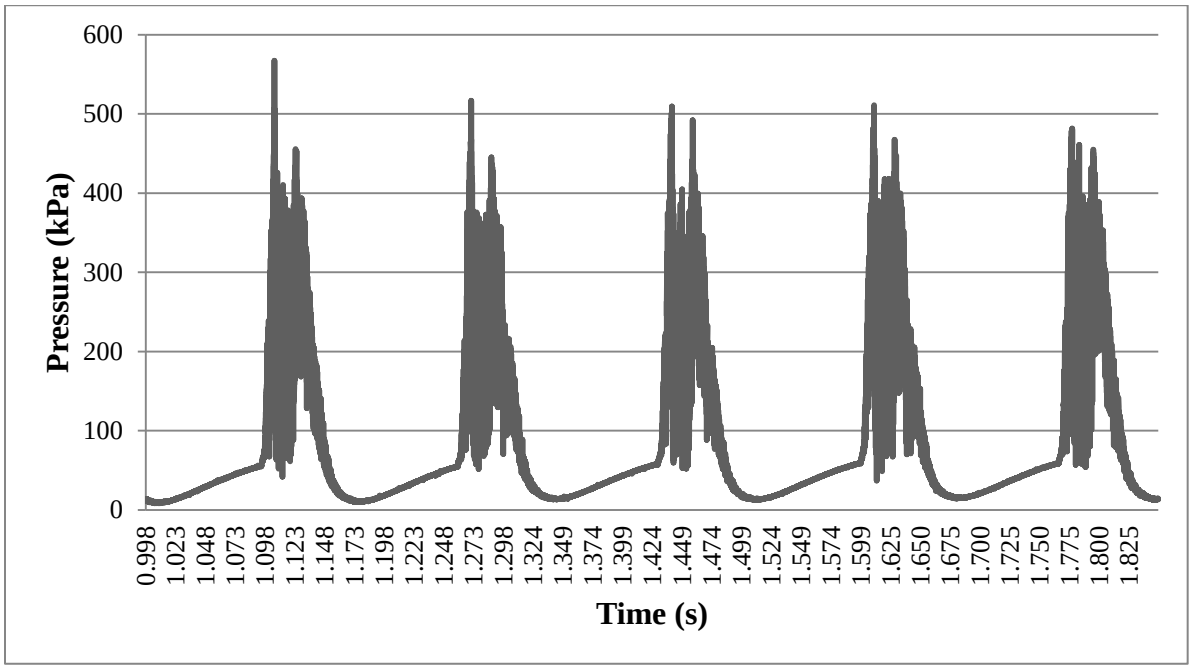

Figure E26 Substrate Pressure Graph for a Supply Pressure of 4.8 MPa Firing at 5 Hz at 30mm SOD

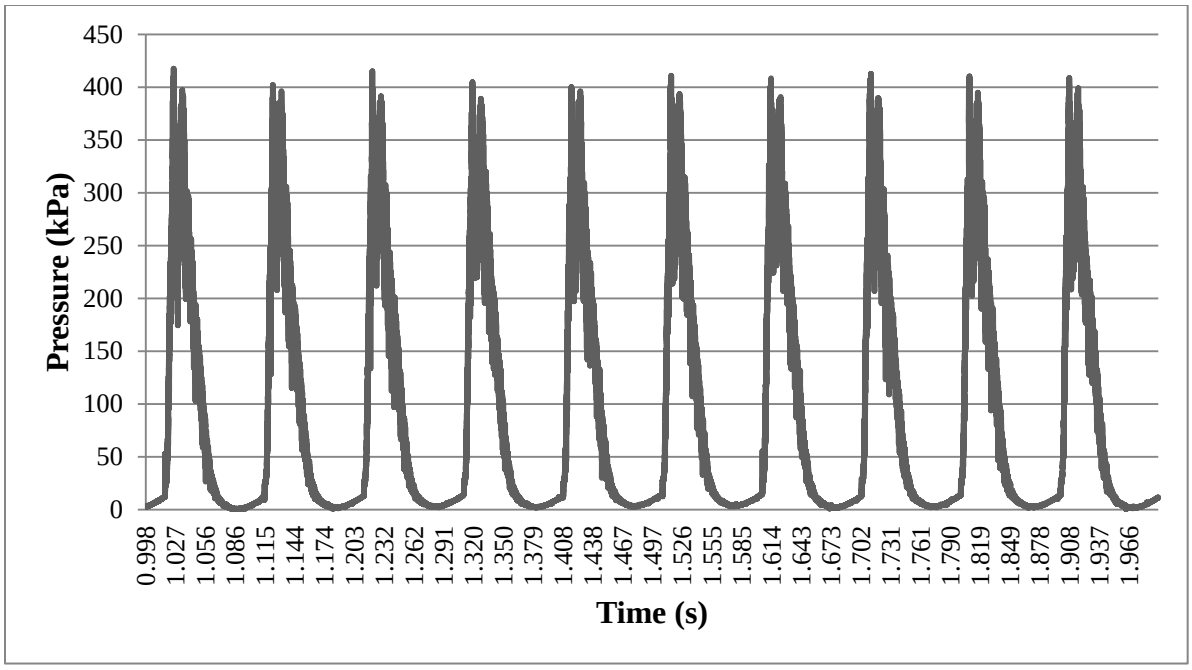

Figure E27 Substrate Pressure Graph for a Supply Pressure of 4.8 MPa Firing at 10 Hz at 10mm SOD

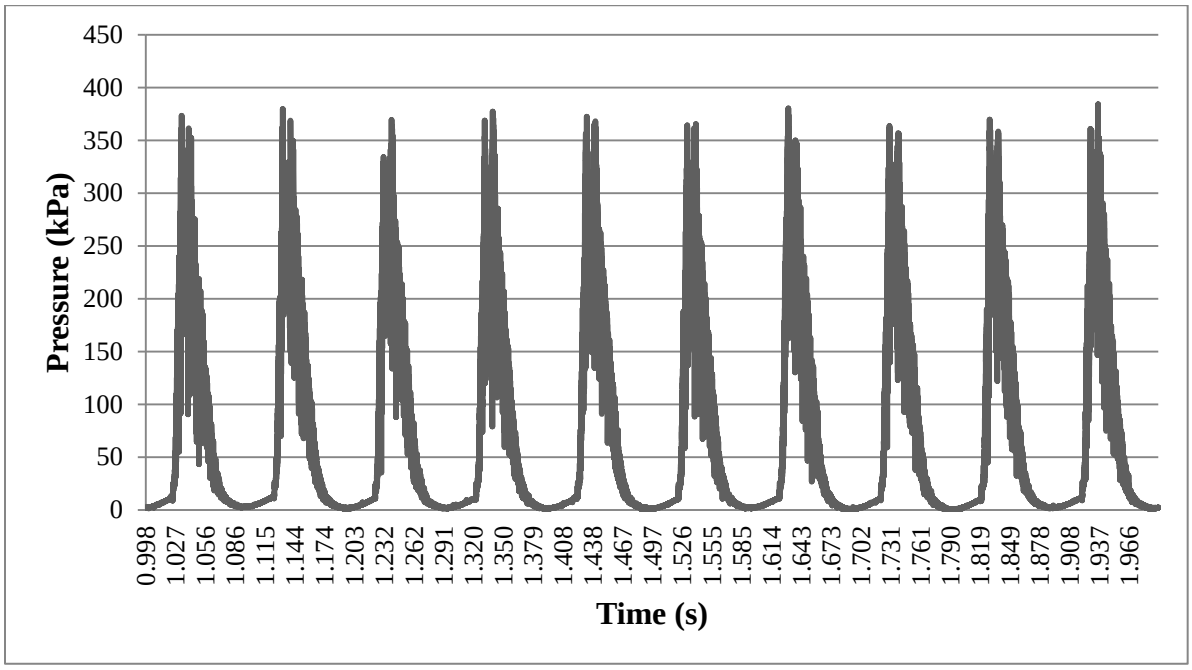

Figure E28 Substrate Pressure Graph for a Supply Pressure of 4.8 MPa Firing at 10 Hz at 20mm SOD

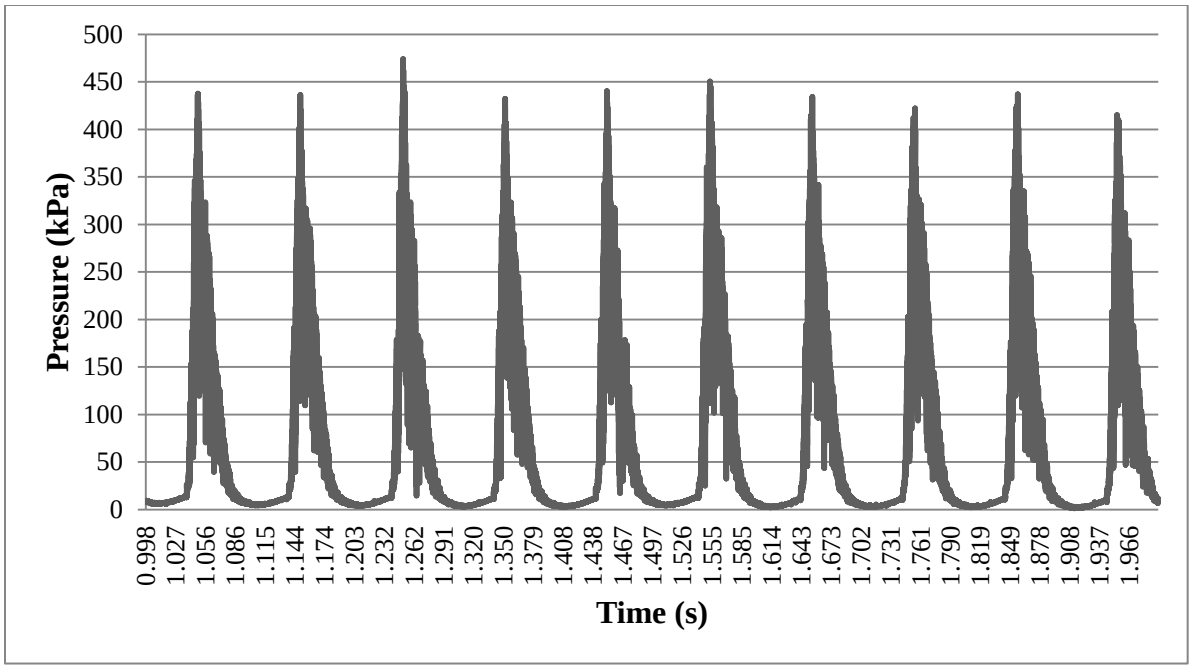

Figure E29 Substrate Pressure Graph for a Supply Pressure of 4.8 MPa Firing at 10 Hz at 30mm SOD

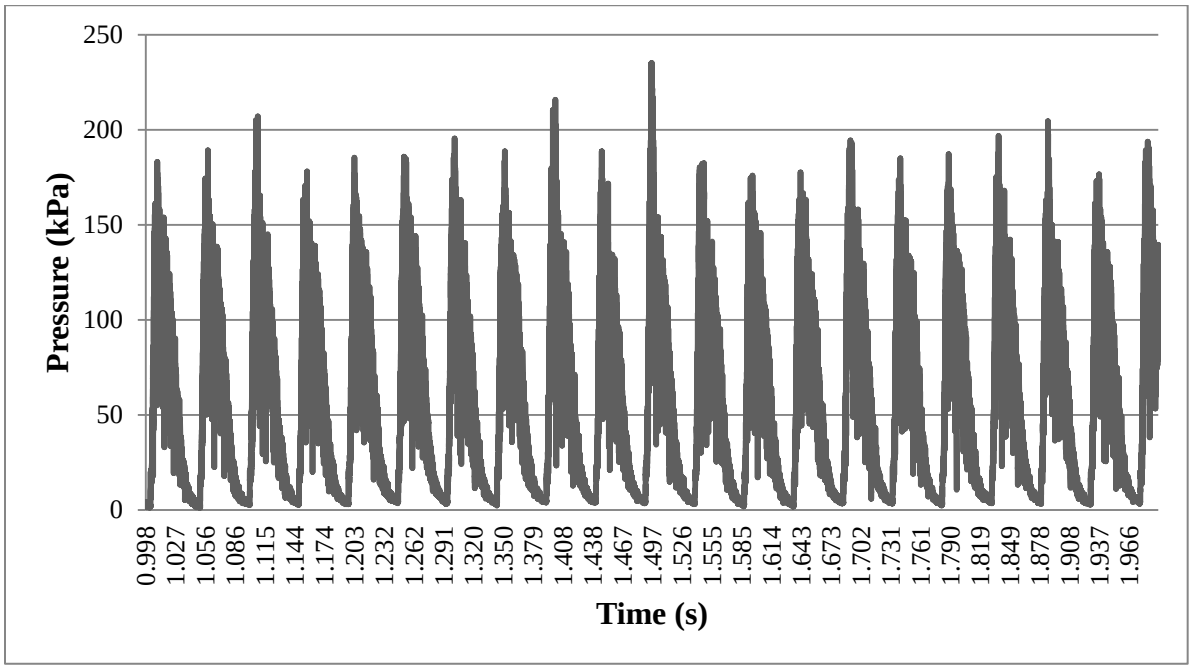

Figure E30 Substrate Pressure Graph for a Supply Pressure of 4.8 MPa Firing at 20 Hz at 10mm SOD

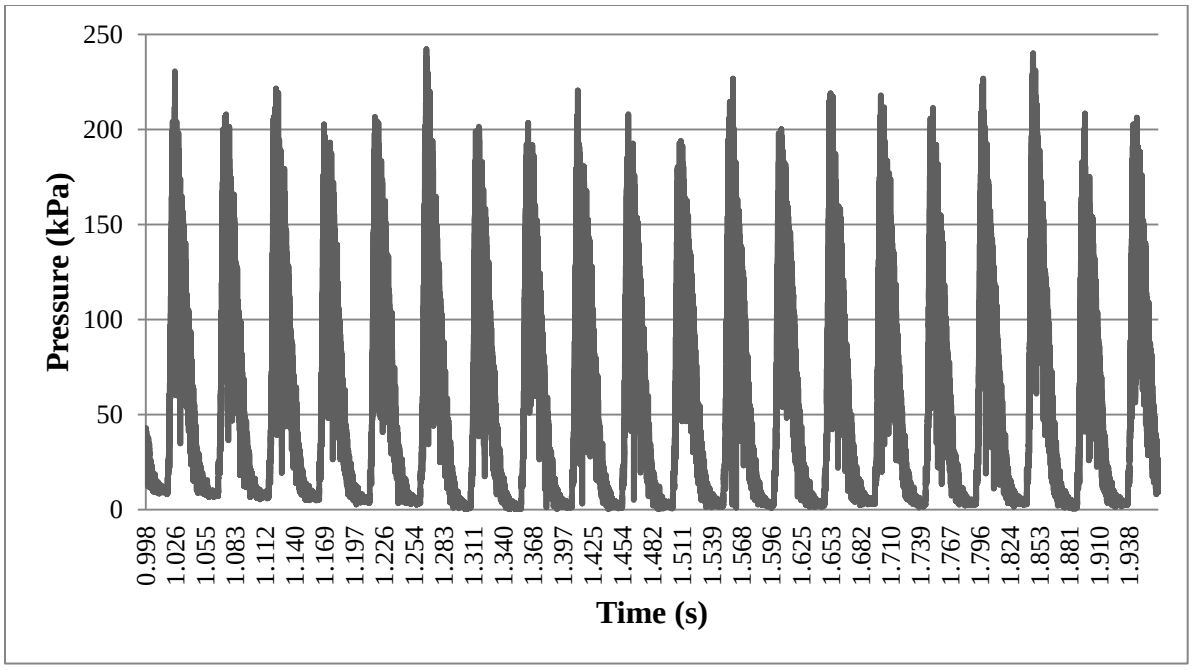

Figure E31 Substrate Pressure Graph for a Supply Pressure of 4.8 MPa Firing at 20 Hz at 20mm SOD

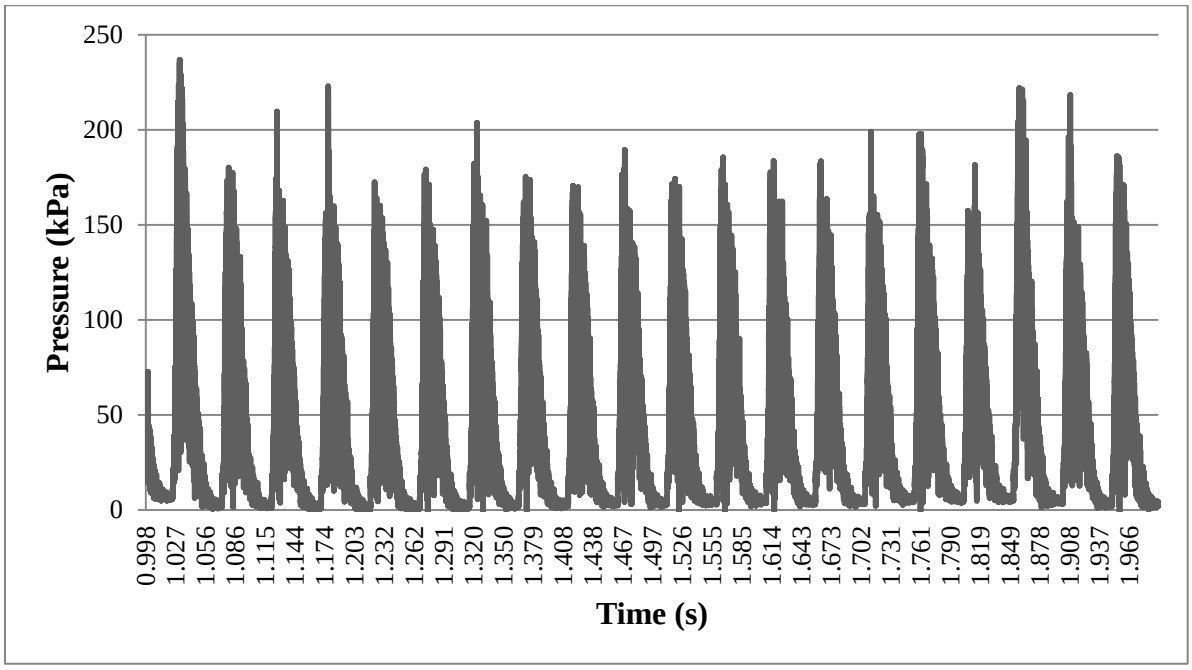

Figure E32 Substrate Pressure Graph for a Supply Pressure of 4.8 MPa Firing at 20 Hz at 30mm SOD

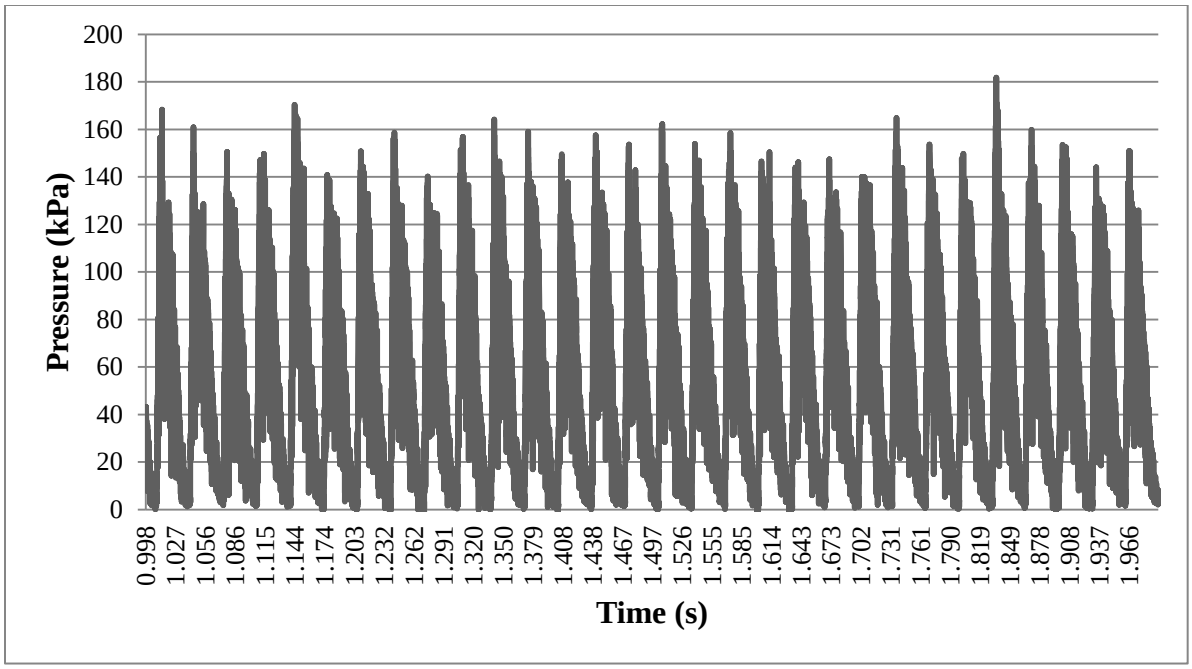

Figure E33 Substrate Pressure Graph for a Supply Pressure of 4.8 MPa Firing at 30 Hz at 10mm SOD

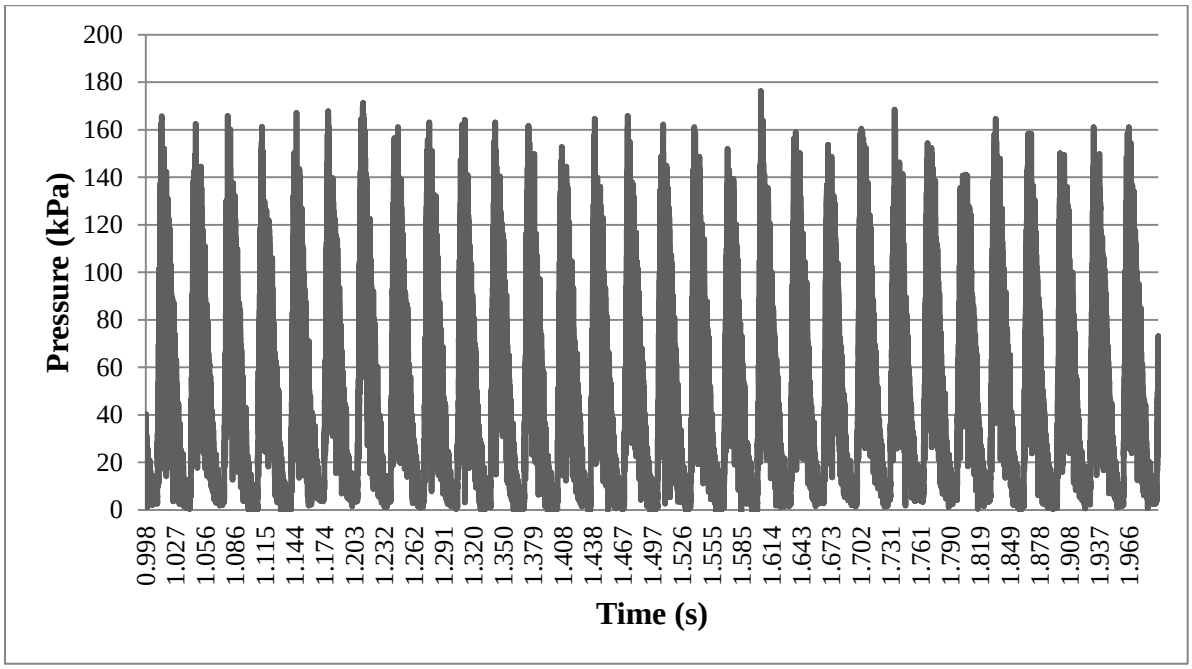

Figure E34 Substrate Pressure Graph for a Supply Pressure of 4.8 MPa Firing at 30 Hz at 20mm SOD

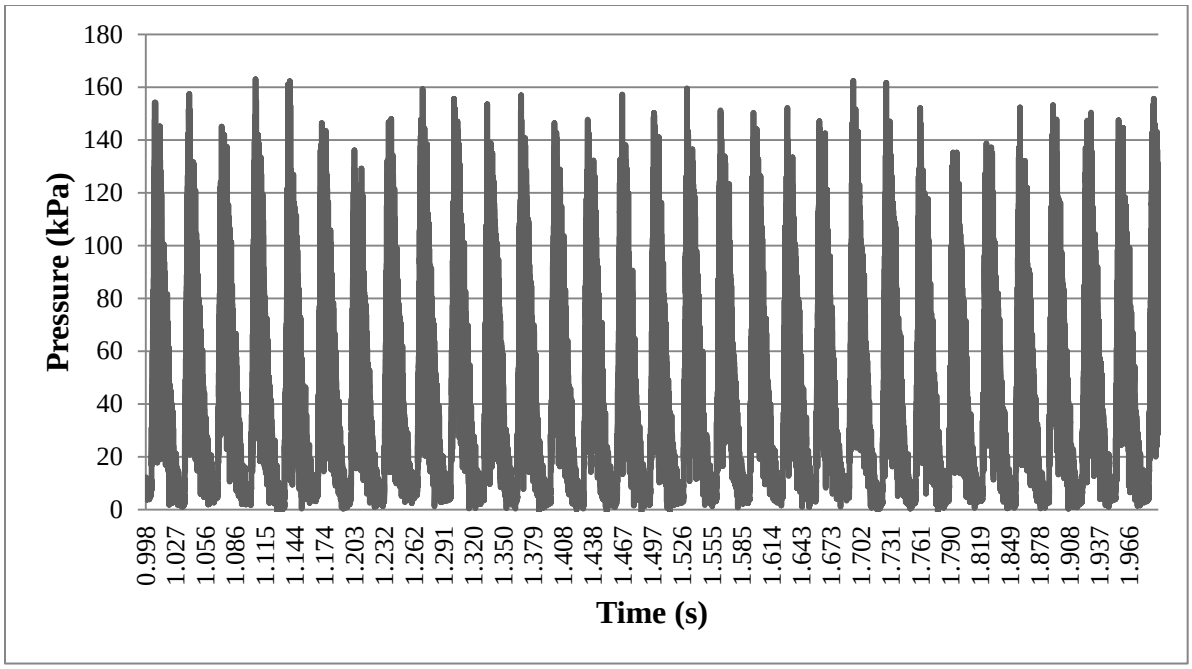

Figure E35 Substrate Pressure Graph for a Supply Pressure of 4.8 MPa Firing at 30 Hz at 30mm SOD

Appendix F Written Permissions from Copyright Holders

ELSEVIER LICENSE
TERMS AND CONDITIONS
Dec 22, 2014

This is an Agreement between Kevin Mrozinski ("You") and Elsevier ("Elsevier"). It consists of your order details, the terms and conditions provided by Elsevier ("Elsevier"), and the payment terms and conditions.

Registered Company Number	1982084
Customer name	Kevin Mrozinski
License number	3326780421138
License date	Feb 12, 2014
Licensed content publisher	Elsevier
Licensed content publication	Elsevier Books
Licensed content title	Principles of Corrosion Engineering and Corrosion Control
Licensed content author	Zaki Ahmad
Licensed content date	2006
Number of pages	56
Start Page	382
End Page	437
Type of Use	reuse in a thesis/dissertation
Portion	figures/tables/illustrations
Number of figures/tables/illustrations	1
Format	electronic
Are you the author of this Elsevier chapter?	No
Will you be translating?	No
Title of your thesis/dissertation	Shock Interaction With Substrate in a Shock Induced Flow
Expected completion date	Jun 2014
Estimated size (number of pages)	150
Elsevier VAT number	GB 494 6272 12

JOHN WILEY AND SONS LICENSE
TERMS AND CONDITIONS
Dec 22, 2014

This Agreement between Kevin Mrozinski ("You") and John Wiley and Sons ("John Wiley and Sons") consists of your license details and the terms and conditions provided by John Wiley and Sons and Copyright Clearance Center.

License Number	3335560069319
License date	Feb 24, 2014
Licensed Content Publisher	John Wiley and Sons
Licensed Content Publication	Wiley oBooks
Licensed Content Title	Thermal Spraying Techniques
Licensed Content Author	Lech Pawlowski
Licensed Content Date	Mar 20, 2008
Pages	47
Type of use	Dissertation/Thesis
Requestor type	University/Academic
Format	Electronic
Portion	Figure/table
Number of figures/tables	1
Original Wiley figure/table number(s)	Figure 3.11
Will you be translating?	No
Title of your thesis / dissertation	Shock Interaction With Substrate in a Shock Induced Flow
Expected completion date	Jun 2014
Expected size (number of pages)	150
Billing Type	Invoice
Terms and Conditions	See Above

SPRINGER LICENSE
TERMS AND CONDITIONS

Dec 22, 2014

This is a License Agreement between Kevin Mrozinski ("You") and Springer ("Springer") provided by Copyright Clearance Center ("CCC"). The license consists of your order details, the terms and conditions provided by Springer, and the payment terms and conditions.

License Number	3534240335821
License date	Dec 22, 2014
Licensed content publisher	Springer
Licensed content publication	Journal of Thermal Spray Technology
Licensed content title	Shock-Wave-Induced Spraying: Modeling and Physics of a New Spray Process
Licensed content author	Mo Karimi
Licensed content date	Jan 1, 2011
Volume number	20
Issue number	4
Type of Use	Thesis/Dissertation
Portion	Figures
Author of this Springer article	No
Order reference number	None
Original figure numbers	Figure 1
Title of your thesis / dissertation	Shock Interaction with Substrate in a Shock Induced Spray Process
Expected completion date	Jan 2015
Estimated size(pages)	120
Terms and Conditions	See Above

ELSEVIER LICENSE
TERMS AND CONDITIONS

Dec 22, 2014

This is a License Agreement between Kevin Mrozinski ("You") and Elsevier ("Elsevier") provided by Copyright Clearance Center ("CCC"). The license consists of your order details, the terms and conditions provided by Elsevier, and the payment terms and conditions.

Supplier	Elsevier Limited The Boulevard,Langford Lane Kidlington,Oxford,OX5 1GB,UK
Registered Company Number	1982084
Customer name	Kevin Mrozinski
License number	3534240729295
License date	Dec 22, 2014
Licensed content publisher	Elsevier
Licensed content publication	Surface and Coatings Technology
Licensed content title	SiC particulate reinforced Al–12Si alloy composite coatings produced by the pulsed gas dynamic spray process: Microstructure and properties
Licensed content author	None
Licensed content date	15 July 2009
Licensed content volume number	203
Licensed content issue number	20-21
Number of pages	11
Start Page	3260
End Page	3270
Type of Use	reuse in a thesis/dissertation
Intended publisher of new work	other
Portion	figures/tables/illustrations
Number of figures/tables/illustrations	1
Format	both print and electronic

Are you the author of this Elsevier article?	No
Will you be translating?	No
Original figure numbers	1
Title of your thesis/dissertation	Shock Interaction with Substrate in a Shock Induced Spray Process
Expected completion date	Jan 2015
Estimated size (number of pages)	120
Elsevier VAT number	GB 494 6272 12
Terms and Conditions	See Above

Measurements of Mean Static Pressure and Far Field Acoustics of Shock Containing Supersonic Jets

Author and Affiliation: Norum, T. D. *(NASA Langley Research Center, Hampton, VA, USA)*; Seiner, J. M. *(NASA Langley Research Center, Hampton, VA, USA)*

Publication Date: Sep 01, 1982
Document ID: 19820025274 *(Acquired Nov 13, 1995)*
Accession Number: 82N33150
Subject Category: ACOUSTICS
Report/Patent Number: NASA-TM-84521, L-15378, NAS 1.15:84521
Document Type: Technical Report
Publisher Information: United States
Contract/Grant/Task Num: RTOP 505-32-03-05
Financial Sponsor: NASA; Washington, DC, United States
Organization Source: NASA Langley Research Center; Hampton, VA, United States
Description: 204p; In English
Distribution Limits: Unclassified; Publicly available; Unlimited

NASA Terms: FAR FIELDS; JET AIRCRAFT NOISE; NOISE PROPAGATION; SHOCK WAVES; SUPERSONIC FLIGHT; DATA BASES; NOISE SPECTRA; PRESSURE MEASUREMENT; SOUND PRESSURE; STATIC PRESSURE; WIND TUNNEL TESTS

ELSEVIER LICENSE
TERMS AND CONDITIONS

Jan 07, 2015

This is a License Agreement between Kevin Mrozinski ("You") and Elsevier ("Elsevier") provided by Copyright Clearance Center ("CCC"). The license consists of your order details, the terms and conditions provided by Elsevier, and the payment terms and conditions.

Supplier	Elsevier Limited The Boulevard,Langford Lane Kidlington,Oxford,OX5 1GB,UK
Registered Company Number	1982084
Customer name	Kevin Mrozinski
License number	3543760719539
License date	Jan 07, 2015
Licensed content publisher	Elsevier
Licensed content publication	Surface and Coatings Technology
Licensed content title	Standoff distance and bow shock phenomena in the Cold Spray process
Licensed content author	J. Pattison,S. Celotto,A. Khan,W. O'Neill
Licensed content date	15 January 2008
Licensed content volume number	202
Licensed content issue number	8
Number of pages	12
Start Page	1443
End Page	1454
Type of Use	reuse in a thesis/dissertation
Portion	figures/tables/illustrations
Number of figures/tables/illustrations	1
Format	both print and electronic
Are you the author of this Elsevier article?	No
Will you be translating?	No
Original figure numbers	1
Title of your thesis/dissertation	Shock Interaction with Substrate in a Shock Induced Spray Process
Expected completion date	Jan 2015
Estimated size (number of pages)	120
Elsevier VAT number	GB 494 6272 12
Terms and Conditions	See Above

ELSEVIER LICENSE
TERMS AND CONDITIONS

Dec 22, 2014

This is a License Agreement between Kevin Mrozinski ("You") and Elsevier ("Elsevier") provided by Copyright Clearance Center ("CCC"). The license consists of your order details, the terms and conditions provided by Elsevier, and the payment terms and conditions.

Supplier	Elsevier Limited The Boulevard,Langford Lane Kidlington,Oxford,OX5 1GB,UK
Registered Company Number	1982084
Customer name	Kevin Mrozinski
License number	3534241287649
License date	Dec 22, 2014
Licensed content publisher	Elsevier
Licensed content publication	Surface and Coatings Technology
Licensed content title	Pulsed-Gas Dynamic Spraying: Process analysis, development and selected coating examples
Licensed content author	B. Jodoin,P. Richer,G. Bérubé,L. Ajdelsztajn,A. Erdi-Betchi,M. Yandouzi
Licensed content date	21 May 2007
Licensed content volume number	201
Licensed content issue number	16-17
Number of pages	8
Start Page	7544
End Page	7551
Type of Use	reuse in a thesis/dissertation
Intended publisher of new work	other
Portion	figures/tables/illustrations
Number of figures/tables/illustrations	2
Format	both print and electronic

Are you the author of this Elsevier article?	No
Will you be translating?	No
Original figure numbers	1, 2
Title of your thesis/dissertation	Shock Interaction with Substrate in a Shock Induced Spray Process
Expected completion date	Jan 2015
Estimated size (number of pages)	120
Elsevier VAT number	GB 494 6272 12
Terms and Conditions	See Above

AIP PUBLISHING LLC LICENSE
TERMS AND CONDITIONS

Dec 22, 2014

License Number	3534241505647
Order Date	Dec 22, 2014
Publisher	AIP Publishing LLC
Publication	Journal of Applied Physics
Article Title	Experimental Study of the Formation of a Vortex Ring at the Open End of a Cylindrical Shock Tube
Author	F. K. Elder Jr.,N. De Haas
Online Publication Date	Jun 15, 2004
Volume number	23
Issue number	10
Type of Use	Thesis/Dissertation
Requestor type	Author (original article)
Format	Print and electronic
Portion	Figure/Table
Number of figures/tables	1
Title of your thesis / dissertation	Shock Interaction with Substrate in a Shock Induced Spray Process
Expected completion date	Jan 2015
Estimated size (number of pages)	120
Terms and Conditions	

AIP Publishing LLC -- Terms and Conditions: Permissions Uses

CAMBRIDGE UNIVERSITY PRESS LICENSE
TERMS AND CONDITIONS

Dec 22, 2014

This is a License Agreement between Kevin Mrozinski ("You") and Cambridge University Press ("Cambridge University Press") provided by Copyright Clearance Center ("CCC"). The license consists of your order details, the terms and conditions provided by Cambridge University Press, and the payment terms and conditions.

License Number	3534251024549
License date	Dec 22, 2014
Licensed content publisher	Cambridge University Press
Licensed content publication	The Journal of Fluid Mechanics
Licensed content title	Experimental and numerical analysis of circular pulse jets
Licensed content author	R. ISHII, H. FUJIMOTO, N. HATTA and Y. UMEDA
Licensed content date	Sep 8, 2000
Volume number	392
Issue number	-1
Start page	129
End page	153
Type of Use	Dissertation/Thesis
Requestor type	Not-for-profit
Portion	Text extract
Number of pages requested	1
Order reference number	None
Territory for reuse	North America Only
Title of your thesis / dissertation	Shock Interaction with Substrate in a Shock Induced Spray Process
Expected completion date	Jan 2015
Estimated size(pages)	120
Terms and Conditions	See Above

ELSEVIER ORDER DETAILS

Dec 22, 2014

This is an Agreement between Kevin Mrozinski ("You") and Elsevier ("Elsevier"). It consists of your order details, the terms and conditions provided by Elsevier ("Elsevier"), and the payment terms and conditions.

Order Number	500953806
Order Date	Dec 22, 2014
Licensed content publisher	Elsevier
Licensed content publication	JSAE Review
Licensed content title	Relation between the flow pattern downstream of duct and the noise
Licensed content author	Masaki Endo,Yuji Futagami,Junjiro Iwamoto
Licensed content date	January 2000
Licensed content volume number	21
Licensed content issue number	1
Number of pages	8
Start Page	125
End Page	132
Type of Use	reuse in a thesis/dissertation
Intended publisher of new work	other
Portion	figures/tables/illustrations
Number of figures/tables/illustrations	1
Format	both print and electronic
Are you the author of this Elsevier article?	No
Will you be translating?	No
Original figure numbers	4
Title of your thesis/dissertation	Shock Interaction with Substrate in a Shock Induced Spray Process
Expected completion date	Jan 2015
Elsevier VAT number	GB 494 6272 12

Detonation Gun Figure Permission:

I hereby give permission to Master of Applied Science in Mechanical Engineering Student at the University of Windsor, Kevin Mrozinski, permission to use and reproduce the diagram of the Detonation Gun in his thesis Shock Interaction With Substrate in a Shock Induced Spray Process.

Rod Mylcraine
Praxair Surface Technician

CSME Conference Permission:

I hereby give permission to Master of Applied Science in Mechanical Engineering Student at the University of Windsor, Kevin Mrozinski, permission to use and reproduce all content including figures and tables from *Shock Induced Spray Process: Flow Visualization of The Substrate Impact Region* presented at the Proceedings of The Canadian Society for Mechanical Engineering International Congress in Toronto held June 1-4, 2014.

Jean Zu | *Professor and Chair*

Department of Mechanical & Industrial Engineering
Faculty of Applied Science & Engineering | University of Toronto

Appendix G Uncertainty Calculations

G.1 Uncertainty in Substrate Peak Pressure

The uncertainty of the peak pressure depended on the uncertainties of the pressure transducer used in the substrate.

This was a PCB Piezotronics 113B28 with the following manufacturing uncertainties:

A sensitivity of +/-14.5 mV/kPa with a 2 mV minimum voltage.

A resolution of 0.007 kPa with a max voltage range of 689.4 kPa.

A temperature coefficient of sensitivity of +/- 0.054%/˚C with an assumption of a range in temperature for all trials of 2 ˚C.

The following equations can be used;

$$W_{PP} = \sqrt{{B_{PP}}^2 + \left(t_{v,95}\, P_{pp}\right)^2} \qquad [40]$$

Where, $$B_{PP} = \sqrt{\left(\frac{E_{min}}{S}\right)^2 + R^2 + [(\Delta T)(T_{CS})(P_{MR})]^2}$$

And, $$P_{PP} = \sqrt{\frac{1}{N-1}\sum_{i=1}^{N}\left(P_{Peak_i} - P_{Peak_{avg}}\right)^2}$$

$t_{v,95}$ is found using the Student t Distribution table using a 95% confidence regularly distributed graph.

The trial with the lowest peak pressure has degree of freedom of 29 and a $t_{v,95}$ value of 2.045.

The trial with the highest peak pressure has degree of freedom of 4 and a $t_{v,95}$ value of 2.776.

Solving the above equations,

The lowest peak pressure uncertainty is +/- 2.68 kPa. With the lowest average peak pressure being 17.49 kPa, this gives an uncertainty percentage of +/- 15.3%.

The highest peak pressure uncertainty is +/- 59.83 kPa. With the highest average peak pressure being 582.80 kPa, this gives an uncertainty percentage of +/- 10.3%.

G.2 Uncertainty in Supply Pressure

The uncertainty of the supply pressure is based on the uncertainty of the reading of the pressure gauge by the operator. A relationship can be developed based on the intervals on the gauge and thickness of the reader needle.

This relationship is:

$$\frac{Y}{X} = \frac{W_{SP}}{I}$$

Where W_{SP} is the uncertainty in the supply pressure, I is the interval of the gauge; in this case 100 PSI, Y is the width of the reader needle and X is the distance between indicators. This is seen more clearly in the example Figure G1.

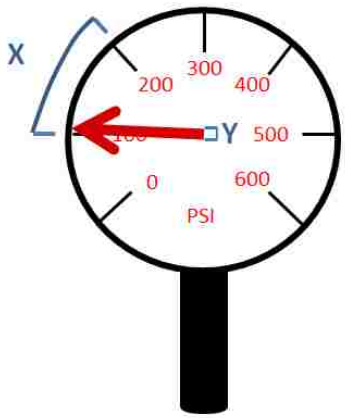

Figure G1 Uncertainty in Pressure Gauge

The value of Y was approximated to be 1/20th the size of X.

Therefore the uncertainty in the supply pressure is +/- 5 PSI or 35 kPa. As the lowest supply pressure used was 2 MPa, the largest supply pressure uncertainty percentage is +/- 1.75%.

G.3 Uncertainty in the Stand off Distance

The Uncertainty in the stand off distance is the uncertainty of the measurement instrument used. Vernier calipers yield an uncertainty of +/- 0.025 mm.

Therefore the uncertainty of the stand off distance is +/- 0.025 mm. As the smallest stand off distance was 10 mm, the largest stand off distance uncertainty percentage is +/- 0.25%.

G.4 Uncertainty in Image Capture Time

The uncertainty in the image capture is based on the ability of the High Speed Camera. Using a conservative approach the maximum time the camera can possibly be off is 1 frame.

So,

$$W_{TF} = \pm T = \pm \frac{1}{F_R}$$

where F_R is the frame rate; in this case 52500 fps.

Therefore the uncertainty of the image capture is +/- 1.91 x10^{-5}s.

G.5 Uncertainty in Phase Duration

The uncertainty of the phase duration is simply the difference between the first frame and the last frame in a phase:

$$\emptyset = t_{LF} - t_{FF}$$

Using the law of propagation of uncertainty equation yields:

$$W_{\emptyset} = \sqrt{\left[\left(\frac{\partial \emptyset}{\partial t_{LF}} W_{TF_{LF}}\right)^2 + \left(\frac{\partial \emptyset}{\partial t_{FF}} W_{TF_{FF}}\right)^2\right]} \qquad [40]$$

Which becomes,

$$W_{\emptyset} = \sqrt{\left[\left(W_{TF_{LF}}\right)^2 + \left(W_{TF_{FF}}\right)^2\right]}$$

Therefore the uncertainty in the phase duration is +/- 2.69 x10^{-5}s.

G.6 Uncertainty in Percentage of Phase Duration

The uncertainty of the percentage of the phase duration is found using the uncertainty in the phase duration found before and the uncertainty in the cycle duration.

Using the law of propagation of uncertainty equation again yields:

$$W_{P\emptyset} = \sqrt{\left[\left(\frac{W_{\emptyset}}{C_D}\right)^2 + \left(\frac{\emptyset W_{C_D}}{(C_D)^2}\right)^2\right]}$$

At very small phase durations, ∅ becomes negligible resulting in:

$$W_{P\emptyset_s} = \sqrt{\left(\frac{W_\emptyset}{C_D}\right)^2} = \frac{W_\emptyset}{C_D}$$

At very large phase durations, ∅ can be assumed to equal the cycle duration resulting in:

$$W_{P\emptyset_L} = \sqrt{\left[\left(\frac{W_\emptyset}{C_D}\right)^2 + \left(\frac{W_{C_D}}{C_D}\right)^2\right]}$$

Since the uncertainty in phase duration is equal to the uncertainty in cycle duration, the percentage phase duration for the 30 Hz cycle at very small phase durations becomes 0.08%. At very large phase durations for the 30 Hz cycle it is 0.11%.

G.7 Uncertainty in Channel Dimensions

Since the vernier calipers were used to measure the width and height of the channel therefore the uncertainty of each dimension is +/- 0.025 mm.

The area of the channel's uncertainty can be obtained from the equation:

$$W_{AC} = \sqrt{[(W_{CH})^2 + (W_{CW})^2]}$$

Therefore the Uncertainty in the area is +/- 0.036 mm^2.

G.8 Uncertainty in Frequency

Uncertainty in the frequency is determined by the uncertainty to read the oscilloscope as well as the uncertainty in the cycle durations of each nominal frequency found in Figure 43.

This can be found using the equation:

$$W_{PP} = \sqrt{{B_F}^2 + \left(t_{v,95}\, P_F\right)^2} \qquad [40]$$

From the oscilloscope, $B_F = 0.01$ Hz

And, $$P_F = \sqrt{\frac{1}{N-1}\sum_{i=1}^{N}\left(f_i - f_{avg}\right)^2}$$

A $t_{v,95}$ of 2.306 is found using the Student t Distribution table using a 95% confidence regularly distributed graph and a degree of freedom of 8.

Solving for the above equations results in:

Nominal Frequency (Hz)	Average Frequency (Hz)	Uncertainty in Frequency (Hz)	Frequency Uncertainty Percentage (%)
5	5.36	0.36	7.25
10	9.80	0.17	1.77
20	20.02	0.47	2.33
30	30.13	0.65	2.16

Vita Auctoris

NAME:	Kevin Mrozinski
PLACE OF BIRTH:	Mannheim, Germany
YEAR OF BIRTH:	1989
EDUCATION:	2015 University of Windsor, Windsor, ON MASc: Mechanical Engineering Candidate 2011 University of Windsor, Windsor, ON BASc: Mechanical Engineering